Michigan Technological University

Digital Commons @ Michigan Tech

Dissertations, Master's Theses and Master's Reports

2016

Rhyolite and Trachyte Formation at Lake City Caldera: Insight from Quantitative Textural and Geochemical Analyses

Jordan Lubbers
Michigan Technological University, jelubber@mtu.edu

RHYOLITE AND TRACHYTE FORMATION AT LAKE CITY CALDERA: INSIGHT
FROM QUANTITATIVE TEXTURAL AND GEOCHEMICAL ANALYSES

By

Jordan E. Lubbers

A THESIS

Submitted in partial fulfillment of the requirements for the degree of

MASTER OF SCIENCE

In Geology

MICHIGAN TECHNOLOGICAL UNIVERSITY

2016

This thesis has been approved in partial fulfillment of the requirements for the Degree of MASTER OF SCIENCE in Geology.

Department of Geological and Mining Engineering and Sciences

Thesis Advisor: *Chad Deering*

Committee Member: *Olivier Bachmann*

Committee Member: *William Rose*

Department Chair: *John Gierke*

Table of Contents

Acknowledgements

Abstract

Lake City Caldera (22.93 ± 0.02 Ma) is the youngest of 15 Tertiary calderas found within the Southern Rocky Mountain Volcanic Field (SRMVF). Extreme topographical relief of the area reveals the three dimensional exposure of a complex, high-k calc-alkaline, magmatic system, which provides us with the opportunity to study, in detail, how large silicic magmas evolve in the subsurface. The Lake City igneous system is comprised of two major units: a resurgent syenite intrusion and the Sunshine Peak Tuff (Lower, Middle, and Upper). Bulk-rock analyses indicate that the Lower and Middle Sunshine Peak tuff are crystal poor and rhyolitic in composition, while the Upper Sunshine Peak Tuff is crystal rich and trachytic in composition. Rhyolite-MELTS modeling and geochemical analyses show that Lake City rhyolites were formed by fractional crystallization of the syenite magma reservoir once it reached ~40% crystallinity. Zoning of these ignimbrites LSPT (76 wt % SiO_2) to MSPT (74 wt% SiO_2) shows that further crystal fractionation occurred following melt extraction from the syenite magma. This is interpreted as occurring within a melt-rich rhyolite cap within the syenite magma reservoir. Geochemical and textural analysis shows that the Upper Sunshine Peak trachyte was formed by later re-melting of a portion of the syenite cumulate. Crystal Size Distributions (CSDs) generated for both the syenite and trachyte show signs of textural coarsening, although trachytes exhibit these signatures to a more advanced degree. Syenite CSDs show characteristics of crystal accumulation, and both units are comprised mainly of glomerocryst networks. Titanium in quartz geothermometry gives temperature estimates for quartz formation across all units and shows that the majority of grains were formed between 735°C and 785°C, further providing evidence for a petrogenic relationship for all the rocks comprising Lake City Caldera. The presence of mafic enclaves within both the syenite and USPT trachyte coupled with reverse zoning noted in trachyte potassium feldspar grains alludes to mafic injection into the magma reservoir being responsible for both the re-melting of the syenite cumulate and the eruption mechanism for all three units of the Sunshine Peak Tuff. These models, for both rhyolite and trachyte production, are consistent with other models put forth for rhyolite production in the shallow crust and the origin of zoned ignimbrites.

1) Introduction

An understanding of the thermomechanical processes that lead to the formation of rhyolite and, in particular, zoned ignimbrites, are topics of ongoing controversy in the geologic community. Mechanisms for how these highly silicic and viscous magmas behave in the subsurface, are formed, and transported are varied among two distinct models: 1) Rhyolites are formed via the partial melting of the lower crust (gabbroic in composition), transported tens of kilometers to the surface, where their ascent pauses briefly (days to weeks), and then are subsequently erupted (Ratajeski et al., 2005). 2) Rhyolites are formed via the remobilization of interstitial magma found in evolved, silicic, magma chambers located in the shallow crust, form both explosive rhyolitic eruptions, and geochemically related silicic cumulates trapped in the subsurface (Bachmann and Bergantz, 2004; Deering and Bachmann, 2010). This study aims test the second model for rhyolite production at the Lake City caldera of the Southern Rocky Mountain Volcanic Field (SRMVF) in Southwest Colorado.

Lake City caldera formed at 22.93 ± 0.02 Ma and is the youngest of 15 Tertiary calderas found in the SRMVF (Figure 1) (Steven and Lipman, 1976; Lipman et al., 1997; Bove et al., 2001). Both extrusive and intrusive rocks are well exposed at Lake City caldera, allowing for the observation of a large, roughly 300 km^3, fossil magmatic system. Over time, uplift has exposed a large portion of the caldera, and when coupled with the extreme topographic relief of the area, much of the caldera that was once hidden in the subsurface can be directly studied. (Hon,1987; Hon and Lipman, 1989).
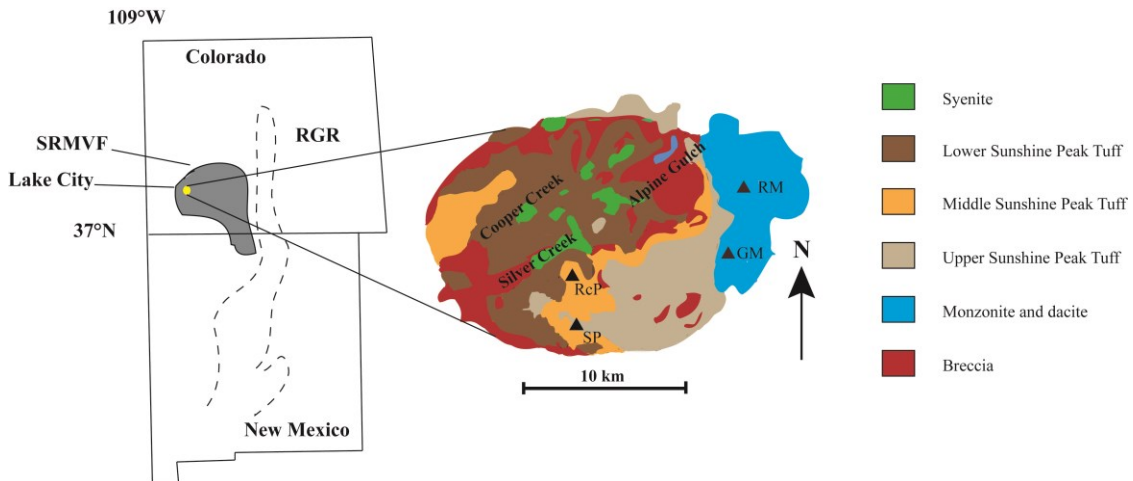
Figure 1: Geologic setting and map of Lake City caldera.

Geochemical and geospatial relationships show that multiple types of magma interacted and co-existed in the reservoir prior to the catastrophic eruption and caldera formation. The three ignimbrite units (Lower Sunshine Peak Tuff (LSPT), Middle Sunshine Peak Tuff (MSPT), and Upper Sunshine Peak Tuff (USPT)) found at Lake City show compositional zonation characteristic of other ignimbrites in the SRMVF. (Hon, 1987; Hon and Lipman, 1989).

1.1 Zoned ignimbrites

Compositioanlly zoned ignimbrites can provide useful insight into the deeper evolution and development of large magmatic systems (e.g., Bacon, 1983; Eichelberger et al., 2000; Hildreth and Wilson, 2007). Pumice samples from these chemically zoned ignimbrites may display small changes in magma type between adjacent ignimbrite units (Hildreth, 1979,1981; Hildreth and Wilson, 2007) or potentially show compositional gaps (Bacon, 1983; Eichelberger et al., 2000). Hildreth (1981) showed that undisturbed fractional crystallization processes can result in gradual chemical zonation in a single magma chamber and could be a mechanism for producing chemically zoned ignimbrites, such as those found at Lake City caldera. Alternatively, separate magma batches could produce compositional variances in ignimbrite units that appear to be zoned ignimbrites. These batches could be from separate magma chambers, or co-exist in a single chemically zoned magma chamber formed from magma replenishment. (Mills et al., 1997; Brown et al., 1998; Eichelberger et al., 2000; Reubi and Nicholls, 2005; Smith et al., 2005). It should be noted, however, that compositional zoning of an ignimbrite does not necessarily mimic the initial zoning of the magma chamber from which the ignimbrite was derived, as zoned ignimbrites can also be influenced by magma interaction during flow in the chamber (Bachman et al., 2002) and conduit (Kennedy and Stix, 2007), as well as ignimbrite transport and deposition on the surface (Branney and Kokelaar, 2003). The range in magma compositions observed, coupled with the well-exposed zoned ignimbrites and intrusions at Lake City caldera (Hon, 1987) make it perfect for studying the processes that occur within a magma reservoir before, and during, eruption events.

2) Geologic background

Lake City caldera is the youngest of 15 Tertiary collapse calderas (Figure 1) within the Southern Rocky Mountain Volcanic Field (SRMVF) (Steven and Lipman, 1976). Lake City caldera, itself, is nested within the 27-29 Ma Uncompahgre-San Juan and Silverton caldera complex (Lipman et al., 1973; Steven and Lipman, 1976). The overwhelming northeast-southwest alignment of this caldera complex was most likely controlled by pre-existing structural weaknesses within the underlying Precambrian country rock related to faults associated with the Colorado lineament (Tweto and Sims, 1963; Luedke and Burbank, 1968; Warner, 1978). The deposition of the Sunshine Peak Tuff (Lower, Middle, and Upper) and associated caldera formation occurred 22.93 ± 0.02 Ma, roughly three Ma after the last eruptive activity related to the older calderas in the area (Mehnert et al., 1973). The caldera is an elongate, oblate shape on the surface, roughly 10 to 12 km in diameter, with the long axis being parallel to regional fault orientations, Uncompahgre caldera, and Eureka graben (Lipman et al., 1978). Paleomagnetic data and $^{40}Ar/^{39}Ar$ dating show that the whole caldera sequence (from the Lower Sunshine Peak Tuff to post collapse dacite intrusions) erupted for between 80,000-330,000 years (Bove et al., 2001). The magmatic system of Lake City shows more of a variety of magma types than older SRMVF systems, and this variation is thought to be associated with the beginnings of regional extensional tectonism and the opening of the Rio Grande Rift (Lipman et al., 1978). Uplift and erosion

are responsible for exposing 1.5 km of zoned intracaldera ignimbrite along with the upper portion of a large, resurgent, syenitic pluton (Hon, 1987). The upper sequence of the intracaldera ignimbrites is well preserved and visible along the southern and eastern edges of the caldera.

2.1 Sunshine Peak Tuff

The intracaldera Sunshine Peak Tuff is comprised of three units, all uniquely distinct in both composition and mineralogy. All three units, however, share characteristics of being densely welded, extremely altered, and locally lithic rich (Hon, 1987). They are divided by large sections of megabreccia (Hon, 1987; Hon and Lipman, 1989). Due to the excellent exposure in three dimensions, megabreccia units can be very accurately mapped, providing confident separation of individual Sunshine Peak Tuff units (Kennedy et al., 2015). The lower unit of the Sunshine Peak Tuff (LSPT) is a high silica rhyolite (76% SiO_2)**.** Mineralogically it is composed of potassium feldspar (sanidine), plagioclase feldspar (anorthoclase), and quartz phenocrysts with trace amounts of biotite and clinopyroxene. These phases make up 30-40% of the intracaldera tuff and 25% of the outflow portion of the tuff (Hon, 1987). The middle unit of the Sunshine Peak Tuff (MSPT) is compositionally rhyolitic (74% SiO_2). Unlike the LSPT, the MSPT has two distinct pumice types rather than one: 1) high-silica rhyolite identical to the LSPT, and 2) quartz trachyte (65% SiO_2, 40-50% crystallinity of sanidine, plagioclase, biotite, and clinopyroxene). Distinguishing between the LSPT and MSPT is done by identifying the presence of biotite flakes and plagioclase in the MSPT, which are the result of the more mafic pumice (Hon, 1987). The upper unit of the Sunshine Peak Tuff (USPT) is a quartz trachyte (67-69% SiO_2). It contains both aforementioned pumice types, and at least two more types of pumice. Geochemical and other petrologic data suggests that the USPT is compositionally similar to the resurgent syenite intrusions found beneath the Sunshine Peak Tuff (Hon, 1987). In this study, it will be the primary unit of concern with respect to the other Sunshine Peak Tuff units when attempted to determine if a relationship exists between the plutonic and volcanic rocks found at Lake City caldera.

2.2 Resurgent Intrusive Unit

Resurgent quartz syenite is exposed within valleys and lower elevation areas in Lake City caldera and along the northern ring fault. These exposures are interpreted as high points in an undulating upper plutonic surface that was emplaced via resurgent activity (Hon, 1987). Mineralogically it is composed of mainly sanidine, minor quartz and hydrous phases, and mafic enclaves.

3) Methods

3.1 Petrography

Petrographic analyses were performed on an Olympus BX53 petrographic and reflected light microscope with an Olympus TH4 halogen lamp power supply unit, attached to a QImaging Retiga 2000R Color camera. The camera was attached to an Apple Imac

with a 27-inch screen and displayed images using Q-Capture Pro 7 imaging software. Photomicrographs were also obtained using this same software. Petrographic analysis was done using standard thickness (30μm) thin sections and thick sections (~200μm), in both plane polarized and cross polarized light.

3.2 iSpectra

Mineralogical mapping and quantification of samples used in both trace element and major element analysis was obtained by using the open source toolbox iSpectra. iSpectra uses spectral image analysis recorded on SEM and EDS systems to assign pixels with similar spectral content to phases, effectively creating very accurate phase maps of an entire thin section (Liebske, 2015). iSpectra runs via IGOR Pro 6.1 or later and is supported on both Windows XP and Mac OS X 10.4 (or later versions of both operating systems). More information on installation, operation, and pixel to phase assignment can be found in Liebske (2015).

3.3 Crystal Size Distributions

Crystal size distributions (CSDs) offer a means of quantitatively describing crystal contents of a magma body as a function of size, and through this we can derive important information about crystal growth, nucleation, and residence time for crystals in a magma chamber (Marsh, 1988). Population density of crystals (n) can be described as:

$$n = n_0 \cdot exp\left[\left\{\frac{-L}{G\tau}\right\}\right]$$

where L is crystal size, G is growth rate, τ is residence time, and n_0 is nucleation density. Linear regression analysis of the CSD curve, a plot of crystal size (L) vs. logarithmic population density of that size [ln(n)] provides a way to describe the growth rate/residence time (slope) and nucleation density (intercept) (Marsh, 1998). Linear CSD populations reflect uninterrupted fractional crystallization processes, therefore, deviations from this straight 'simple' pattern can reflect different processes that have occurred in magma chambers (e.g. Oswald ripening, textural coarsening; Marsh, 1998; Higgins, 1999; Zieg and Marsh, 2002).

For this project CSDs were generated in a multi-step process. Thin sections were digitized and stitched together from individual photomicrographs taken with Q-Capture Pro 7 and a mosaic was created using ImageJ and the MosaicJ plug-in. The digitized thin section mosaics were imported into Adobe Illustrator and as many grains as possible were outlined and filled in. In order to be statistically robust, as many grains as possible per sample need to be outlined. The layer of outlined and filled in grains was then exported back into ImageJ where measurement functions inside the program were used to generate best fit ellipses around each outlined grain. A data table of all long and short axis measurements of each ellipse was generated using similar measurement functions within ImageJ, saved as a .csd file, and imported into CSDCorrections 1.51. Certain assumptions and parameters need to be made when generating a CSD in CSDCorrections 1.51, and for this project they can be found in the results section. These assumptions are a result of the average roundness and fabric of grains observed in each thin section during petrographic analysis. Considering these assumptions and after double checking the area of the thin

11

section as well as the crystallographic parameters in CSDCorrections 1.51, a CSD is generated. Detailes are provided in Appendix 1.

3.4 Microprobe

Major element analyses (Si, Na, Ca, Cl, Fe, Mg, Ti, K, Mn, Al, Cr, Sr, Ba, Ni, V) were conducted on 11 carbon coated, polished, 200μm-thick thick sections were analyzed with a Jeol JXA-8200 electron microprobe (EPMA) at the Institute of Geochemistry and Petrology at ETH Zürich (ETHZ), using wavelength dispersive spectrometry (WDS). Elements were measured as oxides using the PRZ-Armstrong method.

Operation conditions for the EPMA measurements were the following: 1) an accelerating voltage of 15 kV, 2) beam current of 20 nA, 3) the Kα-lines (except for Ba and V using the Lα-line) were used, 4) employed a defocused beam of 20μm for the analyses of biotite and feldspar, and focused beam for the oxide analyses. The measuring time on peaks and backgrounds was 20 s for each element with the exceptions of Na and K, which were measured in the first row for 10 s on both peak and background. All elements were measured in differential mode in order to suppress higher order interferences.

Synthetic and natural standards used for feldspar and biotite measurements were: albite (Si, Na), forsterite (Mg), anorthite (Al, Ca), Rutile (Ti), chromite (Cr), microcline (K), scapolite (Cl), strontianite (Sr), fayalite (Fe), pyrolusite (Mn), bunsenite (Ni), and barite (Ba). Standards for the oxide measurements: wollastonite (Si, Ca), periclase (Mg), corundum (Al), chromite (Cr), elemental Vanadium (V), bunsenite (Ni), rutile (Ti), fayalite (Fe), and pyrolusite (Mn). The quality of the analyses was checked by measuring standards periodically throughout the analyses as well as by recalculation of the mineral stoichiometry.

3.5 Cathodoluminescence

Cathodoluminescence (CL) images were obtained for use in observing Ti zonation in quartz grains. As Ti concentration varies throughout the sample, so does CL emission intensity (Wark and Spear, 2005). Furthermore, Ti concentration in quartz and temperature of crystallization are directly correlated with one another (Watson and Wark, 2006). These two pieces of information can help shed light on changing conditions within a magma chamber as it evolves over time. Cathodoluminescence imaging was conducted at ETHZ and images were obtained from five samples. Here, ~200μm-thick sections, polished to 1μm, carbon-coated samples were analyzed and imaged using a Gatan MiniCL attached to an EMEZ Quanta 200 F SEM using an accelerating voltage of 20 kV and a beam current between 15 and 20 nA.

3.6 Laser Ablation

Laser ablation inductively coupled plasma mass spetcrometry (LA-ICP-MS) was used for the measurement of the trace elements ^{7}Li, ^{11}B, ^{23}Na, ^{27}Al, ^{29}Si, ^{31}P, ^{43}Ca, ^{47}Ti, ^{49}Ti, ^{55}Mn, ^{72}Ge, ^{85}Rb, ^{93}Nb, ^{118}Sn, ^{139}La, ^{140}Ce, ^{146}Nd, ^{157}Gd, and ^{208}Pb in quartz grains and was completed using the Department of Earth Science's Lab at ETH Zürich. Samples were prepared as ~200μm thick, thick sections, polished to 1 μm. Measurements were completed using the Resonetics Resolution 155 193 nm excimer laser using a spot diameter

of 51 μm, a repetition rate of 5 Hz, and energy density of 15 J/cm^2. The ablated material is carried in a mixture of helium and argon gas into the plasma source of a Thermo Element XR high sensitivity sector field ICP-MS equipped with a single triple mode detection system (pulse counting, analog, and Faraday cup). Each analysis starts with 5 "pre-blasts" to clear the surface contamination from the sample, a 10 s measurement of the background with the laser off, and a 30 second integration with the laser firing and ablating the sample. Samples were calibrated using NIST 612 standards (Jochum et al. 2011) and analyzing the standards every 29 sample analyses. Data was reduced using SILLS courtesy of Guillong and others (2008).

4) Results

4.1 Petrography

4.1.1 LSPT, MSPT, rhyolite
The LSPT and MSPT rhyolites are all crystal-poor rhyolites and on average contain less than 20% crystals. The majority of grains are fragmented quartz, plagioclase, or potassium feldspar (Figure 2f). Fragmented grains range in size from 10s of μm to two mm in diameter, with greater than 90% being smaller than 100 μm. Some samples observed have glomerocrysts in them (Figure 2 b, c,). These glomerocrysts are both monomineralic (plagioclase or potassium feldspar) or comprised of both feldspars in the same cluster. Crystals within these glomerocrysts are subhedral with rounded corners on the edges of grains. Glomerocrysts occasionally show alignment of grains (Figure 2c), but also show no alignment of grains (Figure 2b). Grain size for these clusters ranges from 0.25 to 2.0 mm. Potassium feldspar within the rhyolites ranges in size from 10s of μm to multiple cm in length. Within the LSPT and MSPT potassium feldspar phenocrysts are much less abundant and occur as anhedral to subhedral individual grains roughly 0.5 to 1.0 mm in diameter. Plagioclase within rhyolites ranges in size from 10s of μm to multiple cm in length. It is the dominant phenocryst phase (>85%) in the LSPT and MSPT, where it is subhedral to almost anhedral and has less alteration overprinting than potassium feldspar. When in two to five grain monomineralic glomerocrysts, grains are observed to be aligned with one another. Quartz grains occur in all units, are heavily embayed, and anhedral. Quartz occurs in five to ten percent, and is one to five mm in length. Unlike the potassium feldspar, quartz is rarely fragmented and often is found in an oblate spheroid shape.

4.1.2 USPT trachyte
The USPT trachyte porphyry is noticeably different than the rhyolite. Trachyte can be distinguished from the rhyolite by a drastic increase in crystallinity (30-40%), the disappearance of the majority of fragmented grains, appearance of monomineralic potassium feldspar glomerocrysts, and an increase in the size of the potassium feldspar grains within the rocks. Potassium feldspar is the dominant phase within the USPT trachyte, making up greater than 85% of phenocrysts within the rock. Grains range in size from sub-millimeter to multiple centimeters in length (Figure 2e). Grains are anhedral to subhedral and have much of their surface covered by an alteration overprint, sometimes to

13

the extent of appearing spongy and much of the grain being dissolved. Average grain shape is blocky with rounded edges on the corners of the grain. Potassium feldspar also occurs in monomineralic glomerocrysts that have no discernable orientation or fabric to the grains (Figure 2d). Plagioclase represents less than five percent of phenocrysts in the USPT trachyte. It is subhedral, 0.5 through 2.0 mm in length, and has more of an alteration overprint to it than plagioclase found within the LSPT and MSPT rhyolites. It occurs as single phenocrysts or as two to three grain monomineralic glomerocrysts aligned along long faces of the grain. Quartz represents between 5-10% of phenocrysts within the USPT trachyte. Like the rhyolites, quartz grains are oblate spheroid in shape, anhedral, heavily embayed, and one to five mm in length.

4.1.3 Syenite

The syenite at Lake City is heavily altered and porphyritic. Phenocrysts are predominantly potassium feldspar with trace amounts of phenocrysts being plagioclase, quartz, and biotite grains. The syenite is holocrystalline with 40-60% of grains being phenocrysts, and the rest being interstitial material and mafic enclaves. Potassium feldspar occurs both as phenocrysts and interstitial material. It makes up greater than 95% of phenocrysts, is sub-millimeter to multiple centimeters in length, subhedral in shape, and has an alteration overprint on the grain. Alteration is more prevalent on the rims of grains, and some of the megacryst cores are free of alteration. Grains are also rounded along the corners. These phenocrysts also occur as both polymineralic and monomineralic glomerocrysts ranging from one to three cm in diameter. As interstitial material, potassium feldspar is 0.1 through 0.25 mm in diameter, anhedral, and heavily altered. Next to quartz grains, myrmekitic textures were also observed. It makes up roughly 40-50% of interstitial material. Plagioclase occurs in in trace amounts in the syenite as anhedral to subhedral phenocrysts ranging one to three mm in length. They are heavily altered and only identified by their albite and carlsbad twinning. Quartz occurs as both phenocrysts and interstitial material. It makes up between 5-10% of phenocrysts. As phenocrysts, quartz is anhedral, oblate spheroidal in shape, heavily embayed, has very little to no alteration on the surface of the grain, and is one to five mm in length. As interstitial material quartz is anhedral, has no polygonal shape to it, and occurs with potassium feldspar. Here it is 0.1 to 0.25 mm in length, has very little alteration on the surface of grains, and helps outline the borders of larger potassium feldspar phenocrysts.

14
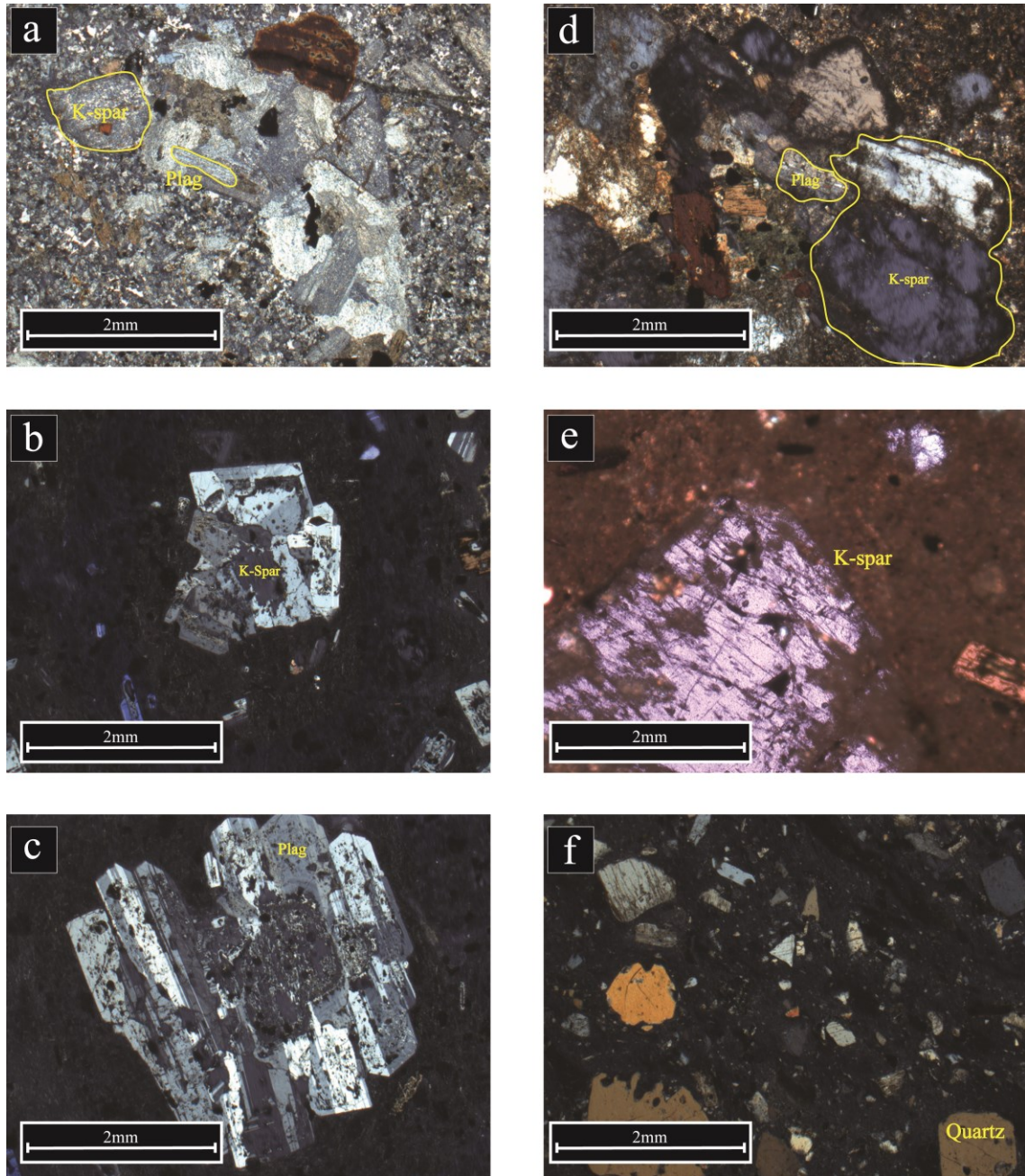
Figure 2: Photomicrographs from samples at Lake City caldera. a) polymineralic feldspar glomerocryst within syenite. b) monomineralic potassium feldspar glomerocryst from trachyte. c) monomineralic plagioclase glomerocryst from pumice within the rhyolite. d) polymineralic feldspar glomerocrysts within trachyte. e) potassium feldspar megacryst with rounded corners from trachyte. f) fragmented grains from pumice within rhyolite.

4.1.4 Mafic Enclaves

Many of the syenite and trachyte samples collected in the field were observed, due to color index, to have what looked like mafic to intermediate composition enclaves within them. This was confirmed upon petrographic analysis. These enclaves are spheroidal in shape, mafic in composition, and range in size from 0.5 to 5.0 cm in diameter (Figure 3). The enclaves consist of plagioclase microlites, and amphibole. Amphibole occurs in

15

subhedral, acicular, laths 0.25 mm to 1.0 cm in length. Plagioclase microlites are heavily altered, making it difficult to determine a definite size. At the hand sample scale contacts look to be sharp, but upon petrographic analysis it can be observed the contacts are more diffuse and crystal populations from both rocks mingle together near the edge of the enclave-syenite contact. This is evidenced by an increase in hydrous minerals within the syenite near the contact.
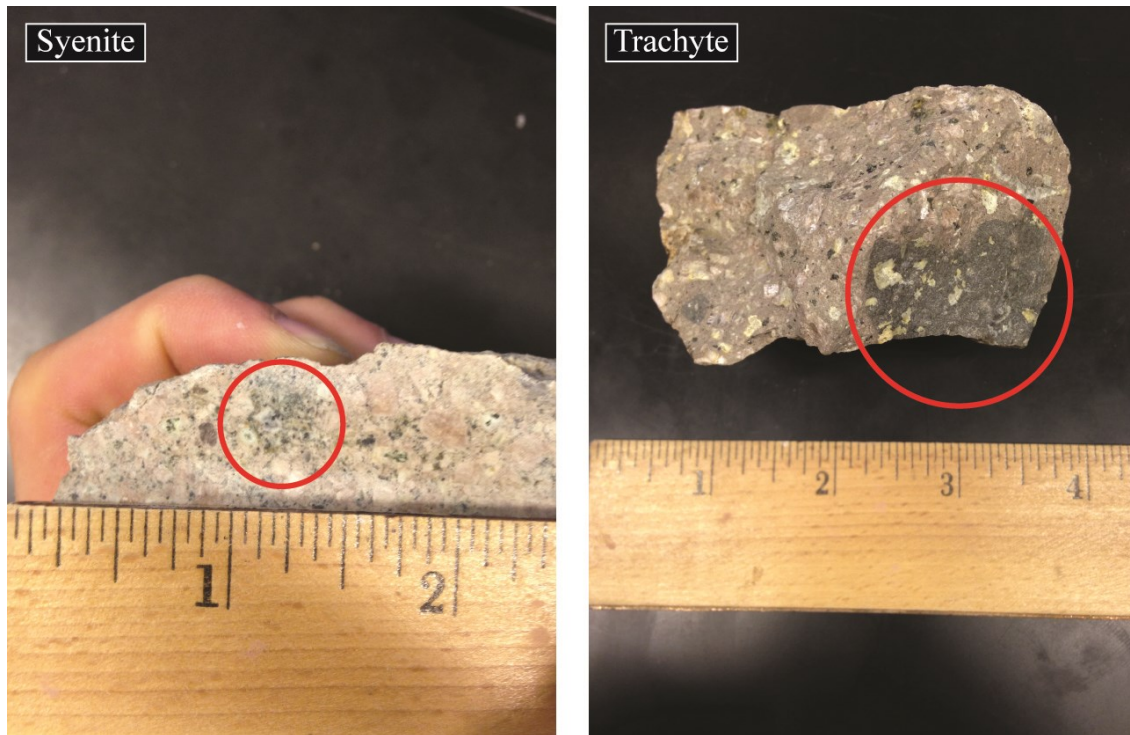
Figure 3: Photographs of mafic enclaves within both syenite and trachyte. Circled areas represent extent of enclaves.

4.1.5 Alteration

Alteration is present in all samples observed. Both clay and silica-rich alteration is present, with clay-rich being more prevalent in the feldspar dominated rocks (syenite) and the silica-rich being more prevalent in the glass matrix rocks (LSPT, MSPT, USPT). Clay-rich alteration forms an overprint on feldspar grains, making the positive identification of some heavily altered feldspars challenging, and only identifiable by the way they go extinct in cross polarized light. Silica-rich alteration typically forms wormy blebs of amorphous silica found in the groundmass of the volcanic. The source of this alteration is most likely the 23 Ma fossil hydrothermal system emplaced after caldera collapse (Hon and Mehnert, 1983).

Alteration is most accurately observed using iSpectra generated phase maps (Figure 4). Phase mapping was completed using iSpectra software courtesy of Liebske (2015). Phase mapping of these samples better illustrates the advanced degree of alteration that rocks at Lake City caldera have been exposed to and how it affects feldspar determination in the samples collected, which is of importance in data acquisition for Crystal Size

16

Distributions (CSDs). The main phase shown in syenite samples is potassium feldspar, but Figure 4 shows that this also may be alteration, because clay-rich alteration also has high K and Al peaks like potassium feldspar and the morphology of some of the pixel clusters is not grain shaped, but rather looks like an overprinting on top of grains.
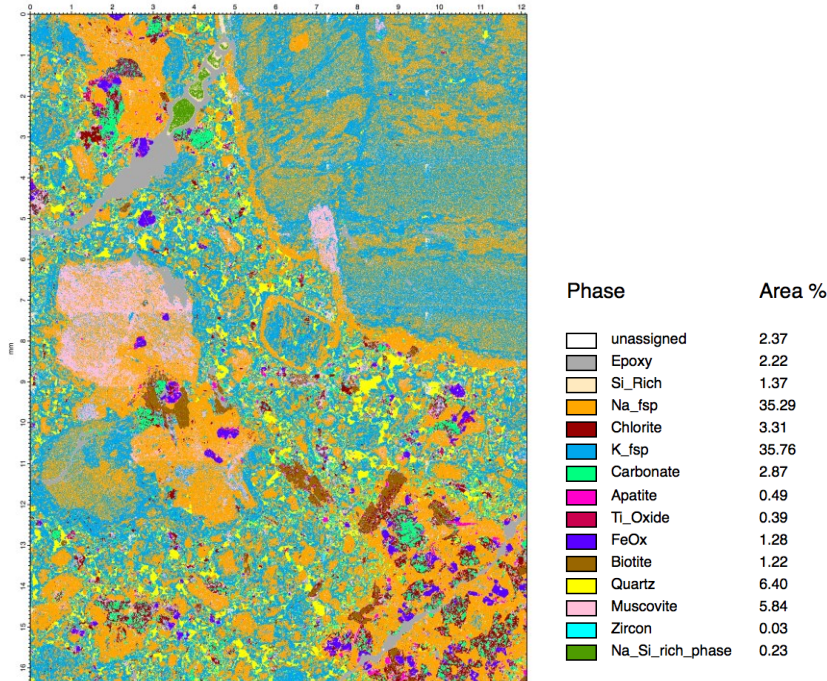
Figure 4: Phase map for sample LCTISY081013-10b (syenite) showing the ambiguity between Na feldspar, K feldspar, and clay alteration of similar chemical makeup.

4.2 Quantitative textural analysis

4.2.1 *Crystal size distributions (CSDs)*

Crystal size distributions were estimated for five samples (three syenite and two trachyte) using CSDCorrections. Trachyte samples are a part of the USPT. All samples have been exposed to hydrothermal alteration, however, despite this alteration, definitive edges to grains were found and outlined via petrographic analysis in order to minimize error. In CSDCorrections variables were dealt with as follows: 1) size scale was log 10 based, 2) ellipses were measured along their major axis, 3) roundness of 0.4 was selected, and 4) a massive fabric was chosen. Individual shape ratios between short, intermediate, and long axes for the grains in each sample are listed in (Figure 5). Vertical bars located at the center of each size bin are directly proportional to uncertainty with each size bin calculation. A brief statistical summary can be found in (Table 1).

All CSDs exhibit a continuous, concave upwards shape, with a negative slope on a semi-logarithmic CSD diagram, however, the concavity is more severe in the syenite samples than the trachyte samples (Figure 5). Due to concavity, linear regression and intercept determination of each CSD is not possible. All CSDs exhibit similar sizes for the

smallest grains found in each sample, however, the largest grains in each sample are extremely variable (5-20mm). This is due to the varying size of megacrysts found in each sample. Syenites are characterized by a sharp decrease in the smallest size bin, exhibited by a concave down hook in the upper left hand portion of the CSD (with the exception of LCITV091114-1C). Sample LCTISY081013-11A exhibits a more kinked shape in its concavity than the other syenite samples, which have more rounded curves to them.

Table 1: Summary of units, rock type, axes parameters, and R-value for each sample used in CSDCorrections

Sample	Unit	Rock Type	Grains counted	Short axis	Inter axis	Long axis	R-value
LCTISY08013-2A	Syenite	Syenite	991	1.00	2.00	2.00	0.807
LCTISY081013-11A	Syenite	Syenite	888	1.00	1.43	1.43	0.966
LCITV091114-1C	Syenite	Syenite	1292	1.00	1.54	1.54	0.774
LC-2004-40B	USPT	Trachyte	156	1.00	2.00	2.00	1.03
LC-2004-40A	USPT	Trachyte	152	1.00	1.82	1.82	1.01
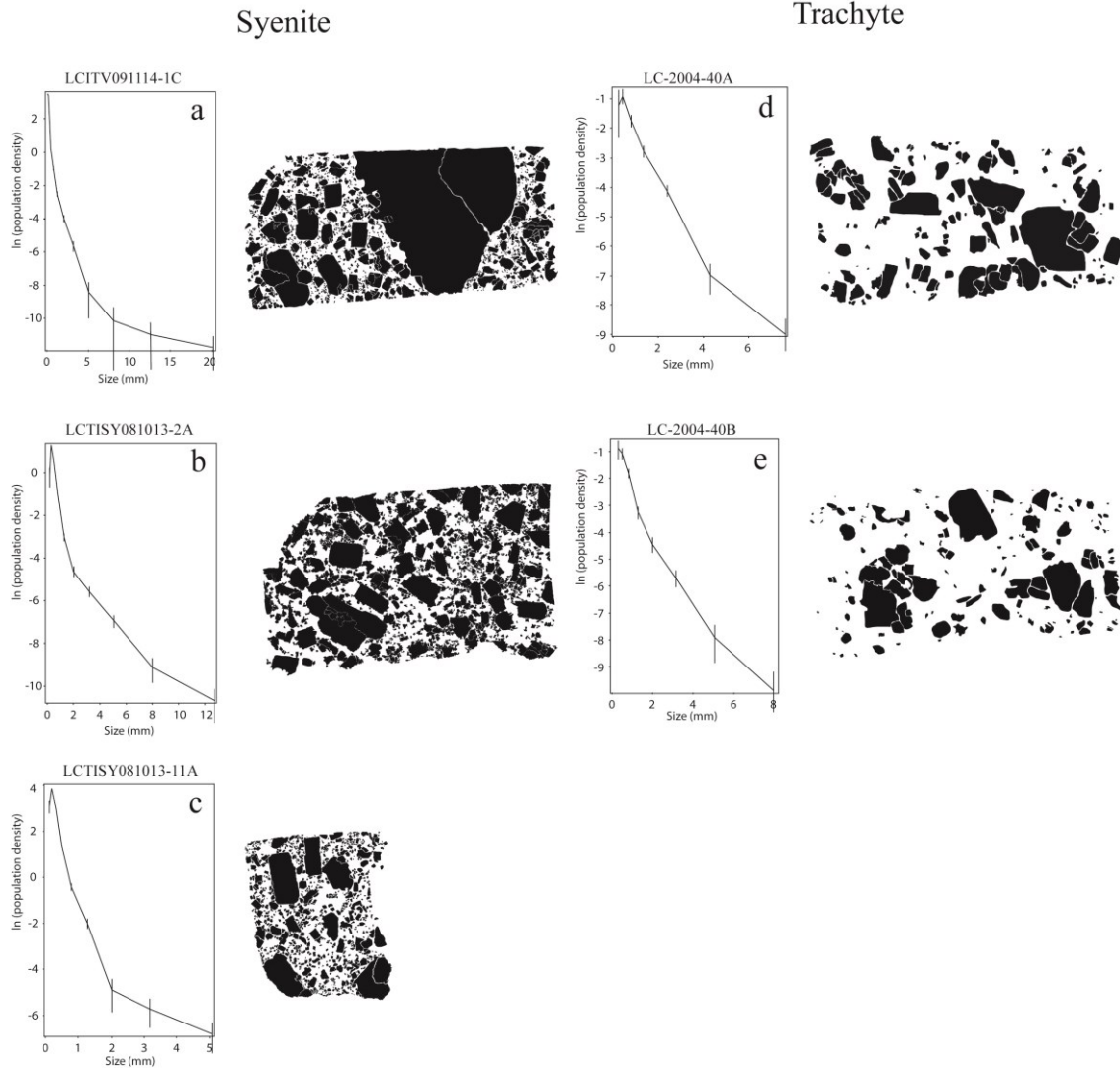
Syenite   Trachyte

Figure 5: Crystal Size Distribution (CSD) plots for potassium feldspar grains within syenite (a, b, c)) and trachyte (d, e) samples at Lake City caldera. Binary images generated from grain outlines are shown to the right of their corresponding CSD to show how different shaped CSDs look in thin section.

4.3 Cathodoluminescence (CL) imaging

Cathodoluminescence (CL) images were obtained for a total of thirty quartz grains from five different samples representative of the rhyolite, trachyte, and syenite. Growth zones in the quartz appear as different shades of grey and represent crystallographic defects (Götze, 2009a). Growth zones were later used as maps for trace element analysis by laser ablation.

Quartz from the trachyte were mostly anhedral and oblate, with a few samples being subhedral and hexagonal. Quartz from the syenite were observed to have fewer

embayments and sieve textures than the trachyte samples (Figure 6 a,c). Embayments in both the syenite and trachyte quartz grains cut across lines of zoning, however, only the syenite grains had bright rims around the edges (Figure 6 a,b,). These rims follow the contour of the embayments, not the original zoning patterns, and are found in the majority of syenite quartz grains. There are a few grains where embayments are parallel to zoning as well, and are unrelated to the high Ti rims found in the syenite (Figure 6a, b).

Zoning observed was both concentric and non-concentric in both samples. In the syenites many samples were observed to have no zoning whatsoever, however the high Ti rim was still present. There is no discernable pattern to the zoning among samples and greyscale variations are random and individual to each sample.
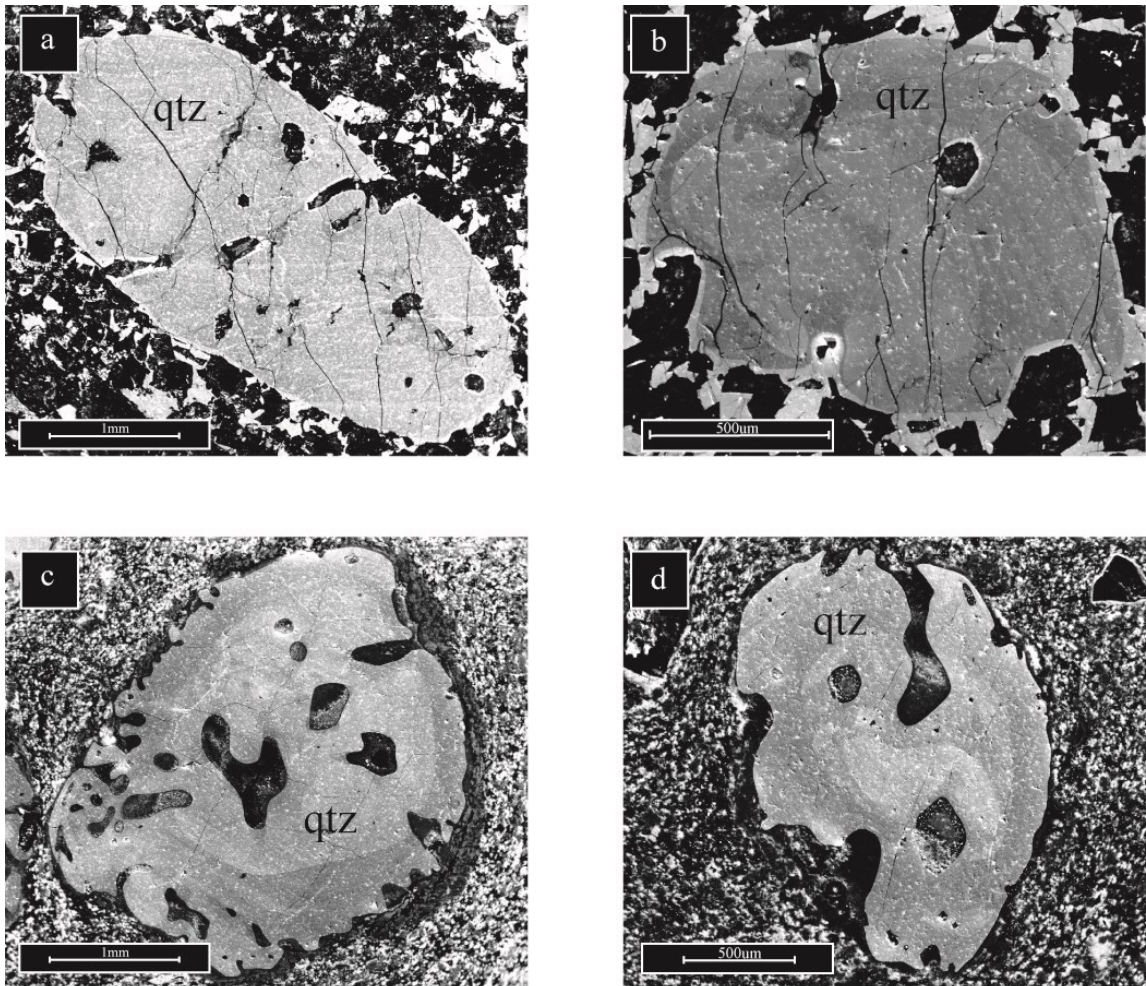
Figure 6: Cathodoluminescence (CL) images for quartz in syenite (a, b) and trachyte (c, d).

4.4 Mineral chemistry

4.4.1 Potassium feldspar

Major element data was obtained via Electron Microprobe Analysis (EPMA) for potassium feldspar, plagioclase feldspar, biotite, magnetite, and ilmenite grains in 11 samples. 325 feldspar analyses from these 11 samples were combined with another 309 analyses from feldspar grains courtesy of Kennedy (2005). 139 oxide analyses were obtained from magnetite and ilmenite grains, however data from these analyses were not used, due to exolution lamellae being present in many of the grains, and therefore, not representative of equilibrium conditions in the magma chamber at the time of the grain's formation. 117 biotite analyses were obtained from the 11 samples as well. Samples analyzed ranged in composition from syenite, trachyte (Upper Sunshine Peak Tuff), unknown mafic intrusive material, high-silica rhyolite (Lower Sunshine Peak Tuff), and low-silica rhyolite (Middle Sunshine Peak Tuff).

When plotted against An, K seems to have two separate groups. One, involving the syenite, shows a high K, population (Figure 7). This is a small subset of syenite analyses. The majority of the data shows a negative, linear correlation between K and An content. Barium concentrations in potassium feldspar grains shows a significant enrichment from syenite to trachyte samples when plotted against An (Figure 7). Potassium feldspars analyzed also exhibit reverse zoning patterns, with rims having higher An and Ba content than the cores of grains (Figure 8).
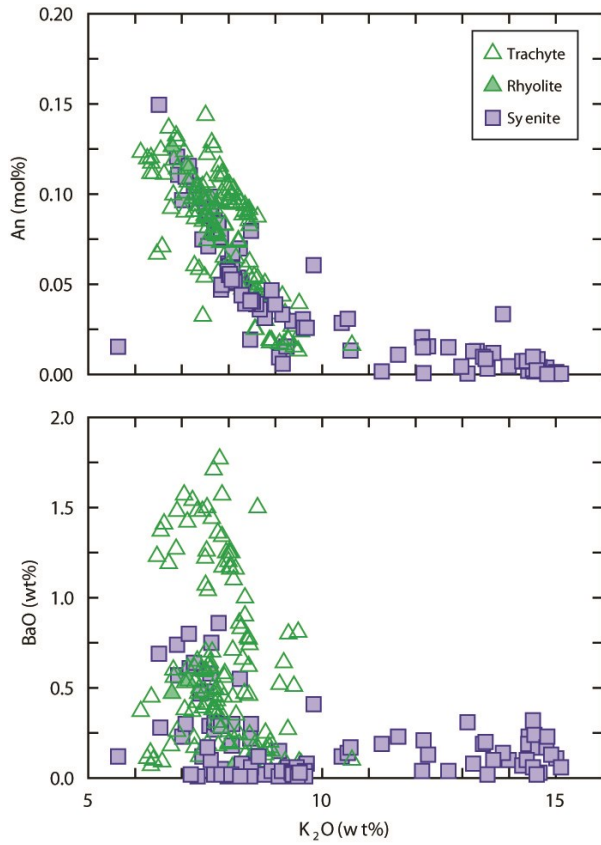
Figure 7: Plots of An content and BaO content against K₂O for potassium feldspar grains in the USPT, LSPT, and Syenite samples.
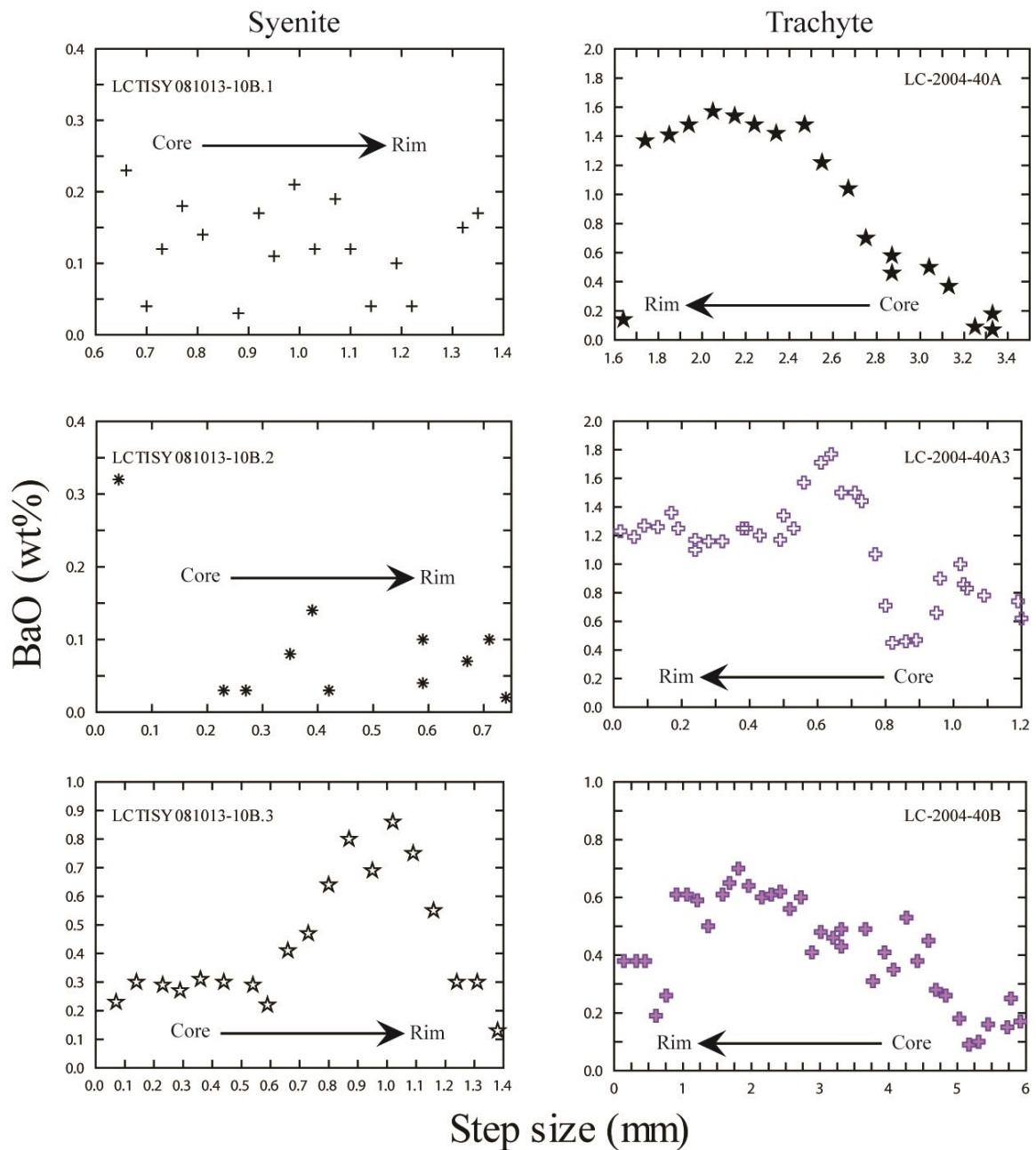
Figure 8: Plots of BaO from potassium feldspar grains in both the syenite and trachyte. Traverses go from core to the rim of the grain.. X-axes show distance between analyses in mm.

4.4.2 Plagioclase

Plagioclase exhibits a poor linear, positive correlation between Sr and An (Figure 9). Only volcanic samples have microprobe data for plagioclase due to its low abundance within the syenite. Plagioclase, is therefore, not a good mineral to study when comparing intrusive and volcanic units at Lake City caldera.

23
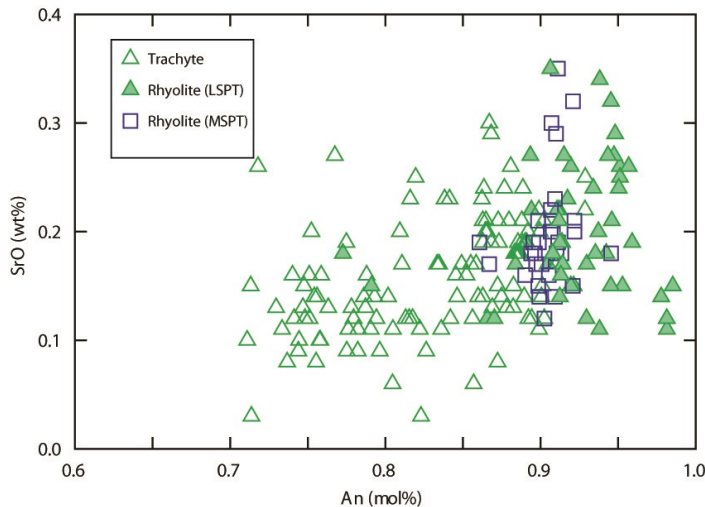
Figure 9: Sr content with varying anorthite content for volcanic rocks at Lake City caldera

4.4.3 Quartz

Quartz trace element chemistry was obtained for 13 samples using laser ablation-inductively coupled plasma-mass spectrometry (LA-ICP-MS). Average trace element compositions for each unit are shown in Table 2. Of the 13 samples, bulk-rock compositions are as follows: one was LSPT (rhyolite), three were MSPT (rhyolite), four were USPT (trachyte), two were syenite, two were monzonite, and one was dacite. Elements focused on from laser ablation were Ti, Al, Li, and Ge. These elements are easily incorporated into the lattice structure of quartz grains as defects (e.g., Sprunt, 1981; Waychunas, 1988; Perny et al., 1992; Stevens Kalceff and Phillips, 1995; Pagel et al., 2000; Gotze et al., 2001). Titanium concentrations in quartz also have the potential to reflect crystallization temperatures of the mineral in the magma chamber (Wark and Watson, 2006; Thomas et al, 2010; Huang and Audetat, 2012). Fractionation processes in granitic magmas can also be examined using Al and Ti concentrations (Mueller et al., 2010), and are, therefore, plotted in (Figure 10). The Ti vs. Al, Ti vs. Li, and Ti vs. Ge plots all show similar trends and overlaps among samples. Figure 10 shows a strong clustering and overlap of analyses from all units. Quartz grains from the USPT, however, show higher Al, Li, and Ge populations than the quartz grains from other units. There are also analyses from some of the syenite that display high Li signatures characteristic of hydrothermal quartz (Breiter et al., 2012). Since there is noticeable hydrothermal alteration present in the rocks, having some analyses of this nature is not surprising. The dominant cluster of analyses have Ti concentrations ranging from 80-150 ppm.

24
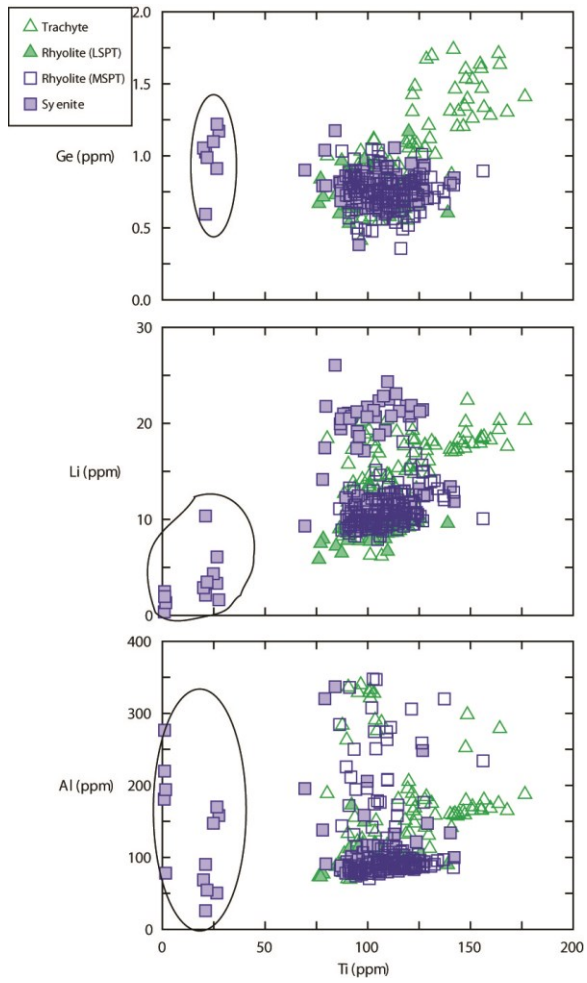
Figure 10: Plots showing how Ti concentration varies against Al, Li, and Ge in quartz grains from units at Lake City caldera. Circled areas are analyses from hydrothermal quartz grains.

Table 2: Average trace element concentrations for all of the units sampled at Lake City caldera in parts per million (ppm).

Element	Unit Syenite	LSPT	MSPT	USPT	Monzonite
Li	13.8	8.97	11.0	14.2	10.50
B	3.23	3.38	2.47	3.13	2.38
Na	25.1	67.1	13.6	16.4	136
Al	109	90.3	124	144	145
Ca	76.9	73.7	79.6	79.3	428
Ti[47]	91.4	101	109	115	148
Ti[49]	93.9	102	111	117	150
Mn	3.13	21.3	.730	1.10	15
Ge	1.04	0.760	0.750	0.950	0.840
Rb	0.47	0.720	0.240	0.220	1.00
Nb	0.060	0.040	0.090	0.020	0.090
Sn	1.01	0.070	0.090	0.070	0.070
La	0.060	0.040	0.040	0.040	0.040
Ce	0.06	0.080	0.06	0.040	0.050
Nd	0.030	0.040	0.060	0.040	0.040
Gd	0.010	0.040	0.020	0.010	0.010
Pb	0.460	1.05	0.680	0.040	1.13

4.4.4 Biotite

Biotite analyses from both volcanic and plutonic units at Lake City caldera show similar geochemical signatures. When plotted against Mg, K shows an overlap between all samples, with a linear positive correlation (Figure 11).
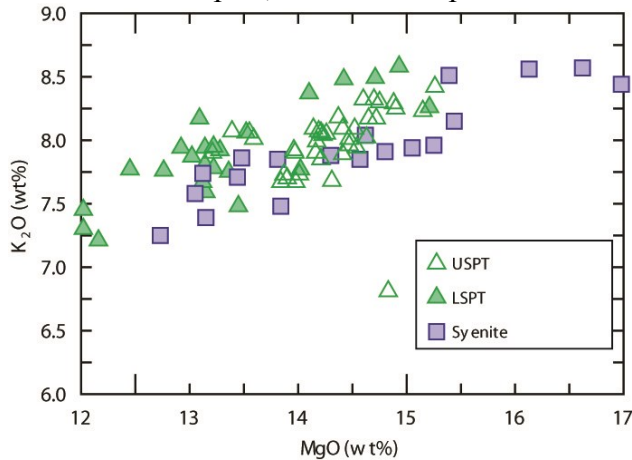
Figure 11: Figure showing K_2O with varying MgO content in biotite analyses from volcanic and plutonic samples at Lake City caldera.

Table 3: EPMA major element compositions in potassium feldspar, plagioclase, and biotite for the highest and lowest Ba samples found in each unit. All values are in weight percent. Note: n.m. = not measured, b.d. = below detection limit.

Unit Sample Mineral	USPT LC-2004-40A3 kspar	USPT LC-2004-40B kspar	USPT LC-2004-40A3 plag	USPT LC-2004-40F plag	USPT LC-2004-40B biotite
SiO_2	63.6	66.5	60.5	57.9	36.8
TiO_2	0.16	0.01	0.06	0.04	7.69
Al_2O_3	20.5	19.2	24.7	25.5	14.8
FeO	b.d.	b.d.	b.d.	0.34	13.3
MnO	b.d.	b.d.	b.d.	b.d.	0.19
MgO	b.d.	b.d.	b.d.	0.01	13.8
CaO	1.21	0.37	5.82	4.87	0.02
Na_2O	4.42	4.51	6.95	7.69	0.72
K_2O	7.81	9.00	1.42	1.51	7.67
BaO	1.77	b.d.	0.32	b.d.	2.25
SrO	0.13	0.03	0.16	0.16	0.00
Cl	n.m.	n.m.	n.m.	n.m.	0.04
Cr_2O_3	n.m.	n.m.	n.m.	n.m.	0.03
NiO	n.m.	n.m.	n.m.	n.m.	0.01
Total	99.5	99.6	100.0	97.9	97.3

Unit Sample Mineral	USPT LC-2004-40B biotite	Syenite LCTISY081013-10B kspar	Syenite LC-2004-17C kspar	Syenite LC-100 plag	Syenite LCTISY081013-10B biotite
SiO_2	66.5	65.0	66.4	65.2	35.9
TiO_2	0.02	0.13	0.04	0.03	7.38
Al_2O_3	19.4	20	18.7	18.7	14.5
FeO	0.21	b.d.	0.17	0.19	15.1
MnO	0.02	b.d.	0.00	0.00	0.270
MgO	0.01	b.d.	0.00	0.00	13.1
CaO	0.66	0.82	0.45	3.96	0.01
Na_2O	5.18	5.04	5.97	8.45	0.66
K_2O	7.92	7.79	8.23	1.33	7.58
BaO	0.09	0.86	0.00	0.08	2.64
SrO	0.03	0.08	0.02	0.10	0.01
Cl	0.01	NM	NM	NM	0.09
Cr_2O_3	0.00	NM	NM	NM	0.06
NiO	0.03	NM	NM	NM	0.03
Total	100	99.7	99.9	98.1	97.2

Table 3 Continued:

Unit	Syenite	MSPT	MSPT	LSPT	LSPT
Sample	LCTISY081013-7B	LC-2004-57C	LC-2004-57C	LC-2004-15D	LC-2004-15D
Mineral	biotite	plag	plag	kspar	kspar
SiO_2	39.1	57.0	66.7	66.6	67.5
TiO_2	3.5	0.06	0.00	0.05	0.04
Al_2O_3	12.4	26.6	18.9	19.9	19.0
FeO	13.5	0.30	0.21	b.d.	b.d.
MnO	0.420	0.00	0.00	b.d.	b.d.
MgO	16.6	0.03	0.01	b.d.	b.d.
CaO	b.d.	8.22	8.39	1.09	0.47
Na_2O	0.72	5.95	6.19	5.26	4.9
K_2O	8.57	1.12	0.74	7.14	8.53
BaO	b.d.	0.26	b.d.	0.54	b.d.
SrO	0.02	0.32	0.18	0.11	0.01
Cl	0.15	n.m.	n.m.	n.m.	n.m.
Cr_2O_3	b.d.	n.m.	n.m.	n.m.	n.m.
NiO	0.06	n.m.	n.m.	n.m.	n.m.
Total	95.0	99.8	101	101	100

Unit	LSPT	LSPT	LSPT	LSPT
Sample	LC-2004-15D	LC-2004-15D	LC-2004-15D	LC-2004-15D
Mineral	plag	plag	biotite	biotite
SiO_2	59.6	51.6	35.9	38.5
TiO_2	0.06	0.06	7.84	5.08
Al_2O_3	25.6	31.2	14.2	13.3
FeO	b.d.	b.d.	16.8	14.8
MnO	b.d.	b.d.	0.41	0.261
MgO	b.d.	b.d.	12.0	14.9
CaO	7.14	13.91	0.07	0.055
Na_2O	6.96	3.24	0.66	0.50
K_2O	0.54	0.22	7.3	8.58
BaO	0.29	b.d.	2.8	0.253
SrO	0.22	0.12	b.d.	0.008
Cl	n.m.	n.m.	0.12	0.202
Cr_2O_3	n.m.	n.m.	b.d.	0.020
NiO	n.m.	n.m.	0.01	b.d.
Total	100	100	98.1	96.5

4.4.5 Fe-Ti oxides

Due to the presence of exolution lamellae indicating disequilibrium (Figure 12) within the majority of oxide grains the data could not be used for geothermometry.

a   b
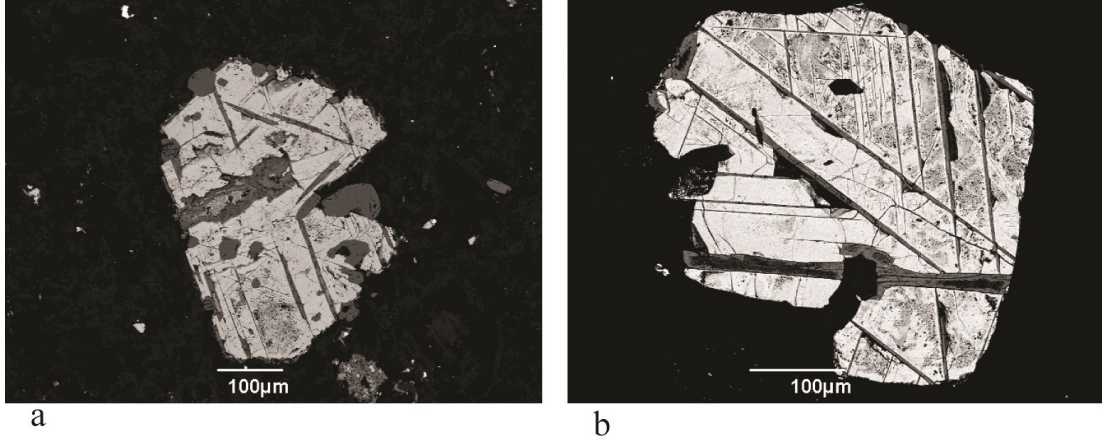
Figure 12: Backscattered electron (BSE) images for oxides within trachyte at Lake City caldera. a) LC-2004-40A b) LC-2004-40A3.

4.6 Geothermometry

4.6.1 Titanium in quartz geothermometry

Temperatures for quartz crystallization in the magma chamber were calculated initially using three different equations from Watson and Wark (2006), Thomas and others (2010), and Huang and Audetat (2012) respectively.

(1)

$$T\,(°C) = \left[\frac{-3765}{log\left[\frac{X_{Ti}^{qtz}(ppm)}{\alpha_{TiO_2}}\right] - 5.69}\right] - 273$$

(2)

$$T(°C) = \left[\frac{60952 - 1741 \cdot P(kbar)}{R\left[\ln\left(X_{TiO_2}^{quartz}(ppm)\right) - \ln(\alpha_{TiO_2}) - 1.52\right]}\right] - 273$$

(3)

$$T(°C) = \left[\frac{-2794.3 - (660.53 \cdot P(kbar)^{.35})}{log\left(X_{TiO_2(mol\%)}^{quartz}\right) - 5.6459}\right] - 273$$

where T is temperature in degrees Celsius, α_{TiO_2} is activity of TiO₂ in the system, X_{Ti}^{qtz} is the concentration of quartz in ppm (Wark and Watson, 2006; Huang and Audetát, 2012) or mole fraction (Thomas et al., 2010), R is the gas constant 8.3145 J/K, and P is the pressure of the system in kbar. Pressure is considered in both equations 2 and 3, and, therefore, temperatures were calculated for varying depths throughout the upper crust for each equation (Figure 13). A statistical summary of these temperature

calculations can be seen in Table 4. Equation 1 gives the highest average temperature estimates across all samples measured, while equation 2 estimates the lowest average temperatures. For equations that incorporate temperature (2 and 3), shallower depths used in the equation result in lower temperatures estimated for quartz formation. Boxes represent the middle two quartiles of temperature estimates, while "whiskers" represent the upper and lower quartile temperature estimates. Outlier temperature estimates are shown by black dots.
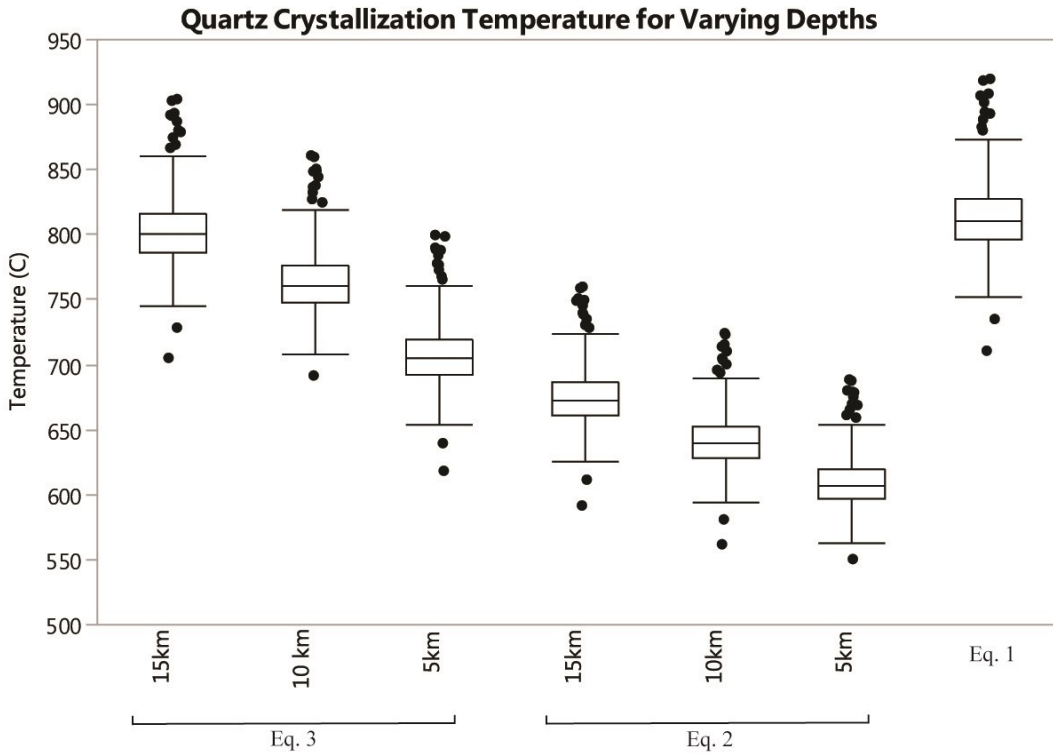
Figure 13: Box and whisker plot for temperatures calculated using equations 1, 2, and 3. Temperatures were calculated for depths of 5, 10, and 15 km with the Huang and Audetat (2012) and Thomas et al. (2010) geothermometers.

Depth	Wark & Watson -	Thomas et al. 2010			Huang & Audetat 2012		
		5km	10km	15km	5km	10km	15km
Mean	815	610	643	676	709	765	804
Std. Deviation	27	19	20	21	23	24	26
Std. Error Mean	1.3	1.0	1.0	1.0	1.1	1.1	1.2
Upper 95% Mean	817	612	645	678	711	767	807
Lower 95% Mean	812	608	641	674	706	763	802
N	460	460	460	460	460	460	460

4.6.2 Two Feldspar and Fe-Ti oxide geothermometry

Temperatures calculated from Ti concentration in quartz were compared to temperatures calculated with the Giorso and Evans (2008) Fe-Ti oxide geothermometer available online from OFM Research's Computational Thermodynamics (CT) server (http://ctserver.ofm-research.org/OxideGeothrm/OxideGeothrm.php). Oxide data was obtained from EPMA analysis, but despite a large number of oxides being analyzed, very few analyses were able to be used for geothermometry, as they were not representative of magma chamber conditions due to re-equilibration from hydrothermal alteration. One a pair of analyses was able to be used to generate a temperature of 759 degrees from sample LC-2004-16C (Figure 14).

Figure 14: Input and results for the Ghiorso and Evans (2008) Fe-Ti oxide geothermometer.

Temperature estimates generated from Ti in quartz geothermometers were also compared to temperatures generated using the two feldspar geothermometer from Putirka (2008) for samples from the USPT. Only this unit was used, because, in order for the geothermometer to be accurate plagioclase and potassium feldspar grains in volcanic samples must either be touching or rim analyses within the same sample, and the USPT was the only unit that contained both types of feldspars and met these requirements, while still passing the equilibrium test. While equilibrium test numbers

for Δ-a(An), Δ-a(Ab), and Δ-a(Or) should be 0 to reflect true thermodynamic equilibrium, the values calculated for the USPT were within range of equilibrated samples from Elkins and Grove (1990), and their calculated temperatures were, therefore, deemed viable (Table 5).

Table 5: Temperatures generated using the two feldspar geothermometer from Putirka (2008).

Sample	Unit	Pressure (kbar)	Temp	Equilibrium Test		
				Δ-a(An)	Δ-a(Ab)	Δ-a(Or)
LC-2004-40A2	**USPT**	2.70	887	-0.10	-0.01	-0.03
LC-2004-40A2	**USPT**	2.70	920	0.24	-0.04	-0.06
LC-2004-40A3	**USPT**	2.70	856	-0.20	-0.01	0.01
LC-2004-40A3	**USPT**	2.70	884	0.13	0.01	-0.09
LC-2004-40B	**USPT**	2.70	896	0.07	0.01	-0.21

After comparison to temperatures calculated from Fe-Ti oxides and two feldspar geothermometry it was decided that the Huang and Audetat (2012) equation fit these temperatures best and also incorporated pressure into the equation, which is important in discerning the evolution of the magma system that formed the rocks found at Lake City caldera. It was then used to calculate quartz crystallization temperatures for each individual unit found at Lake City (Figure 15).
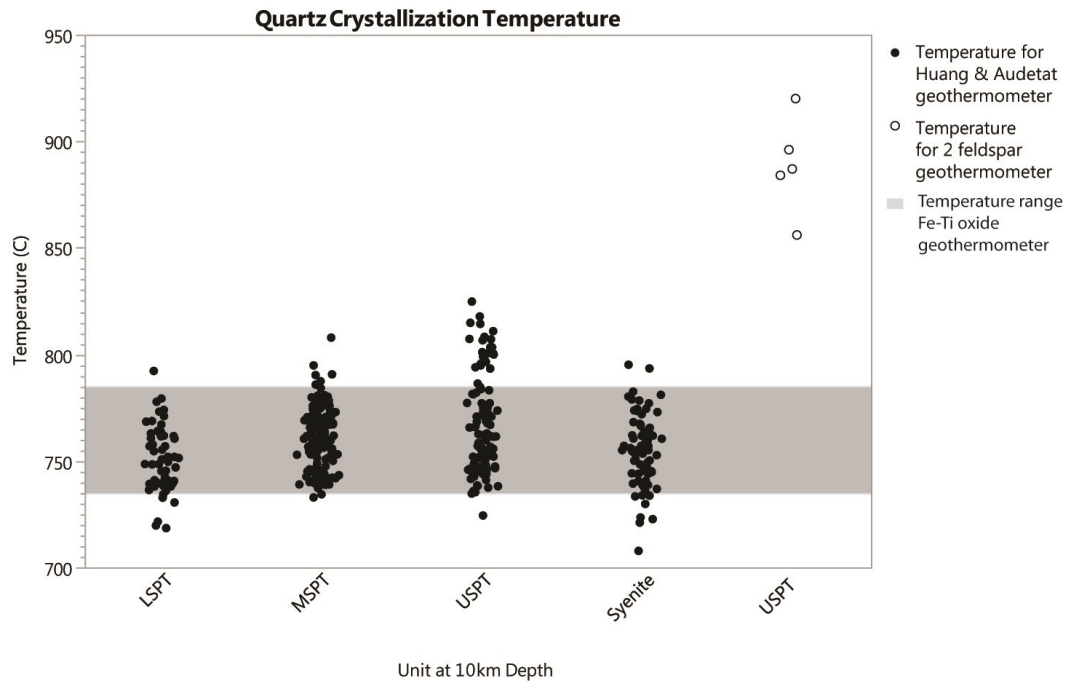
Figure 15: Quartz crystallization temperatures for all units at Lake City caldera using the Huang and Audetat (2012) equation. Temperatures are compared to Putirka (2008) two feldspar as well as Ghiorso and Evans (2008) Fe-Ti oxide geothermometer temperatures. 10km depth was used as it most accurately matched Fe-Ti oxide and two feldspar geothermometry. Temperature range for Fe-Ti geothermometry was calculated by adding ±25°C error.

5) Discussion

Mechanisms for how rhyolite magmas behave in the subsurface, are formed, and transported are varied among two distinct models: 1) Rhyolites are formed by the partial melting of the lower crust (gabbroic in composition), transported tens of kilometers to the surface, where their ascent pauses briefly (days to weeks), and then are subsequently erupted (e.g. Ratajeski et al., 2005). 2) Rhyolites are formed by extraction of interstitial melt in equilibrium with an intermediate reservoir located in the shallow crust, which requires a related complementary silicic cumulate to be trapped in the subsurface (Bachmann and Bergantz, 2004; Deering and Bachmann, 2010). The models of Bachman and Bergantz (2004) and Deering and Bachmann (2010) are tested here by integrating quantitative textural analyses, thermodynamic modeling, and geochemistry.

5.1 Origin of Sunshine Peak rhyolite

Bachmann and Bergantz (2004) suggested a mechanism for the formation of crystal-poor rhyolites within the upper crust by extraction from an intermediate mush. Hindered settling was invoked as the physical mechanism of crystal-liquid separation because it adjusts Stoke's settling law by taking into account the crystal fraction in a magma body. Druitt & Bacon (1989), Bachmann et al. (2002), Schmitt et al. (2003), for example, have shown that around crystallinities of 35-45vol.%, intermediate bodies of magma have evolved enough by crystallization processes to produce rhyolitic composition melts and, at crystallinities of 50-55vol.%, now rheologically behave as solids (Rigid Percolation Threshold, RPT; Vigneresse et al., 1996), therefore, halting convection processes within the magma chamber. It is this high degree of crystallization that allows interstitial rhyolitic composition melt to form by crystal fractionation. It has already been shown that some unzoned ignimbrites are crystal-poor erupted equivalents of silicic plutons located deeper in the subsurface (Cashman & Blundy, 2000; Bachmann et al., 2002; Schmitt et al., 2003). However, the Sunshine Peak eruption is a zoned ignimbrite that includes a range of compositions from rhyolite to trachyte. Kennedy et al. (2014) suggested that the trachyte is the erupted equivalent to the resurgent syenite intrusion within the caldera and that the rhyolite was derived from this magma. This model was further tested in this study using a combination of thermodynamic modeling to determine the conditions of crystal-liquid separation, and quantitative textural and geochemical analysis to determine the processes involved in the rhyolite formation.

5.1.1 Thermodynamic modeling

Thermodynamic modeling was completed using rhyolite-MELTS for Excel (Gualda and Ghiorso, 2015). Bulk-rock data from syenite compositions of Kennedy (2005) were used to run the models. Samples were run, not with the intention of determining the exact composition of crystallizing phases within the Lake City magmatic system, but rather to discern: 1) whether or not it was possible to derive rhyolitic composition melt by fractional crystallization of the syenite observed in the field; 2) crystallinity at which the melt became rhyolite in composition; 3) the enthalpy,

temperature, thermal buffering relationship across the crystallization history of the Lake City magmatic system. All runs were done at one degree temperature intervals and were isobaric.

Syenite crystallization simulations shown were run using sample 1Tsyd. This sample was representative of all syenite compositions. The minute differences in composition observed throughout the Lake City syenite showed invariant MELTS results across all conditions tested and, therefore, only this sample is shown in the results. Simulations run were for varying pressures (1, 1.5, and 2 kbar), varying water contents (4, 5, 6, 7 wt. %) for each pressure, and from ~0-100% crystallinity. Starting at exactly 100% melt and ending at exactly 100% crystallinity was not of major concern, as the important interval of crystallinity surveyed for these simulations was between 40% and 70% when the melt was rhyolitic in composition and the mechanical state of the system was optimal for melt extraction.

Across all simulations, drastic increases in crystal mass fraction occur when the magma reaches 55%-60% crystallinity (Figure 18). The melt reaches a rhyolitic composition in all simulations at ~40% crystallinity (Figure 19). These crystallinities are consistent with the 40-60% phenocrysts observed in the syenites. The only simulations that showed compositions similar to the LSPT rhyolite (75% SiO_2), however, were when the conditions were at 4% H_2O at 1 kbar, 5% H_2O at 1 kbar, 6% H_2O at 1 kbar, and 7% H_2O at 1kbar. Latent heat plotted against liquid fraction also can show when the majority of crystallization takes place. Peaks in Figure 17 show where the enthalpy of the system is controlled by latent heat of crystallization and is thermally buffered (Sliwinksi et al., 2015). The highest SiO_2 rhyolite formed directly correlates with $\Delta H/\Delta T$ peaks in Figure 17. At higher crystallinities (> 40-45%), quartz saturation is reached (Figure 18) and, therefore, the melt cannot further evolve in SiO_2; however, the system has already reached a high-silica rhyolite composition similar to the Sunshine Peak rhyolite. The results of these models indicate that the crystallization occurred across varying depths and water contents in the shallow crust (1-2kbar and 4-7% H_2O) and that the syenite/trachyte intermediate magma was in equilibrium with a rhyolite melt around 55%-60% crystallinity. These results are, therefore, consistent with the rhyolite being produced in a thermally buffered magma reservoir in the shallow crust by hindered settling. The approximate timescales for accumulation of crystals within the Lake City magma reservoir by hindered settling (Bachmann and Bergantz, 2004) can be predicted by calculating settling velocities using the following equation:

(4)

$$U_{hs} = \frac{(1-c)^2}{(1+c^{\frac{1}{3}})^{\frac{5c}{3(1-c)}}} \cdot \left(\frac{2r^2 g \Delta \rho}{9\mu}\right)$$

Where U_{hs} is settling velocity, c is crystal fraction, r is the radius of the crystal, g is acceleration due to gravity, and μ is the dynamic viscosity of the melt. Given the size of the crystals and viscosity of the melts this process would have occurred over thousands to tens of thousands of years in the Lake City magmatic system.
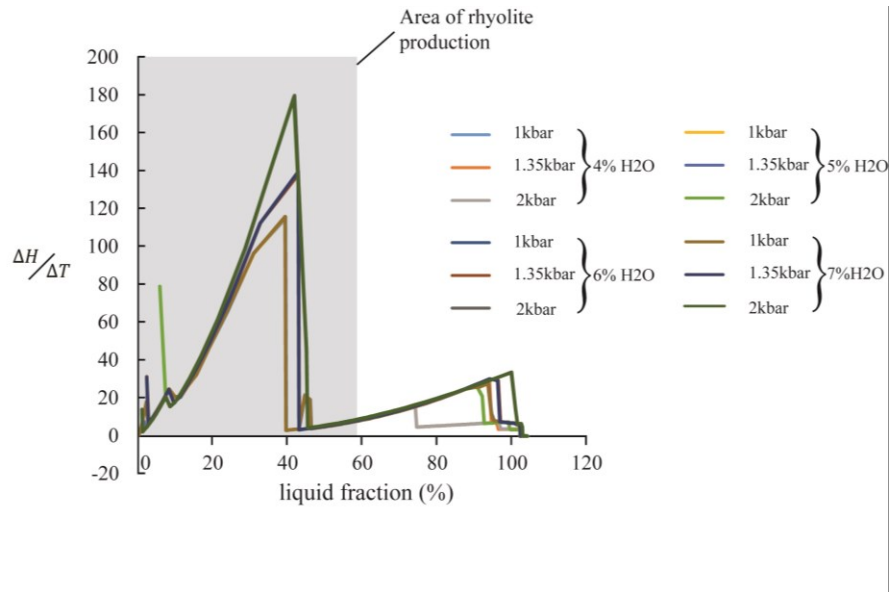
Figure 16: Latent heat vs liquid fraction profiles for syenite generated via rhyolite-MELTS. Pressures ranging from 1-2kbar at 4-7 wt% H_2O are plotted. The grey area represents the point at which the remaining liquid becomes rhyolitic in composition. Peaks in latent heat represent thermal buffering related to crystallization.
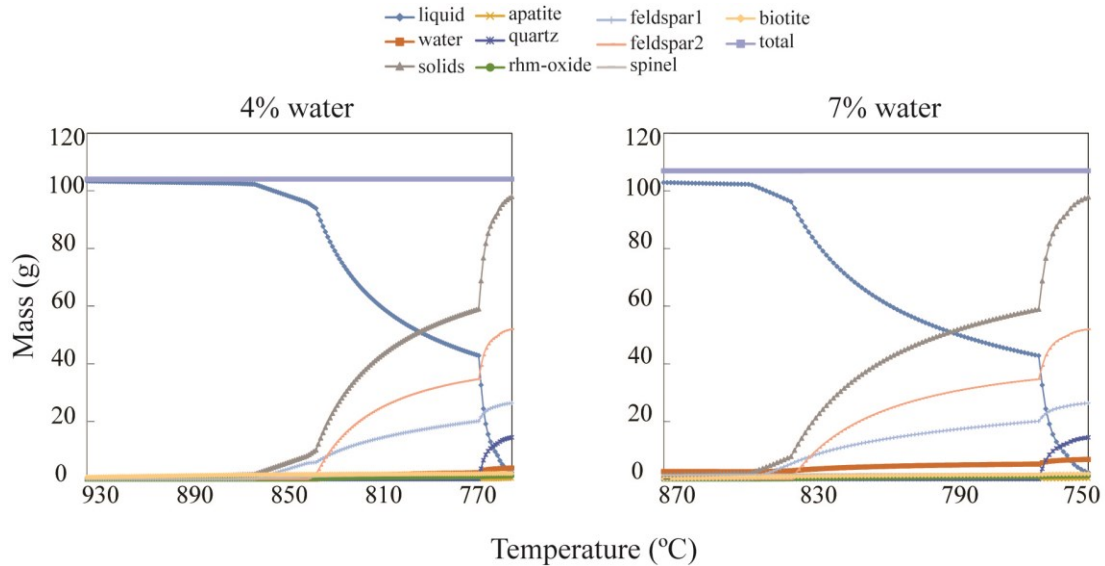
Figure 17: Examples of rhyolite-MELTS simulation runs showing mass fraction of different mineral phases across different temperatures for syenite sample 1Tsyd. Runs shown are 4% and 7% water by weight, a pressure of 1.35

kbar, and illustrate how the bulk of crystallization happens in a small temperature range. For all rhyolite MELTS data, see appendix NUMBER.

5.1.2 Geochemical evidence

Geochemical evidence also can provide insight into rhyolite formation by crystal fractionation of syenite. Figure 19 shows how, within potassium feldspar, as An decreases within samples, K increases. This is a classic example of crystal fractionation modeled after Bowen (1922). As the magma at Lake City evolves and crystallizes, Ca is preferentially incorporated into plagioclase over Na causing the An contents to decrease as incompatible K increases.
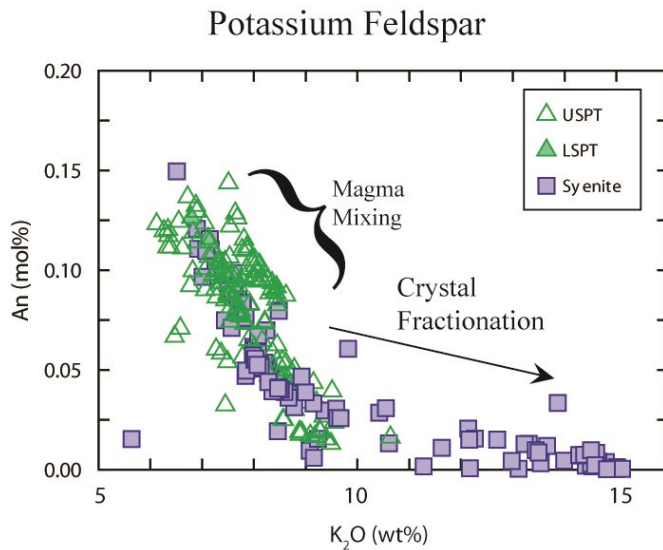
Figure 18: Figures showing fractionation and mixing trends within k-spar grains.

5.1.3 Textural evidence for syenite cumulate formation

Glomerocrysts are ubiquitous within igneous rocks from around the world. Studying them offers a unique look at the 'building blocks' of igneous fabrics observed in both plutonic and volcanic rocks (Jerram, 2003). Glomerocrysts are also ubiquitous in all plutonic and volcanic units from Lake City caldera (Figure 2 a,b,c,d). In a spatial distribution analysis of the syenite textures using CSDCorrections a numerical value, the R-value, is calculated to estimate the degree of clustering or ordering of grains within rocks by comparing fabrics observed to ordered and random distributions of spheres within 3D space (Jerram, 2003). R-value estimates for syenites range between 0.77 and 0.97, which, regardless of melt porosity, indicates clustered frameworks in the rock (Jerram, 2003) (Figure 20).
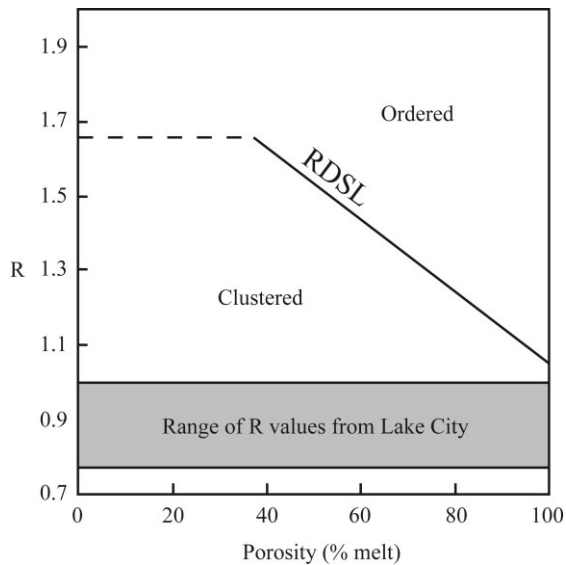
Figure 19: Plot of R value against porosity in the magma chamber modeled after Jerram (2003). Grey areas are the range of R values for Lake City rocks, while RDSL is the Random Distribution of Spheres Line.

A mechanism for the formation of glomerocrysts put forward by Schwindinger and Anderson (1989) uses synneusis (the swimming together and subsequent attachment via surface tension) of crystals in a melt rich environment. By this logic it stands to reason that, megaglomerocrysts found in the syenite, composed exclusively of potassium feldspar megacrysts, could form by similar processes in melt channels driven by textural coarsening as the magma becomes highly crystalline (>40 vol.%) rather than early on in the evolution of the magma system when it is crystal poor. This, however, is not the only proposed origin for glomerocrysts within rocks found at Lake City.

Clustering of grains can also provide evidence for melt extraction and hindered settling. As rhyolitic melt is extracted from interstitial spaces within the rheologically locked syenite, remaining crystals will start to compact and cluster together, due to pore space being much more compressible than interstitial magma. Thermal buffering of the system, as alluded to earlier, could allow a greater time for this to occur, increase extraction efficiency, and allow for a greater degree of clustering to take place (Figure 20). Crystal size distributions also show concave upwards curves, a characteristic of crystal of accumulation within a magma chamber (Higgins, 2006), and help provide evidence for the syenite being a residual cumulate (Figure 21). These concave upwards curves exhibit high populations of small grains and large grains, while showing an absence of intermediate size grains. This reflects a somewhat bimodal crystal population where large grains represent accumulated crystals in the reservoir and small populations represent late crystallizing interstitial material. The results of this textural analysis indicate that the syenite is a silicic cumulate.
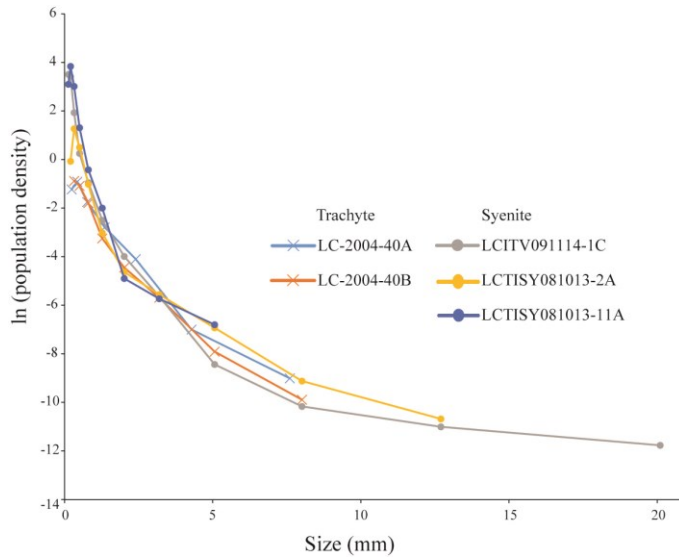
Figure 20: All CSDs generated for trachytes and syenites. All CSDs show concave upwards slopes and exhibit signs of crystal accumulation.

5.1.4 Model for rhyolite production

Figure 22 shows a proposed model, based on Bachmann and Bergantz (2004), for rhyolite production in the upper crust. Intermediate syenite magma, initially crystal poor, is in a state of convection. At this time, early formed crystals are forming glomerocrysts and crystal network chains (Figure 22a). As crystallinity increases to roughly 45%-50%, the system stops convecting and now behaves as a rheologically locked solid. The liquid is now rhyolitic in composition and starts to be extracted by mechanical processes such as hindered settling and filter pressing. The system is also thermally buffered around 40%-50% crystallinity (Figure 17), keeping the reservoir from crystallizing completely, and, therefore, allowing for a greater degree of melt extraction to take place (Figure 22b). After the majority of the interstitial melt has been extracted, a rhyolite cap is now formed near the roof of the magma reservoir (Figure 22c). Chemical zonation, driven by density differences within the magma takes place, giving the geochemical variance observed between units at the surface.

38
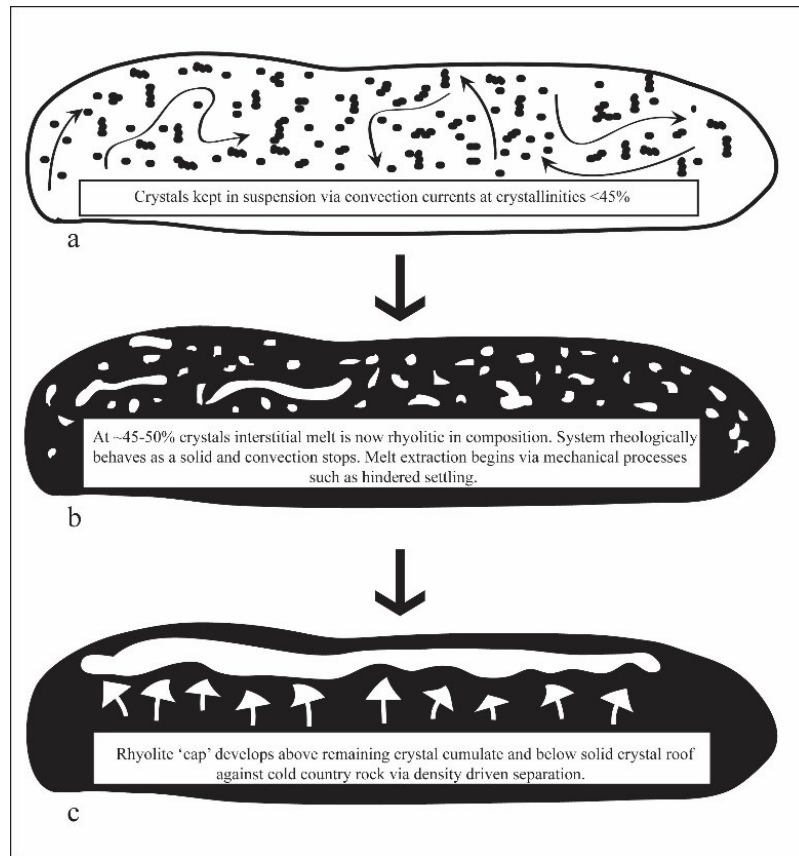
Figure 21: Cartoon modeled after Bachmann and Bergantz (2004) illustrating rhyolite cap formation as crystallinity increases in silicic magma chambers. White space represents melt, and black space represents solid crystal phases.

5.2 Plutonic-Volcanic connection

One would expect both geochemical and textural similarities between syenite and trachyte units if they are genetically related. More specifically, geochemical and textural signatures would indicate that the trachyte was formed by the re-melting, and subsequent eruption of, the newly re-melted syenite. In order for this to happen, evidence for an open-system must also be present. If they are not genetically related, the geochemistry and textural analysis will show this as well. Bulk-rock analyses from Kennedy (2005) show, however, that the syenite and trachyte are similar in composition. In addition, there is abundant evidence of open-system processes indicated by the ubiquity of mafic enclaves found in both the syenite and trachyte (e.g. Figure 3). In the section, the relationship between the resurgent syenite intrusion and trachyte is further examined.

5.2.1 Textural evidence for trachyte and syenite relationship

The comparison (size, shape, mineralogy, fabrics) of glomerocrysts between the syenite and trachyte samples is of crucial importance in determining whether or not the trachyte is derived from the syenite. Upon petrographic analysis it can be seen that the dominant glomerocryst style found in both the syenite and trachyte is polymineralic

feldspar glomerocrysts with no discernable fabric or alignment of grains within the clusters. Glomerocrysts found within the trachyte, on average, are larger in size than those found in the syenite, but this might be because these would survive textural coarsening and remobilization better than smaller grain size glomerocrysts. It should also be noted, however, that smaller grain size glomerocrysts also exist in the trachyte. Other than a slight size difference between the two units, the glomerocrysts are very similar. They are comprised of the same minerals (predominately potassium feldspar, with minor plagioclase and biotite), have no orientation or fabric to the grains, are subhedral with rounded corners on the feldspar grains, and on average 0.5-0.75mm in length. Monomineralic potassium feldspar megaglomerocrysts are most likely not related to the polymineralic glomerocrysts, due to them being formed later on by textural coarsening. These monomineralic glomerocrysts, however, are found almost exclusively within the USPT trachyte. The similarities in size, shape, mineralogy, and fabrics of the trachyte and syenite are consistent with them being genetically related.

5.2.2 Geochemical signatures as evidence for trachyte and syenite relationship

Since Frondel (1934) first put forth that using compositional variations in quartz was of little significance for paragenetic interpretations, numerous studies (e.g. Suttner and Leininger, 1972; Schrön et al., 1988; Blankengurg et al., 1934) have shown the contrary. Modern techniques allow for trace element data to be gathered from quartz grains to a high degree of accuracy and, therefore, be used in comparing quartz grains with both similar and different chemical signatures. This, combined with CL imaging, offers a unique insight into compositional zoning observed within the grain, as well as compositional changes occurring within the environment of which quartz grains are formed (Müller et al., 2003). Comparison of CL of quartz from different geologic environments yields significant differences, most of which are not visible in transmitted and polarized light (Ramseyer et al., 1988; Götze et al., 2001; Götze, 2009a). These differences are usually due to defects found within the quartz grain. Götze (2009a) has illustrated that even though the ideal structure of quartz is composed of a 3-D lattice of $[SiO_4]^{4-}$ tetrahedra, elements such as Al, Ti, Ge, Fe, P, H, Li, and Na can fill in for Si as the cation in individual tetrahedrons. For the most part, however, visible CL differences are due to compositional variances in either Al or Ti. Compositional variations of Ti in quartz can also be used to infer temperature conditions at the time of quartz formation (Wark and Watson, 2006; Thomas et al., 2010; Huang and Audetat, 2012), and for this study it was used to identify different growth zones in individual quartz grains.

Temperature estimates for Lake City quartz grains suggest that the trachyte and syenite existed under similar conditions, with the majority of temperatures generated from the Huang and Audetat (2012) geothermometer being within the same range (Figures 13 and 15). This indicates the possibility of the syenite undergoing initial crystallization, coarsening, and cooling, until it was interrupted by injection of the hotter mafic magma. Interstitial melt, previously evacuated by hindered settling (Bachmann and Bergantz, 2004) is also reheated to the point of eruption along with re-melted syenite. The small subset of analyses that are higher temperature than all of the other units could be from the bottom of the magma chamber and, therefore, exposed to

40

higher temperatures when mafic magma was first intruding into the body of syenite. Melt channels created due to textural coarsening would allow a permeable pathway for these grains and newly melted syenite liquid to be extracted without being blocked by the heavily crystalline mush that has already formed.

Quartz grains show significant geochemical overlap across all units when Ge, Li, and Al are plotted against Ti (Figure 10). Although there is a population of trachyte samples with high Ge, Li, and Al, the majority of analyses are all clustered together, also indicating the possibility of quartz from all units coming from the same place. These same overlapping trends can also be seen when An is plotted against K for potassium feldspar. These plots show an overlap between all samples at Lake City and indicate the possibility that all feldspars within the rocks found are derived from a magma body of similar composition (Figure 7). Trace element data from quartz, combined with major element data from feldspar analyses, are both consistent with the trachyte and syenite being genetically related.

5.3 Evidence for an open-system

5.3.1 Disequilibrium textures
According to MacKenzie et al. (1982) rock textures are: "geometrical relationships among component crystals of a rock and any amorphous materials that may be present". They include elements such as crystallinity, grain size, crystal shapes and morphologies, and mutual relationships between crystals present within a given rock. Although these characteristics are undoubtedly important in describing, classifying, and understanding the petrogenesis of igneous rocks, evidence for disequilibrium in textures offer a unique look at discerning potential interaction between two different bodies of magma and provide evidence for an open-system.

The source for an increase in thermal energy, and therefore, cause for the disequilibrium textures observed in the Lake City rocks, is most likely a result of the input of mafic to intermediate magma into the reservoir during pre-eruptive magmatic activity. This mafic material is found in the form of mafic enclaves. Mafic enclaves are commonly found as spheroidal blebs in the syenite ranging from two to over five centimeters in diameter. Upon further petrographic analysis, they are primarily composed of plagioclase microlites and acicular amphibole laths alluding to them being basaltic in composition. (Figure 3).

Rocks at Lake City show many characteristics of disequilibrium. Both plagioclase and potassium feldspars exhibit rounded corners (Figure 2). These are areas of highest energy on a crystal and, therefore, areas that will be preferentially subjected to the effects of an increase in temperature. In order to achieve a lower overall energy in the magmatic system, these sharp and pointed corners will dissolve and melt back (Higgins, 2006) first. This results in the appearance of rounded corners to feldspar grains. The vast majority of feldspar grains observed within all rocks from Lake City exhibit these rounded corners. The same increase in thermal energy that results in rounded corners on feldspar grains, also will dissolve small grain populations back into the melt in order to lower the overall energy of the system. This textural coarsening is

evidenced by CSDs (Figure 21) and petrography (Figure 2) in rocks at Lake City. Some potassium feldspar grains also exhibit a spongy cellular texture. These textures can form due to dissolution of grains in the silicic host magma by hotter, more mafic, magma and has been shown experimentally by Tsuchiyama and Takhashi (1983). Spongy cellular textures can also be due to rapid decompression driven dissolution in a dry, crystal bearing magma (Hibbard, 1995), however, combined with other textural information which indicates thermal driven dissolution, this mechanism for spongy cellular potassium feldspar seems unlikely.

Quartz crystals also exhibit signs of disequilibrium. Quartz grains are heavily embayed, with the majority of these embayments cutting across internal zoning (Figure 6). Embayments that cross-cut zoning are generally agreed to be from dissolution (e.g. Judd, 1883; Bain, 1925). A probable mechanism for this is shown by the work of Donaldson and Henderson (1988), whereby volatile bubbles at the coring front of the embayment provide a site to transport solutes to the surrounding melt. Volatiles would almost certainly be present within the Lake City syenite, as the presence of hydrous phases such as amphibole (within the mafic enclaves) and biotite (within the syenite) indicate that water saturation has occurred.

5.3.1 Crystal size distributions

Understanding the relationship between naturally observed textures, experimental data, and their petrogenesis in comagmatic igneous rocks has long been a topic of debate in the geologic community (Marsh, 1998). It is no secret that rock textures observed in the field can be created by experimentation, dating back to those of James Hall (1805). Since that time detailed kinetic models have been created, however, they are restrictive with regards to magma chamber conditions at the time of crystal formation (e.g. Dowty, 1980; Kirkpatrick, 1983; Brandeis et al., 1984; Hort and Spohn, 1991a). Crystal size distributions (CSDs) offer a quantitative procedure for describing crystallinity as a function of size and of creating a model of crystal nucleation and growth in magmatic systems (Marsh, 1988).

Much work has been done since Marsh (1988) first tried to use crystal size distributions in the explanation and modeling of crystallization processes in magmatic systems (e.g Higgins, 1991, 1995, 1999; Jerram 2003; Marsh 1998; Spillar, 2014). Various shaped CSD curves, slopes, y-intercepts, and kinks have now been interpreted as distinct igneous rock forming processes (Higgins, 2006). Samples from Lake City caldera, with their concave upwards, and sometimes kinked, CSDs can be similarly interpreted. Higgins (1998) invoked the process of textural coarsening as a mechanism for explaining the disappearance of small grain size populations in anorthositic rocks, and the same can be seen in the rocks from Lake City caldera when transitioning from syenites to trachytes (Figure 21). Textural coarsening in open-systems based off of Higgins (2006) and the work of DeHoff (1991) is portrayed as a flattening of slope (Figure 22b) and illustrates the dissolution of small grain populations back into magma. The disappearance of these small grain populations allows for flow channels to be formed within the magma and provides a location for megacryst formation (Figure 22a). When compared to actual data from Lake City, it can be seen that Lake City exhibits signs of textural coarsening (Figure 23).
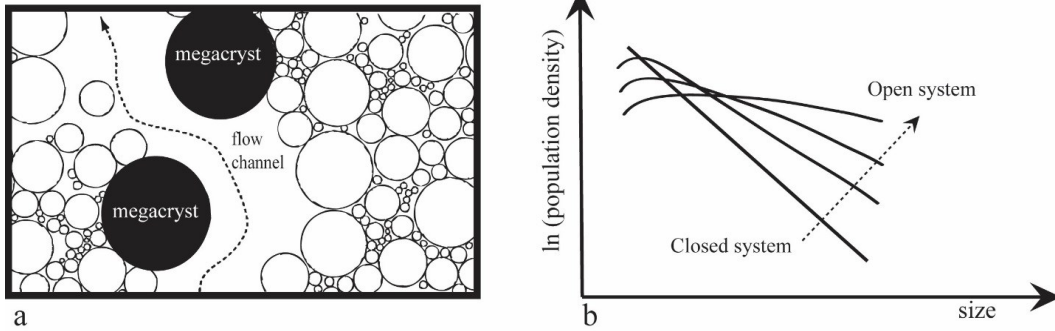
Figure 22: a) Figure modeled after Higgins (2006) illustrating how textural coarsening creates megacrysts within a magma chamber. b) Figure modeled after Higgins (2006) showing how CSDs look in both open and closed systems from rocks that have been texturally coarsened.
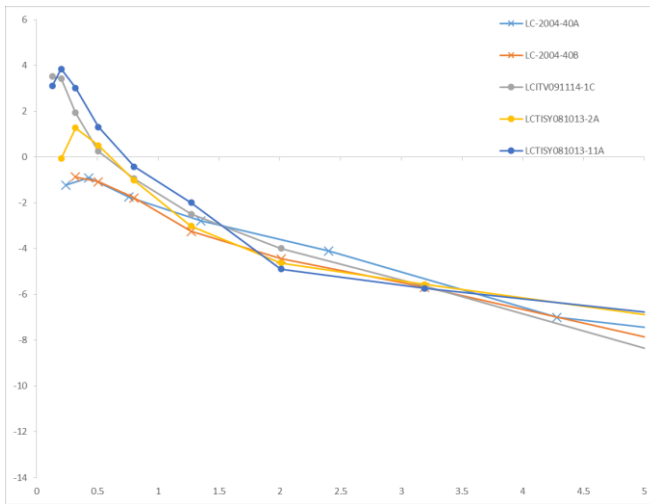
Figure 23: Figure showing the left-hand portion of all CSDs generated for Lake City Caldera in order to emphasize the disappearance of small grain size populations in all samples: a classic signature of textural coarsening. This, combined with the similar appearance to Higgins (2006) open-system CSD illustrations, is consistent with the trachyte having formed in an open, rather than closed system.

Megacrysts are ubiquitous within syenites from Lake City and often times occur in clusters (Figure 2d). Crystal size distributions for rocks at Lake City caldera show a shallowing of slope as well as a disappearance of small grain size populations from syenite to trachyte (Figure 5a,b,c to 5d,e, 23). Small grain populations in low abundance relative to megacryst and glomerocryst populations in Lake City trachytes suggests that textural coarsening occurred. Due to trachytes sampled being composed primarily of larger phenocrysts and megacrysts, it is likely that input of mafic material was able to move beyond melt channel formation and succeed in significant re-melting of the syenite in the areas that are closer in proximity to mafic injections.

Syenite CSDs, as well as being concave upwards, are also sometimes kinked (Figure 5). Spillar (2014) suggested that heterogeneous nucleation was the mechanism that led to the formation of kinked CSDs. In contrast, Marsh (1998) uses kinked, concave upwards CSDs to represent a sequence of two nucleation events, and, therefore, a mixing of two grain size populations. Although heterogeneous nucleation almost certainly took place within the magma at Lake City caldera, as it is

43

thermodynamically much easier to grow crystals this way, the presence of mafic enclaves suggests two separate nucleation events occurring within the rocks also being extremely probable. Mafic magma would interrupt initial crystallization within the syenite by the melting back of small crystal populations, subsequently forming megacrysts. Higgins (1999) shows that a crystal mush coarsening in an open-system will increase permeability by the dissolution of small grains, lead to focusing in fluid flow in the areas of dissolution, and preferentially grow megacrysts in these areas, effectively creating a positive feedback loop. It is also highly probable, that both heterogeneous nucleation and a combination of two separate crystal populations is responsible for the kinked CSDs observed in syenites.

Potassium feldspar grains from the trachyte exhibit more linear, negative, sloped CSDs than the syenites and they have a slight downwards concavity to them in the small grain size bins. These shapes reflect a higher ratio of large grain size populations to small populations. This is indicative of dissolution of small grains to the extreme extent where only larger grains and megacrysts are left within the melt, and the subsequent eruption of this newly 'syenite derived' magma preserves these crystal size distributions. The presence of large megacrysts within these samples is likely due to them being areas of lower energy in the system. Melting in igneous systems always begins at the eutectic point, and as such megaglomerocrysts (glomerocrysts comprised of mostly megacrysts) would be exempt from being melted back as they are comprised only of potassium feldspar and, therefore, refractory. As temperature continues to increase melt channels are formed and grown to the point where they eventually disappear as focused fluid flow is replaced by convection when crystallinity drops to a low enough fraction. At this point there is enough syenite melt to form the volume of trachyte observed at the surface. Bachmann and Bergantz (2004) show that silicic magma bodies on the order of 10^3-10^4 km^3 only need ~10% melt extraction to produce the volumes of volcanics derived from them. Similar logic can be used here to produce the amount of trachyte observed.

5.3.3 Barium zonation in potassium feldspar

Barium distribution throughout potassium feldspars offers another way to examine the process of melting of syenite in order to form the trachyte (Bachmann et al., 2014). Potassium feldspar grains from the syenite show little to no variation in the amount of Ba from core to rim and average around 1,000-3,000 ppm (Figure 8). Using the highest possible partition coefficient (~20; e.g., Nash and Crecraft, 1985), this would yield Ba concentrations in the melt of 50-150 ppm. Conversely, trachyte potassium feldspar grains show reverse zoning (high Ba rims). These rims contain between 6,000 and 16,000 ppm (Figure 8), whereas cores are similar in composition to the syenite. Using the same partition coefficients, melt composition can be estimated at 300-800 ppm at the time trachyte feldspar core formation. Higher Ba concentrations are most likely due to mass transfer from the mafic magma to the syenite mush. Enclaves observed in hand sample and thin section have diffuse boundaries, making mass transfer extremely probable (Figure 3). Evidence for mass transfer from mafic injection also comes in the form of high Ti rims on quartz grains (Figure 6a). It is no surprise that mafic magma has higher Ti concentrations than more evolved, silicic

magma, and pending the amount of mafic magma injected, could significantly increase the composition of Ti in areas of the newly re-melted syenite that are close in proximity to mafic injection sites. This would explain why only syenite hosted quartz grains have these high Ti rims, and not trachyte hosted quartz grains, as mafic material most likely never came within direct contact with the bulk of trachyte erupted. It is also probable that high Ba rims on potassium feldspar grains are a combination of both slow Ba diffusion and mass transfer from mafic injections into the magma chamber. Rims on potassium feldspar grains, however, along with having high Ba concentrations, also have higher An content than cores of grains and exhibit reverse zoning. This suggests an input of new mafic material being mainly responsible for high Ba concentration and provides further evidence for an open-system. Another explanation for high Ba rims could also be that Ba was locally enriched by dissolution of potassium feldspar and later enriched in the feldspars as the system began to crystallize again (Bachmann et al. 2014).

5.3.4 Mechanism for trachyte production

Figure 24 illustrates a proposed mechanism for trachyte petrogenesis by the re-melting of a syenite cumulate. After the majority of crystal/melt separation takes place to form the LSPT and MSPT rhyolite, resurgent mafic magma is injected into the reservoir. This mafic material increases the thermal energy and temperature of the syenite cumulate, causing textural coarsening to take place in localized areas near mafic input. Resurgent mafic activity most likely is episodic, and textural coarsening advanced to the point where melt channels graded into areas that are melt-rich, similar to Figure 22a. Episodic mafic activity could also help explain why some of the megacrysts found in the syenite are larger than the megacrysts found in the trachyte, as they were most likely exposed to more textural coarsening events post trachyte eruption. Similar to Figure 22c, a trachyte cap formed in the syenite. Melt channels formed by textural coarsening would provide fluid pathways for trachyte liquid to reach the top of the reservoir and accumulate there until enough of an overpressure was created by mafic injections to cause eruption.
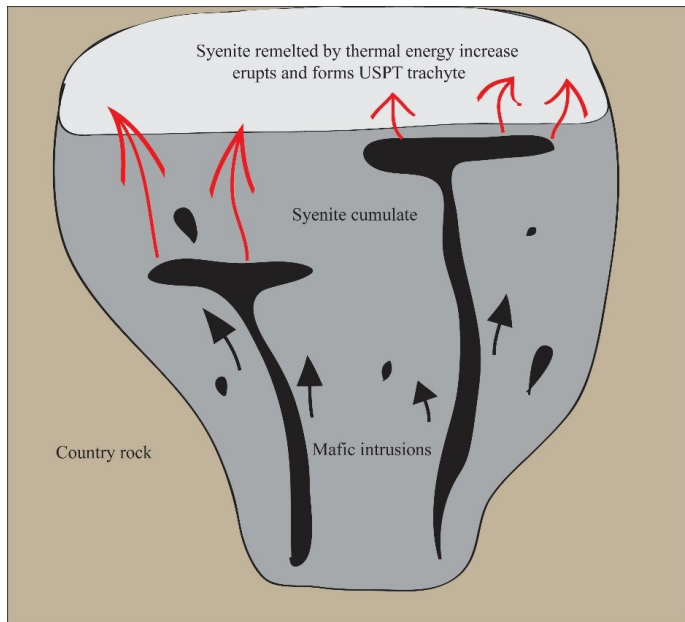
Figure 24: Cartoon illustrating trachyte petrogenesis via the re-melting of a syenite cumulate. Black arrows indicate the travel direction of mafic intrusions, while red arrows represent vast amounts of thermal energy they supply to the surrounding syenite cumulate.

6) Conclusions

1)   Rhyolites found at Lake City caldera (LSPT, MSPT) were generated by fractional crystallization of a syenitic magma body (now observed as a syenite pluton). Rhyolite-MELTS modeling shows that the rhyolite was produced at ~40% crystallinity. At this point the system became thermally buffered by latent heat of crystallization, rhyolite melt was extracted by hindered settling, and later erupted.

2)   Trachyte (USPT) was formed by the re-melting of a crystalline-mush syenite magma reservoir. Textural data provides evidence for this re-melting in the form of the presence of mafic enclaves within the syenite and disequilibrium textures in both the syenite and trachyte. Geochemical similarities (both major and trace elements) between the two are also consistent with the two being genetically related.

3)   The cause of both re-melting of syenite to form the USPT and eruption of all units at Lake City is injection of mafic magma to the syenite magma chamber. Evidence for this lies in the presence of mafic enclaves found in the syenite, mass transfer between mafic enclaves and syenite shown by geochemical data, and disequilibrium textures observed in feldspars by petrographic analysis and quartz by cathodoluminescence (CL) imaging.

7) References

- Bachmann, O., & Bergantz, G. W. (2004). On the origin of crystal-poor rhyolites: extracted from batholithic crystal mushes. Journal of Petrology, 45(8), 1565-1582.

- Bachmann, O., Deering, C. D., Lipman, P. W., & Plummer, C. (2014). Building zoned ignimbrites by recycling silicic cumulates: insight from the 1,000 km3 Carpenter Ridge Tuff, CO. Contributions to Mineralogy and Petrology, 167(6), 1-13.
- Bachmann, O., Dungan, M. A. & Lipman, P. W. (2002). The Fish Canyon magma body, San Juan volcanic field, Colorado: rejuvena- tion and eruption of an upper crustal batholith. Journal of Petrology 43, 1469–1503.
- Bacon, C.R. (1983). Eruptive history of Mount Mazama and Crater Lake Caldera, Cascade Range, USA: Journal of Volcanology and Geothermal Research, 18, 57-115.
- Bain, G. W. (1925). Skeleton quartz crystals. Am. Min, 10, 435.
- Blankenburg, H., Götze, J., Schulz, J. (1994). Quarzrohstoffe. Deutscher Verlag für Grundstoffindustrie, Leipzig Stuttgart, 296
- Bove, D.J., Hon, K., Budding, K.E., Slack, J.F., Snee, L.W. and Yeoman, R.A. (2001). Geochronology and geology of late Oligocene through Miocene volcanism and mineralization in the western San Juan Mountains, Colorado: U. S. Geological Survey Professional Paper, Report: 1642.
- Bowen, N. L. (1922). The reaction principle in petrogenesis. The Journal of Geology, 30(3), 177-198.
- Brandeis, G., Jaupart, C., & Allègre, C. J. (1984). Nucleation, crystal growth and the thermal regime of cooling magmas. Journal of Geophysical Research: Solid Earth, 89 (B12), 10161-10177.
- Branney, M.J., Kokelaar, P. (2002). Pyroclastic density currents and the sedimentation of ignimbrites: Geological Society London Memoir 27, 143.
- Breiter, K., Svojtka, M., Ackerman, L., Svecova, K. (2012). Trace element composition of quartz from the Variscan Altenberg-Teplice caldera (Krusne hory/Erzgebirge Mts, Czech Republic/Germany): Insights into the volcano-plutonic complex evolution, Chemical Geology, 326-327, 36-50.
- Brown S.J.A, Wilson C.J.N., Cole J.W., Wooden J. (1998). The Whakamaru group ignimbrites, Taupo Volcanic Zone, New Zealand: evidence for reverse tapping of a zoned silicic magmatic system: Journal of Volcanology and Geothermal Research, 84, 1-37.
- Cashman, K. & Blundy, J. (2000). Degassing and crystallization of ascending andesite and dacite. Philosophical Transactions of the Royal Society of London 358, 1487–1513.
- DeHoff, R.T. (1991). A geometrically general theory of diffusion controlled coarsening. Acta Metallurgica et Materialia, 39(10), 2349-2360.
- Dowty, E. (1980). Crystal growth and nucleation theory and the numerical simulation of igneous crystallization. Physics of magmatic processes. Princeton University Press, Princeton, 419-485.

o Druitt, T. H. & Bacon, C. R. (1989). Petrology of the zoned calcalkaline magma chamber of Mount Mazama, Crater Lake, Oregon. Contributions to Mineralogy and Petrology 101, 245–259.

o Eichelberger, J.C., Chertkoff, D.G., Dreher, S.T. and Nye C.J. (2000). Magmas in collision; rethinking chemical zonation in silicic magmas: Geology, 28, 603-606.

o Elkins, L., Grove, T. (1990). Ternary feldspar experiments and thermodynamic models. American Mineralogist, 75 (5-6), 544-559.

o Frondel, C. (1934), Origin of the segmental coloration of amethyst and smoky quartz. Am Mus Novitates 758: 1–15

o Ghiorso, M., Evans, B. (2008). Thermodynamics of rhombohedral oxide solid solutions and a revision of the Fe-Ti two-oxide geothermometer and oxygen-barometer. American Journal of Science, 308(9), 957-1039.

o Gualda G.A.R., Ghiorso M.S. (2015) MELTS_Excel: A Microsoft Excel-based MELTS interface for research and teaching of magma properties and evolution. Geochemistry, Geophysics, Geosystems 16(1), 315-324

o Glazner, A. F., Coleman, D. S., & Bartley, J. M. (2008). The tenuous connection between high-silica rhyolites and granodiorite plutons. Geology, 36(2), 183-186.

o Götze J., Plötze M., Habermann D. (2001). Origin, spectral characteristics and practical applications of the cathodoluminescence (CL) of quartz: a review. Mineral Petrol 71: 225–250

o Götze, J. (2009). Chemistry, textures and physical properties of quartz-geological interpretation and technical application. Mineralogical Magazine,73(4), 645-671.

o Götze, J. (2012). Application of cathodoluminescence microscopy and spectroscopy in geosciences. Microscopy and Microanalysis, 18(06), 1270-1284.

o Götze, J., Plötze, M., & Habermann, D. (2001). Origin, spectral characteristics and practical applications of the cathodoluminescence (CL) of quartz–a review. Mineralogy and petrology, 71(3-4), 225-250.

o Guillong, M., Meier, D. L., Allan, M. M., Heinrich, C. A., & Yardley, B. W. (2008). Appendix A6: SILLS: a MatLab-based program for the reduction of Laser Ablation ICP-MS data of homogeneous materials and inclusions.Mineralogical Association of Canada Short Course, 40, 328-333.

o Hall, J. (1805). III. Experiments on Whinstone and Lava. Transactions of the Royal Society of Edinburgh, 5(01), 43-75.

o Hibbard, M. J. (1995). Petrography to petrogenesis (No. 552.2 HIB).

o Higgins, M. D. (1991). The origin of laminated and massive anorthosite, Sept Iles layered intrusion, Quebec, Canada. Contributions to Mineralogy and Petrology, 106(3), 340-354.

o Higgins, M. D. (1998). Origin of anorthosite by textural coarsening: quantitative measurements of a natural sequence of textural development.Journal of Petrology, 39(7), 1307-1323.

o Higgins, M. D. (1999). Origin of megacrysts in granitoids by textural coarsening: a crystal size distribution (CSD) study of microcline in the Cathedral Peak Granodiorite, Sierra Nevada, California. Geological Society, London, Special Publications, 168(1), 207-219.

o Higgins, M. D. (2006). Quantitative textural measurements in igneous and metamorphic petrology. Cambridge University Press.

o Hildreth, E.W. (1979). The Bishop Tuff: evidence for the origin of compositional zonation in silicic magma chambers In: Chapin, C.E., and Elston, W.E. (eds.) Ash-Flow Tuffs: Geological Society of America Special Paper, 180, 43-72.

o Hildreth, E.W. (1981). Gradients in silicic magma chambers: Implications for lithospheric magmatism: Journal of Geophysical Research, 86, 10153-10192

o Hildreth, W., Wilson, C.J.N. (2007). Compositional zoning of the Bishop Tuff: Journal of Petrology, 48, 951-999.

o Hon, K. and Mehnert, H.H. (1983). Compilation of revised ages of volcanic units in the San Juan Mountains, Colorado: Recalculated K-Ar age determinations using IUGS constants. U.S. Geol. Surv., Open-File Rep., 83-668, 1-14.

o Hon, K., and Lipman, P.W. (1989). Western San Juan caldera complex: In: Lipman, P.W. (ed.) Oligocene-Miocene San Juan volcanic field, Colorado. New Mexico Bureau of Mines and Mineral Resources Memoir, 46, 350-380.

o Hon, K.A. (1987). Geologic and petrologic evolution of the Lake City Caldera, San Juan Mountains, Colorado. PhD Thesis, University of Colorado.

o Hort, M., & Spohn, T. (1991). Crystallization calculations for a binary melt cooling at constant rates of heat removal: implications for the crystallization of magma bodies. Earth and planetary science letters, 107(3), 463-474.

o Huang, R., Audétat, A. (2012). The titanium-in-quartz (TitaniQ) thermobarometer: A critical examination and re-calibration, Geochimica et Cosmochimica Acta, 84, 75-89, ISSN 0016-7037, http://dx.doi.org/10.1016/j.gca.2012.01.009.

o Jerram, D. A., Cheadle, M. J., & Philpotts, A. R. (2003). Quantifying the building blocks of igneous rocks: are clustered crystal frameworks the foundation?. Journal of Petrology, 44(11), 2033-2051.

o Jochum, K. P., Weis, U., Stoll, B., Kuzmin, D., Yang, Q., Raczek, I., Günther, D. (2011). Determination of reference values for NIST SRM 610–617 glasses following ISO guidelines. Geostandards and Geoanalytical Research, 35(4), 397-429.

o Judd, J. W., & Cole, G. A. (1883). On the basalt-glass (tachylyte) of the Western Isles of Scotland. Quarterly Journal of the Geological Society, 39(1-4), 444-465.

o Kennedy, B. (2005). Magmatic Processes Associated With the Development of Large Silicic Calderas, PhD Thesis, McGill University.

o Kennedy, B., Stix, J., Hon, K., Deering, C., & Gelman, S. (2015). Magma storage, differentiation, and interaction at Lake City caldera, Colorado, USA. Geological Society of America Bulletin, B31305-1.

o Kennedy, B.M., and Stix, J. (2007). Magmatic processes associated with caldera collapse at Ossipee ring dyke, New Hampshire: Geological Society of America Bulletin, 119, 1-2, 3-17.

o Kirkpatrick, R. J. (1981). Kinetics of crystallization of igneous rocks. Rev. Mineral; (United States), 8.

o Liebske, C. (2015). iSpectra: An Open Source Toolbox for The Analysis of Spectral Images Recorded on Scanning Electron Microscopes. Microscopy and Microanlysis, 21, 1006, doi: 10.1017/S1431927615014336

- Lipman, P.W., Doe, B.R, Hedge, C.E., and Steven, T.A. (1978). Petrologic evolution of the San Juan vo1canic field, southwestern Colorado: Pb and Sr isotope Geological Society of America Bulletin, 89; 59-82.
- Lipman, P.W., Dungan, M.A. and Bachmann, O. (1997). Comagmatic granophyric granite in the Fish Canyon Tuff, Colorado; implications for magma-chamber processes during a large ash-flow eruption: Geology, 25, 915-918.
- Lipman, P.W., Steven, T.A., Luedke, R.G. and Burbank, W.S. (1973). Revised volcanic history of the San Juan, Uncompahgre, Silverton, and Lake City calderas in the western San Juan Mountains, Colorado. U.S. Geol. Surv., J. Res., 1, 627--642.
- Luedke, R. G., & Burbank, W. S. (1968). Volcanism and cauldron development in the western San Juan Mountains, Colorado. Cenozoic volcanism in the southern Rocky Mountains, RC Epis, ed., Colo. Sch. Mines Quart, 68, 175-208.
- MacKenzie, W. S., Donaldson, C. H., & Guilford, C. (1982). Atlas of igneous rocks and their textures. Longman.
- Marsh, B. D. (1988). Crystal size distribution (CSD) in rocks and the kinetics and dynamics of crystallization. Contributions to Mineralogy and Petrology, 99(3), 277-291.
- Marsh, B. D. (1998). On the interpretation of crystal size distributions in magmatic systems. Journal of Petrology, 39(4), 553-599.
- Mehnert, H.H., Lipman, P.W. and Steven, T.A. (1973). Age of the Lake City caldera and related Sunshine Peak Tuff, western San Juan Mountains, Colorado. Isochron/West, 6: 31--33.
- Mills, J.G., Jr., Saltoun, W.S., and Vogel T.A. (1997). Magma batches in the Timber Mountain magmatic system, Southwestern Nevada Volcanic Field, Nevada, USA: Journal of Volcanology and Geothermal Research, 78, 185-288.
- Müller, A., René, M., Behr, H. J., & Kronz, A. (2003). Trace elements and cathodoluminescence of igneous quartz in topaz granites from the Hub Stock (Slavkovský Les Mts., Czech Republic). Mineralogy and Petrology, 79(3-4), 167-191.
- Müller, A., van den Kerkhof, A.M., Behr, H.-J., Kronz, A., Koch-Müller, M. (2010). The evolution of late-Hercynian granites and rhyolites documented by quartz — a review. Earth and Environmental Science Transactions of the Royal Society of Edinburgh, 100, 185–204.
- Nash, W.P., Crecraft, H.R. (1985). Partition coefficients for trace elementsin silicic magmas. Geochim Cosmochim Acta 49:2309–2322
- Pagel, M., Barbin, V., Blanc, P., Ohnenstetter, D. (2000). Cathodoluminescence in geosciences. Springer, Berlin Heidelberg New York Tokyo, 514
- Perny, B., Eberhardt, P., Ramseyer, K., Mullis, J., Pankrath, R. (1992). Microdistribution of aluminium, lithium and sodium in a quartz: possible causes and correlation with shored lived cathodoluminescence. Am Mineral 77: 534–544
- Putirka, K., (2008) Thermometers and barometers for volcanic systems. Reviews in Mineralogy and Geochemistry, 69 (1), 61-120.
- Ramseyer, K., Baumann, J., Matter, A., & Mullis, J. (1988). Cathodoluminescence colours of alpha-quartz. Mineralogical Magazine, 52(368), 669-677.
- Ratajeski, K., Sisson, T. W., & Glazner, A. F. (2005). Experimental and geochemical evidence for derivation of the El Capitan Granite, California, by partial melting of

hydrous gabbroic lower crust. Contributions to Mineralogy and Petrology, 149(6), 713-734.

o Ruebi, O. and Nicholls, I., A. (2005). Structure and Dynamics of a Silicic Magmatic System Associated with Caldera-Forming Eruptions at Batur Volcanic Field, Bali, Indonesia: Journal of Petrology, 46, 1367-1391.

o Schmitt, A. K., Lindsay, J. M., de Silva, S. & Trumbull, R. B. (2003). U–Pb zircon chronostratigraphy of early-Pliocene ignimbrites from La Pacana, north Chile: implications for the formation of stratified magma chambers. Journal of Volcanology and Geothermal Research 120, 43–53.

o Schrön, W., Schmädicke, E., Thomas, R., Schmidt, W. (1988). Geochemische Untersuchungen an Pegmatitquarzen. Z geol Wissensch 16: 229–244

o Schwindinger, K. R., & Anderson Jr, A. T. (1989). Synneusis of Kilauea Iki olivines. Contributions to Mineralogy and Petrology, 103(2), 187-198.

o Sliwinski, J. T., Bachmann, O., Ellis, B. S., Dávila-Harris, P., Nelson, B. K., & Dufek, J. (2015). Eruption of Shallow Crystal Cumulates during Explosive Phonolitic Eruptions on Tenerife, Canary Islands. Journal of Petrology, egv068.

o Smith V., Shane, P. and Nairn., I (2005). Trends in rhyolite geochemistry, mineralogy, and magma storage during the last 50 kyr at Okataina and Taupo volcanic centres, Taupo Volcanic Zone, New Zealand: Journal of Volcanology and Geothermal Research, 148, 372-406.

o Špillar, V., & Dolejš, D. (2014). Kinetic model of nucleation and growth in silicate melts: implications for igneous textures and their quantitative description. Geochimica et Cosmochimica Acta, 131, 164-183.

o Sprunt, E. (1981). Causes of quartz cathodoluminescence colours. Scan Electron Micr 1981: 525–535

o Steven, T.A., Lipman, P.W. (1976). Calderas of the San Juan volcanic field, southwestern Colorado. U.S: Geological Survey Professional Paper, Report P 0958.

o Stevens-Kalceff, MAS, Phillips, M.R (1995). Cathodoluminescence microcharacterisation of the defect structure of quartz. Phys Rev B 52, 3122–3134

o Suttner, L.J., Leininger, R.K. (1972). Comparison of the trace element content of plutonic, volcanic, and metamorphic quartz from southwestern Montana. Geol Soc Am Bull 83, 1855–1862

o Thomas J. B., Watson E. B., Spear F. S., Shemella P. T., Nayak S.K. and Lanzirotti A. (2010). TitaniQ under pressure: the effect of pressure and temperature on the solubility of Ti in quartz. Contrib. Mineral. Petrol. 160, 743–759.

o Tsuchiyama, A., & Takahashi, E. (1983). Melting kinetics of a plagioclase feldspar. Contributions to Mineralogy and Petrology, 84(4), 345-354.

o Tweto, O., & Sims, P. K. (1963). Precambrian ancestry of the Colorado mineral belt. Geological Society of America Bulletin, 74(8), 991-1014.

o Vigneresse, J.-L., Barbey, P. & Cuney, M. (1996). Rheological transitions during partial melting and crystallization with application to felsic magma segregation and transfer. Journal of Petrology 37, 1579–1600.

o Wark, D. A., Watson, E. B. (2006). TitaniQ: a titanium-in-quartz geothermometer. Contrib. Mineral. Petrol. 152, 743–754.

o   Warner, L. A. (1978). The Colorado lineament: a middle Precambrian wrench fault system. Geological Society of America Bulletin, 89(2), 161-171.

o   Waychunas, G.A. (1988). Luminescence, X-ray emission and new spectroscopies. In: Hawthrone FC (ed) Spectroscopic methods in mineralogy and geology. Rev Mineral 18, 639–698

o   Zhang, Y., Cherniak, D.J. (2010). Diffusion in minerals and melts: theoretical background. In: Zhang Y, Cherniak DJ (eds) Diffusion in minerals and melts. Rev Mineral Geochem 72:5–60

o   Zieg, M. J., & Marsh, B. D. (2002). Crystal size distributions and scaling laws in the quantification of igneous textures. Journal of Petrology, 43(1), 85-101.

Appendix 1: Crystal Size Distribution Walkthrough

Methodology created and used by referring and adding to the work of Michael D Higgins.

Equipment Needed

- Petrographic Microscope
- Camera attached to microscope and computer
- Windows computer capable of running programs listed below

Programs Used

- ImageJ
    - MosaicJ (plug-in)
        - http://bigwww.epfl.ch/thevenaz/mosaicj/
    - TurboReg (plug-in)
        - http://bigwww.epfl.ch/thevenaz/turboreg/
- Q-Capture Pro 7 or equivalent image taking software
- CSD Corrections 1.51
    - http://www.uqac.ca/mhiggins/csdcorrections.html
- Adobe Illustrator

Digitizing Image

1. Turn Computer, microscope and camera on
2. Open Q-Capture Pro 7 (Camera must be on before this happens or live feed will not register)
3. In the tool bar click on "Live Preview" button.
    a. This opens up the live feed of the microscope. You should now see exactly what you see through the eye pieces of the microscope.
4. Use the smallest power objective (preferably 2x) and take pictures of the entire thin section in a grid format making sure to overlap the images slightly
    a. The overlap will be used to automatically stitch the images together later.

To take pictures:

1. Use "Auto Exposure" on the right of the screen to get correct brightness.
    a. Only if too dark or too light. Do NOT do on every image because when compiled, the individual image colors will not match up enough.
2. Use default settings for everything else except for gamma (Υ). Set this to 2.00
3. NOTE: Focus in microscope is different than on computer screen, so account for this when taking pictures. Make the image clear on screen.
4. Take picture of area using "Capture" Button in the upper left or Ctrl+Shift+K
    a. Continue doing this in a grid like fashion (see grid below) until thin section is completed
5. Save the picture to a predetermined folder. Name the folder after your sample.

      a.   It is recommended to save pictures in groups of 5 as you progress, in case something crashes

How to label the photos:
- Start with the sample name and include the number in each photo, so stitching the photos together is organized and doesn't get mixed up.

   o Start with the corner of your sample. A standard thin section is roughly a 8x6 grid, so you should end up with 48 photomicrographs for each thin section

Corner	+1	+2	+3	+4	+5	+6	+7
+15	+14	+13	+12	+11	+10	+9	+8
+16	+17	+18	+19	+20	+21	+22	+23
+31	+30	+29	+28	+27	+26	+25	+24
+32	+33	+34	+35	+36	+37	+38	+39
+47	+46	+45	+44	+43	+42	+41	+40

Creating a mosaic of your thin section

5. Open ImageJ
   a. Under the "Plug-ins" tab open Mosaic J
6. Go to File>Open>Image or Ctrl+O
   a. This will open the images one by one and is easier and less complicated than opening an image sequence
7. Select the first image in your thin section (Thin section name corner)
8. Once it opens in MosaicJ click on it in the bottom portion of the screen and it will be moved into your workspace. You can then click and drag it anywhere in the workspace you choose.
   a. This is how we will be stitching the photomicrographs together.
9. Continue doing this for the entire first row
   a. Since you overlapped the photomicrographs slightly when they were initially taken, use these areas of overlap (focus in on certain grains/fractures/pore spaces that match up) and overlay them as best as possible. Zoom in if you have to.
      i. It does not need to be an exact fit, as the algorithm that runs MosaicJ will use colors and shades to match things up exactly, but do the best you can to make things more accurate.
10. Once you have the entire first row manually stitched together, File>Create Mosaic. This will create a fully stitched together .TIFF file of your image.
   a. Later on you can create a duplicate as a .jpg file to reduce image size. The quality will still be good enough.
   b. Save each row in your sample folder as Row1, Row2, Row3…etc.
   c. The reason we do not stitch together all 48 images at once is, that, MosaicJ sometimes crashes, and processing 48 images takes a VERY LONG TIME, so by breaking the thin section up into rows, work can be saved, and the processing doesn't take as long.

11. Repeat steps 9 and 10 for all of your rows.
12. Once you have all of the rows fully stitched together, repeat steps 7-10 only this time use the row .TIFF files you have just created instead of the individual photomicrographs.
    a. This will produce a fully stitched together digitized thin section image. Save one copy as a .TIFF file and one as a .jpg file.
        i. Illustrator can only handle files of a certain size, so we will be using the .jpg file to outline the grains used for making a CSD.

Outlining grains using Adobe Illustrator

We need to outline as many grains as possible in order to make the CSD statistically valid. Minimum 400 grains. If doing an intrusive rock, this should not be an issue at all. It is not hard, just time consuming and tedious.
1. Open Illustrator and open Sample.jpg
2. Outline and Fill in the grains with a color that stands out against the actual photomicrograph in a separate layer than the original photomicrograph. This will give you an exportable layer of grain outlines.
    a. It is recommended to make the outline color of the grains white, so even if the grains are touching it will look like there is a very fine white boundary dividing each grain.
        i. Touching grains will give inaccurate results later on.
3. Export grain outline layer as .jpg file and save it as Outline.jpg or something along those lines.

Creating a CSD using CSDcorrections
1. Open ImageJ and open Outline.jpg
2. We need to make the image binary (black/white). To do this:
    a. Process>Binary>Make Binary
3. We also need to set the scale for the measurements of grain sizes. To do this:
    a. Analyze>Set Scale
        i. This is dependent upon the objective you were taking photomicrographs on and assigns a certain amount of pixels to a numerical distance.
            1. The easiest way to do this is probably by drawing a line along a noticeable/large grain in ImageJ and using the "Measure" function to obtain the number of pixels it is in length. Then use a ruler or some other measuring device to measure the actual length of the grain under microscope. You now have your Distance in pixels and known distance needed to create your conversion. MAKE SURE YOUR UNITS ARE CORRECT.
        ii. Make sure you check the box "Global"
4. Analyze>Set measurements
    a. Select: Area; Centroid; Fit Ellipse
    b. Set decimal places to 4
5. Analyze the image

- a. Analyze>Analyze particles
  - i. Size (pixel^2) set to: 1-Infinity
  - ii. Show box set to: Ellipses
    - 1. This will show you the ellipses created around each grain so you can double check as to whether or not it is accurately creating one ellipse for each grain. If not, the grains may be touching, which can result from an error when outlining them in the first place.
  - iii. Check the boxes: Display results, Clear results, exclude edge particles
    - 1. This will create a table of your results with the columns Area, X, Y, Major, Minor, Angle
6. We now need to make a .csd file for use in CSD Corrections. To do this:
   - a. Plugins>CSD Output
     - i. Save the file as sample_name.csd. Close Log window.
7. Open CSDCorrections 1.51 and open sample_name.csd
8. Check that the area is OK
9. Check that the Intermediate and Long parameters are OK.
   - a. You shouldn't have to do anything here
10. Estimate the roundness of your grains.
    - a. Use your best judgement for the AVERAGE roundness for grains throughout the whole sample
11. Estimate the Fabric from the rock and image
12. Press Calculate
13. You have now created a CSD and it will be displayed in a tab along the top of the CSDCorrections window.
    - a. Data tables and images can be copied to other programs (Word Processor, Draw Program, Microsoft Excel)

Appendix 2: Electron Microprobe Analyses

Feldspars

Table 6: Feldspar electron microprobe analyses

Sample	Rock Type	SiO2	TiO2	Al2O3	CaO	SrO	BaO	Na2O	K2O	Total
10B_plag1.1-line1	Syenite	63.2	0	19.5	0.0	0.02	0.23	0.33	14.4	98.1
10B_plag1.1-line10	Syenite	71.8	0	15.3	0.0	0	0.21	0.29	12.2	99.9
10B_plag1.1-line11	Syenite	66.0	0.01	19.8	0.1	0.02	0.12	6.99	5.64	99.0
10B_plag1.1-line12	Syenite	65.2	0.04	18.8	0.0	0.03	0.19	0.68	14.4	99.5
10B_plag1.1-line13	Syenite	65.8	0.04	19.2	0.4	0.03	0.12	3.57	10.4	99.7
10B_plag1.1-line14	Syenite	65.4	0.02	19.1	0.3	0.03	0.04	2.1	12.1	99.2
10B_plag1.1-line15	Syenite	64.8	0.05	19.0	0.1	0.03	0.1	1.01	14.0	99.2
10B_plag1.1-line16	Syenite	66.9	0.01	19.8	0.2	0.05	0.04	8.58	4.18	99.9
10B_plag1.1-line17	Syenite	65.3	0.03	18.9	0.0	0.01	0	0.4	15.0	99.8
10B_plag1.1-line18	Syenite	65.0	0.01	19.6	0.1	0.05	0.15	4.77	9.08	98.9
10B_plag1.1-line19	Syenite	65.1	0	18.7	0.0	0.04	0.17	0.7	14.6	99.4
10B_plag1.1-line2	Syenite	66.7	0.07	19.6	0.8	0.07	0.04	5.44	7.8	101
10B_plag1.1-line20	Syenite	63.0	0.01	19.6	0.0	0	0.24	0.32	14.5	98.2
10B_plag1.1-line3	Syenite	66.7	0.06	19.4	0.7	0.02	0.12	5.47	7.44	100
10B_plag1.1-line4	Syenite	66.9	0.03	19.5	0.6	0.01	0.18	5.13	8.07	101
10B_plag1.1-line5	Syenite	65.9	0.03	19.1	0.4	0.06	0.14	3.48	10.6	99.9
10B_plag1.1-line6	Syenite	65.8	0	19.3	0.2	0.04	0.03	4.48	9.24	99.3
10B_plag1.1-line8	Syenite	63.9	0.01	18.8	0.1	0	0.17	0.38	14.8	98.3
10B_plag1.1-line9	Syenite	65.2	0	18.6	0.0	0.05	0.11	0.41	15.0	99.5
10B_plag2.1-line1	Syenite	63.7	0.03	19.7	0.1	0.01	0.32	0.34	14.5	99.1
10B_plag2.1-line10	Syenite	64.8	0.04	18.8	0.6	0.02	0.14	0.96	13.9	99.5
10B_plag2.1-line11	Syenite	64.3	0.03	19.2	0.1	0.03	0.03	0.39	14.7	98.9
10B_plag2.1-line12	Syenite	65.1	0.04	18.8	0.2	0.02	0	1.49	13.3	99.1
10B_plag2.1-line13	Syenite	65.4	0	19.0	0.1	0	0	0.8	14.3	99.8
10B_plag2.1-line14	Syenite	65.0	0	18.8	0.2	0.02	0	0.47	14.6	99.2
10B_plag2.1-line15	Syenite	65.3	0.01	18.8	0.2	0.05	0.1	1.16	13.7	99.4
10B_plag2.1-line16	Syenite	65.6	0.03	19.0	0.2	0.04	0.04	1.95	12.7	99.7
10B_plag2.1-line17	Syenite	65.4	0	18.8	0.1	0.01	0.07	0.68	14.3	99.4
10B_plag2.1-line18	Syenite	65.2	0.03	18.8	0.1	0	0.1	0.63	14.4	99.4

Sample	Rock Type	SiO2	TiO2	Al2O3	CaO	SrO	BaO	Na2O	K2O	Total
10B_plag2.1-line19	Syenite	65.5	0.01	18.9	0.1	0.04	0.02	1.45	13.5	99.6
10B_plag2.1-line2	Syenite	67.0	0	19.4	0.5	0	0	5.08	8.41	101
10B_plag2.1-line20	Syenite	65.5	0	18.7	0.2	0.03	0.06	0.58	14.5	99.8
10B_plag2.1-line21	Syenite	65.1	0	19.2	0.0	0.03	0.02	0.53	14.6	99.7
10B_plag2.1-line3	Syenite	66.8	0	19.2	0.5	0.03	0	5.05	8.32	100
10B_plag2.1-line4	Syenite	67.1	0.02	19.3	0.5	0	0	5.07	8.28	100
10B_plag2.1-line5	Syenite	66.9	0	19.4	0.5	0.02	0	5.13	8.28	100
10B_plag2.1-line6	Syenite	66.8	0	19.3	0.5	0.03	0.03	5.16	8.24	100
10B_plag2.1-line7	Syenite	67.2	0	19.5	0.6	0.05	0.03	5.11	8.2	101
10B_plag2.1-line8	Syenite	66.1	0	19.3	0.4	0.05	0	4.59	8.69	99.3
10B_plag2.1-line9	Syenite	65.4	0.01	18.9	0.2	0.02	0.08	1.58	13.2	99.6
10B_plag3.1	Syenite	66.3	0.04	19.8	0.5	0.05	0.05	5.29	7.84	100
10B_plag3.2	Syenite	66.3	0.03	19.5	0.6	0.02	0.02	5.05	7.99	99.7
10B_plag3.3	Syenite	66.5	0.06	19.4	0.7	0	0	5.35	7.57	99.9
10B_plag3.4	Syenite	66.9	0.01	19.6	0.6	0	0	5.04	8.03	100
10B_plag3.5	Syenite	66.2	0.04	19.5	0.6	0.05	0	5.09	8.08	99.7
10B_plag4.1	Syenite	65.7	0.12	20.0	1.0	0.04	0.57	5.56	6.92	100
10B_plag4.2	Syenite	65.4	0.09	20.2	1.0	0.05	0.58	5.1	7.61	100
10B_plag4.3	Syenite	65.6	0.1	19.8	0.9	0.08	0.48	5.21	7.52	99.9
10B_plag4.4	Syenite	65.5	0.07	20.3	1.1	0.09	0.61	5.27	7.17	100
10B_plag4.5	Syenite	65.3	0.07	20.3	1.1	0.07	0.74	5.5	6.9	100
10B_plag5.1-line1	Syenite	66.1	0.08	20.0	0.9	0	0.23	5.72	7.01	100
10B_plag5.1-line10	Syenite	65.6	0.07	20.2	1.0	0.06	0.47	5.4	7.4	100
10B_plag5.1-line11	Syenite	65.7	0.1	20.1	1.0	0.09	0.64	5.36	7.26	100
10B_plag5.1-line12	Syenite	65.5	0.1	20.3	1.1	0.11	0.8	5.27	7.15	101
10B_plag5.1-line13	Syenite	65.2	0.1	20.5	1.4	0.08	0.69	5.73	6.51	100
10B_plag5.1-line14	Syenite	65.0	0.13	20.0	0.8	0.08	0.86	5.04	7.79	100
10B_plag5.1-line15	Syenite	65.6	0.09	20.0	0.9	0.08	0.75	5.09	7.63	100
10B_plag5.1-line16	Syenite	63.7	0.09	20.1	0.7	0.02	0.55	4.64	8.24	98.4
10B_plag5.1-line17	Syenite	65.9	0.11	20.0	1.0	0.06	0.3	5.48	7.08	100
10B_plag5.1-line18	Syenite	65.6	0.06	19.8	0.9	0	0.3	4.6	8.48	99.9
10B_plag5.1-line19	Syenite	64.4	0.09	19.4	0.2	0.02	0.13	2.06	12.3	98.9
10B_plag5.1-line2	Syenite	66.0	0.02	19.7	0.7	0.02	0.3	5.43	8.08	100
10B_plag5.1-line20	Syenite	65.8	0.03	19.2	0.2	0.03	0.17	3.47	10.6	99.6
10B_plag5.1-line3	Syenite	66.1	0.04	19.9	0.9	0.02	0.29	5.38	7.59	100
10B_plag5.1-line4	Syenite	66.2	0.06	19.6	0.8	0.05	0.27	5.24	7.69	100

Sample	Rock Type	SiO2	TiO2	Al2O3	CaO	SrO	BaO	Na2O	K2O	Total
10B_plag5.1-line5	Syenite	66.0	0.07	19.9	0.9	0.05	0.31	5.29	7.7	100
10B_plag5.1-line6	Syenite	65.9	0.06	19.9	0.9	0.05	0.3	5.2	7.78	100
10B_plag5.1-line7	Syenite	66.4	0.06	19.8	0.8	0.02	0.29	5.05	7.84	100
10B_plag5.1-line8	Syenite	65.2	0.12	19.2	0.2	0.04	0.22	4.91	8.46	99.3
10B_plag5.1-line9	Syenite	63.7	0.05	19.0	0.8	0.02	0.41	3.55	9.82	98.8
15D_plag1.1	LSPT	61.4	0.05	24.1	5.5	0.15	0.23	7.69	0.56	100
15D_plag1.2	LSPT	60.9	0.05	24.4	5.9	0.17	0.22	7.74	0.42	100
15D_plag1.3	LSPT	60.7	0.09	24.5	5.9	0.18	0.2	7.41	0.65	100
15D_plag1.4	LSPT	61.7	0.07	24.1	5.3	0.11	0.25	7.42	1.3	100
15D_plag1.5	LSPT	59.1	0.06	26.0	7.4	0.15	0.13	6.92	0.41	101
15D_plag2.1	LSPT	58.5	0.1	25.9	7.8	0.22	0.22	6.42	0.57	100
15D_plag2.2	LSPT	58.9	0.09	26.1	7.6	0.22	0.23	6.53	0.62	101
15D_plag2.3	LSPT	58.8	0.06	26.1	7.7	0.19	0.22	6.47	0.63	101
15D_plag2.4	LSPT	59.4	0.1	25.2	6.9	0.23	0.19	6.79	0.72	100
15D_plag2.5	LSPT	59.6	0.06	25.6	7.1	0.22	0.29	6.96	0.54	101
15D_plag3.1	LSPT	67.0	0.01	19.2	0.5	0.01	0.05	5.1	8.29	100
15D_plag3.2	LSPT	67.7	0.03	19.3	0.5	0.03	0	5.1	7.98	101
15D_plag3.3	LSPT	67.4	0.04	19.1	0.5	0.04	0.05	4.76	8.54	101
15D_plag3.4	LSPT	67.6	0.04	19.1	0.5	0	0.06	5.22	8.08	101
15D_plag3.5	LSPT	67.5	0.04	19.0	0.5	0.01	0	4.9	8.53	101
15D2_plag1.1	LSPT	60.3	0.08	24.4	7.2	0.12	0.06	7.16	0.72	101
15D2_plag1.2	LSPT	61.4	0.06	24.9	6.5	0.12	0.19	7.16	0.84	101
15D2_plag1.3	LSPT	61.0	0.08	24.9	6.6	0.14	0.26	7.03	0.82	101
15D2_plag1.4	LSPT	66.6	0.05	19.9	1.1	0.11	0.54	5.26	7.14	101
15D2_plag1.5	LSPT	66.7	0.03	20.1	1.2	0.07	0.47	5.55	6.79	101
15D2_plag2.1	LSPT	53.0	0.08	30.1	12.6	0.15	0.02	3.9	0.24	101
15D2_plag2.2	LSPT	50.9	0.07	31.6	14.3	0.11	0	3.05	0.18	101
15D2_plag2.3	LSPT	51.6	0.06	31.2	13.9	0.12	0	3.24	0.22	101
15D2_plag2.4	LSPT	51.8	0.08	31.2	13.8	0.17	0.01	3.42	0.22	101
16c_plag1.1	unknown	38.6	4.6	13.2	0.0	0	0.79	0.3	8.41	98.0
16c_plag1.2	unknown	36.4	5.04	14.3	0.0	0	1.41	0.39	8.25	98.2
16c_plag1.3	unknown	36.9	5.08	14.0	0.0	0	1.22	0.44	8.27	97.8
16c_plag1.4	unknown	39.3	4.23	12.5	0.0	0	0.26	0.22	8.62	96.9
16C_plag2.1-line1	unknown	59.9	0.08	25.1	6.4	0.13	0.21	7.2	0.57	100
16C_plag2.1-line10	unknown	60.9	0.08	24.7	5.8	0.13	0.13	7.56	0.66	100
16C_plag2.1-line11	unknown	59.6	0.06	25.4	6.5	0.18	0.18	7.15	0.58	100
16C_plag2.1-line12	unknown	60.8	0.08	24.8	6.0	0.14	0.27	7.33	0.78	101
16C_plag2.1-line13	unknown	60.6	0.08	24.4	5.8	0.16	0.24	7.32	0.88	100
16C_plag2.1-line14	unknown	60.4	0.07	24.6	5.9	0.2	0.34	7.41	0.88	100

Sample	Rock Type	SiO2	TiO2	Al2O3	CaO	SrO	BaO	Na2O	K2O	Total
16C_plag2.1-line15	unknown	60.7	0.07	24.6	6.0	0.18	0.4	7.34	0.99	101
16C_plag2.1-line16	unknown	61.3	0.06	24.3	5.3	0.15	0.42	7.28	1.24	101
16C_plag2.1-line17	unknown	61.1	0.05	24.5	5.8	0.18	0.31	7.36	0.94	100
16C_plag2.1-line18	unknown	60.9	0.08	24.4	5.9	0.15	0.26	7.18	0.87	100
16C_plag2.1-line19	unknown	60.0	0.1	24.9	6.1	0.18	0.23	7.2	0.72	99.9
16C_plag2.1-line2	unknown	60.4	0.07	24.8	6.2	0.16	0.16	7.18	0.59	100
16C_plag2.1-line20	unknown	60.2	0.07	24.9	6.1	0.18	0.26	7.29	0.74	100
16C_plag2.1-line3	unknown	60.6	0.08	24.8	6.1	0.15	0.31	7.35	0.66	100
16C_plag2.1-line4	unknown	60.3	0.05	24.6	6.0	0.14	0.27	7.52	0.67	99.9
16C_plag2.1-line5	unknown	66.2	0.06	20.9	2.1	0.06	0.14	8.48	2.09	100
16C_plag2.1-line6	unknown	66.1	0.07	20.6	2.1	0.1	0.12	8.39	2.07	99.8
16C_plag2.1-line7	unknown	60.5	0.06	24.7	6.2	0.14	0.21	7.29	0.6	99.9
16C_plag2.1-line8	unknown	60.3	0.04	24.9	6.3	0.11	0.2	7.04	0.61	100
16C_plag2.1-line9	unknown	60.1	0.07	25.4	6.5	0.14	0.22	7.28	0.56	101
16C_plag3.1	unknown	50.4	1.06	3.1	22.0	0	0.01	0.55	0.03	100
16C_plag3.2	unknown	57.3	0.09	27.1	8.7	0.19	0.14	5.86	0.43	100
16C_plag3.3	unknown	58.6	0.1	26.1	7.5	0.2	0.23	6.69	0.55	100
16C_plag3.4	unknown	55.8	0.09	28.0	9.8	0.26	0.14	5.5	0.35	101
16C_plag3.5	unknown	60.1	0.08	25.2	6.7	0.18	0.28	7.14	0.53	101
16C_plag4.1	unknown	51.3	0.06	31.0	13.7	0.17	0.07	3.56	0.25	101
16C_plag4.2	unknown	52.2	0.09	30.7	12.1	0.09	0	3.99	0.66	101
16C_plag4.3	unknown	52.5	0.05	30.2	12.7	0.16	0.04	4.03	0.37	101
16C_plag4.4	unknown	51.4	0.06	30.8	13.3	0.15	0	3.69	0.22	100
16C_plag4.5	unknown	50.9	0.06	31.5	13.9	0.16	0	3.41	0.23	101
16C_plag5.1	unknown	51.8	0.06	31.1	13.4	0.18	0.04	3.59	0.32	101
16C_plag5.2	unknown	51.7	0.06	31.0	13.0	0.19	0	3.76	0.29	101
16C_plag5.3	unknown	50.6	0.06	31.9	14.0	0.14	0.06	3.28	0.16	101
16C_plag5.4	unknown	51.8	0.1	31.3	13.6	0.16	0.02	3.62	0.34	102
16C_plag5.5	unknown	51.8	0.09	30.9	13.2	0.14	0	3.73	0.32	101
40A2_plag1.1	USPT	64.9	0.1	20.5	1.1	0.07	0.56	5.72	6.83	99.9
40A2_plag1.2	USPT	66.0	0.08	20.3	0.9	0.07	0.53	5.51	7.07	101
40A2_plag1.3	USPT	65.9	0.06	20.1	0.9	0.08	0.47	5.37	7.35	100
40A2_plag1.4	USPT	66.2	0.1	20.1	0.9	0.03	0.42	5.53	7.31	101
40A2_plag1.5	USPT	66.3	0.03	19.9	0.8	0.08	0.39	5.3	7.45	101
40A2_plag1.6	USPT	65.9	0.08	20.2	1.0	0	0.36	5.11	7.83	101
40A2_plag1.7	USPT	66.1	0.05	20.3	1.0	0.05	0.36	5.13	7.76	101
40A2_plag2.1-line1	USPT	66.6	0.08	20.1	1.0	0.06	0.1	6.11	6.39	101
40A2_plag2.1-line10	USPT	64.7	0.12	20.5	1.0	0.15	1.48	5.01	7.44	101

Sample	Rock Type	SiO2	TiO2	Al2O3	CaO	SrO	BaO	Na2O	K2O	Total
40A2_plag2.1-line11	USPT	65.1	0.11	20.4	1.0	0.09	1.22	5.16	7.5	101
40A2_plag2.1-line12	USPT	65.7	0.11	20.3	1.0	0.07	1.04	4.97	7.56	101
40A2_plag2.1-line13	USPT	65.7	0.09	19.9	1.0	0.09	0.7	5.12	7.65	101
40A2_plag2.1-line14	USPT	65.6	0.12	19.9	0.9	0.05	0.58	4.91	7.92	100
40A2_plag2.1-line15	USPT	66.0	0.07	20.0	0.9	0.11	0.46	5.29	7.7	101
40A2_plag2.1-line16	USPT	66.0	0.09	19.9	0.9	0.06	0.5	5.18	7.66	101
40A2_plag2.1-line17	USPT	65.5	0.08	19.9	0.9	0.06	0.37	5.57	7.22	99.9
40A2_plag2.1-line18	USPT	66.3	0.08	19.1	0.5	0	0.09	4.07	9.51	99.9
40A2_plag2.1-line19	USPT	66.7	0.07	19.8	0.8	0.04	0.18	5.88	6.77	100
40A2_plag2.1-line2	USPT	66.9	0.03	19.9	0.9	0.05	0.14	6.08	6.33	101
40A2_plag2.1-line20	USPT	66.6	0.02	20.0	1.0	0.05	0.07	6.1	6.34	100
40A2_plag2.1-line21	USPT	66.6	0.03	20.0	1.0	0.05	0.11	6.22	6.26	100
40A2_plag2.1-line3	USPT	65.2	0.09	20.5	1.1	0.15	1.37	5.53	6.55	101
40A2_plag2.1-line4	USPT	64.2	0.12	19.8	1.0	0.11	1.41	5.39	6.62	99.0
40A2_plag2.1-line5	USPT	65.2	0.14	20.6	1.2	0.15	1.48	5.25	6.9	101
40A2_plag2.1-line6	USPT	64.7	0.12	20.6	1.2	0.17	1.57	5.19	7.05	101
40A2_plag2.1-line7	USPT	64.3	0.14	20.7	1.1	0.11	1.54	5.12	7.23	101
40A2_plag2.1-line8	USPT	64.5	0.13	20.6	1.0	0.13	1.48	5.09	7.33	101
40A2_plag2.1-line9	USPT	64.9	0.1	20.2	1.1	0.14	1.42	5.1	7.12	100
40A2_plag3.1	USPT	60.1	0.03	25.3	6.8	0.13	0.11	7.06	0.8	101
40A2_plag3.2	USPT	60.0	0.09	25.7	6.9	0.21	0.11	6.8	0.77	101
40A2_plag3.3	USPT	60.3	0.04	25.6	6.4	0.15	0.07	6.98	0.84	101
40A2_plag3.4	USPT	60.7	1.16	23.0	4.5	0.09	0.19	6.08	3.53	99.8
40A2_plag3.5	USPT	59.8	0.09	25.8	6.8	0.11	0.07	7.02	0.76	101
40A2_plag3.6	USPT	61.0	0.04	24.6	5.3	0.08	0.06	7.43	1.23	100
40A2_plag4.1	USPT	66.3	0.09	20.2	0.9	0.08	0.22	5.6	7.26	101
40A2_plag4.2	USPT	66.5	0.06	19.6	0.8	0	0.06	4.81	8.21	100
40A2_plag4.3	USPT	66.8	0.08	19.8	0.7	0.04	0.07	4.77	8.45	101
40A2_plag4.4	USPT	66.0	0.06	19.9	0.8	0.04	0.25	5.02	8.21	101
40A2_plag4.5	USPT	66.7	0.05	20.0	0.8	0.01	0.19	5.4	7.55	101
40A3_plag1-line1	USPT	64.9	0.09	20.7	1.3	0.16	1.23	5.53	6.47	101
40A3_plag1-line10	USPT	64.8	0.08	20.2	1.0	0.09	1.16	4.63	8.15	100
40A3_plag1-line11	USPT	64.6	0.12	20.2	1.1	0.09	1.25	4.78	8.06	100
40A3_plag1-line12	USPT	64.3	0.1	20.3	1.1	0.13	1.25	4.71	8.02	100

Sample	Rock Type	SiO2	TiO2	Al2O3	CaO	SrO	BaO	Na2O	K2O	Total
40A3_plag1-line13	USPT	64.5	0.11	20.3	1.0	0.1	1.2	4.48	8	100
40A3_plag1-line14	USPT	64.3	0.13	20.3	1.1	0.09	1.17	4.7	8.02	100
40A3_plag1-line15	USPT	64.4	0.1	20.3	1.1	0.1	1.34	4.74	7.86	100
40A3_plag1-line16	USPT	64.7	0.14	20.1	1.0	0.15	1.25	4.54	8.01	100
40A3_plag1-line17	USPT	64.1	0.1	20.1	1.2	0.11	1.57	4.71	7.86	100
40A3_plag1-line18	USPT	63.7	0.15	20.6	1.3	0.1	1.71	4.51	7.68	100
40A3_plag1-line19	USPT	63.6	0.16	20.5	1.2	0.13	1.77	4.42	7.81	99.8
40A3_plag1-line2	USPT	65.0	0.12	20.6	1.3	0.14	1.19	5.47	6.72	101
40A3_plag1-line20	USPT	63.9	0.11	20.4	1.0	0.11	1.5	4.35	8.62	100
40A3_plag1-line21	USPT	63.3	0.12	20.0	1.3	0.05	1.5	4.47	7.54	98.6
40A3_plag1-line22	USPT	64.0	0.13	20.7	1.3	0.11	1.44	4.68	7.64	100
40A3_plag1-line23	USPT	64.1	0.1	20.5	1.5	0.17	1.07	4.78	7.51	100
40A3_plag1-line24	USPT	65.4	0.1	20.1	1.0	0.08	0.71	4.77	8.09	101
40A3_plag1-line25	USPT	65.1	0.06	19.9	1.1	0.08	0.45	4.59	8.09	99.7
40A3_plag1-line26	USPT	65.2	0.05	19.9	1.0	0.07	0.46	4.59	8.44	99.9
40A3_plag1-line27	USPT	65.4	0.08	19.8	1.0	0.08	0.47	4.69	8.34	100
40A3_plag1-line28	USPT	65.0	0.07	19.9	1.0	0.11	0.66	4.61	8.3	99.9
40A3_plag1-line29	USPT	64.7	0.08	19.9	1.0	0.03	0.9	4.57	8.35	99.8
40A3_plag1-line3	USPT	64.7	0.12	20.5	1.3	0.16	1.27	5.38	6.88	101
40A3_plag1-line30	USPT	64.7	0.07	20.1	1.0	0.14	1	4.64	8.35	100
40A3_plag1-line31	USPT	64.7	0.11	20.2	1.1	0.12	0.86	4.56	8.23	100
40A3_plag1-line32	USPT	65.0	0.08	20.1	1.0	0.13	0.83	4.67	8.26	100
40A3_plag1-line33	USPT	64.8	0.1	19.8	1.0	0.07	0.78	4.52	8.41	99.8
40A3_plag1-line34	USPT	64.6	0.06	20.0	0.9	0.08	0.74	4.68	8.45	99.7
40A3_plag1-line35	USPT	65.2	0.07	20.0	0.9	0.1	0.62	4.55	8.43	100
40A3_plag1-line36	USPT	64.8	0.08	19.8	1.0	0.09	0.77	4.48	8.43	99.6
40A3_plag1-line4	USPT	64.6	0.12	20.2	1.1	0.12	1.26	5.04	7.53	100
40A3_plag1-line5	USPT	63.8	0.13	20.2	1.2	0.12	1.36	4.7	7.77	99.5
40A3_plag1-line6	USPT	64.4	0.13	20.5	1.1	0.15	1.25	4.71	7.95	100
40A3_plag1-line7	USPT	64.4	0.13	20.4	1.2	0.11	1.17	4.61	7.87	100
40A3_plag1-line8	USPT	64.5	0.15	20.2	1.1	0.15	1.1	4.69	8.11	100
40A3_plag1-line9	USPT	64.4	0.1	20.2	1.1	0.2	1.16	4.51	8.04	99.9
40A3_plag3.1	USPT	58.3	0.05	25.9	7.6	0.19	0.2	6.53	0.93	100
40A3_plag3.2	USPT	60.5	0.06	24.7	5.8	0.16	0.32	6.95	1.42	100
40A3_plag3.3	USPT	61.3	0.05	24.3	5.5	0.1	0.22	7.19	1.54	101
40A3_plag3.4	USPT	60.7	0.03	24.2	5.4	0.11	0.26	7.35	1.45	99.9
40A3_plag3.5	USPT	61.5	0.05	24.3	5.3	0.1	0.21	7.58	1.17	101
40A3_plag4.1	USPT	66.4	0.04	19.7	0.6	0.02	0.24	4.94	8.45	101
40A3_plag4.2	USPT	66.4	0.05	19.6	0.5	0.01	0.04	4.76	8.73	100

Sample	Rock Type	SiO2	TiO2	Al2O3	CaO	SrO	BaO	Na2O	K2O	Total
40A3_plag4.3	USPT	66.3	0.01	19.4	0.5	0.03	0.04	4.43	8.91	99.9
40A3_plag4.4	USPT	66.3	0.03	19.5	0.6	0.01	0.09	4.81	8.62	100
40A3_plag4.5	USPT	65.9	0.05	19.7	0.6	0	0.06	4.69	8.55	99.8
40A3_plag4.6	USPT	66.5	0.02	19.5	0.5	0	0	4.64	8.55	100
40A3_plag4.7	USPT	65.7	0.04	19.5	0.5	0.03	0.05	4.43	9.15	99.7
40A3_plg2.1	USPT	66.0	0.03	19.4	0.6	0.07	0.13	4.68	8.78	99.8
40A3_plg2.2	USPT	66.3	0.03	19.6	0.6	0.03	0.13	4.75	8.36	100
40A3_plg2.3	USPT	65.9	0.01	19.5	0.6	0.03	0.2	5.07	8.01	99.5
40A3_plg2.4	USPT	66.2	0.04	19.8	0.5	0.05	0.19	5.37	8	100
40B_plag1.1-line1	USPT	66.2	0.05	19.7	0.8	0.05	0.38	5.6	7.06	100
40B_plag1.1-line10	USPT	65.3	0.06	19.8	1.0	0.09	0.61	5.26	7.13	99.5
40B_plag1.1-line11	USPT	66.1	0.08	20.0	1.0	0.08	0.65	5.47	7.33	101
40B_plag1.1-line12	USPT	65.4	0.09	20.2	0.9	0.07	0.7	5.27	7.51	100
40B_plag1.1-line13	USPT	65.3	0.1	19.9	0.9	0.05	0.64	5.21	7.6	99.9
40B_plag1.1-line14	USPT	66.1	0.08	20.2	1.0	0.08	0.6	5.23	7.41	101
40B_plag1.1-line15	USPT	65.4	0.05	20.2	0.9	0.02	0.61	5.04	7.62	100
40B_plag1.1-line16	USPT	66.0	0.08	20.1	0.9	0.05	0.62	5.25	7.56	101
40B_plag1.1-line17	USPT	65.5	0.07	20.1	0.9	0.04	0.56	4.89	7.91	100
40B_plag1.1-line18	USPT	66.2	0.07	20.1	0.9	0.07	0.6	5.42	7.51	101
40B_plag1.1-line19	USPT	65.9	0.08	19.9	0.7	0.07	0.41	5.39	7.54	100
40B_plag1.1-line2	USPT	66.5	0.09	20.0	0.8	0.05	0.38	5.2	7.72	101
40B_plag1.1-line20	USPT	63.2	0.05	19.2	0.5	0.06	0.48	5.26	7.49	96.4
40B_plag1.1-line21	USPT	66.3	0.08	19.8	0.8	0.04	0.46	5.24	7.7	101
40B_plag1.1-line22	USPT	66.5	0.06	19.9	0.7	0.05	0.49	5.04	7.82	101
40B_plag1.1-line23	USPT	66.2	0.09	20.2	0.8	0.06	0.43	5.23	7.75	101
40B_plag1.1-line24	USPT	66.1	0.07	19.9	0.8	0.08	0.49	5.25	7.73	101
40B_plag1.1-line25	USPT	66.2	0.05	19.8	0.8	0.08	0.31	5.22	7.74	100
40B_plag1.1-line26	USPT	66.3	0.06	19.9	0.8	0.06	0.41	5.24	7.72	101
40B_plag1.1-line27	USPT	66.2	0.09	19.7	0.7	0.01	0.35	4.95	8.16	100
40B_plag1.1-line28	USPT	66.2	0.09	20.0	0.8	0.03	0.53	5.5	7.28	101
40B_plag1.1-line29	USPT	66.3	0.04	19.9	0.8	0.03	0.38	5.3	7.69	101
40B_plag1.1-line3	USPT	66.5	0.03	20.0	0.8	0.05	0.38	5.22	7.66	101
40B_plag1.1-line30	USPT	65.9	0.04	19.7	0.7	0.03	0.45	5.19	7.9	100
40B_plag1.1-line31	USPT	66.4	0.06	19.8	0.7	0.04	0.28	5.21	7.84	101

Sample	Rock Type	SiO2	TiO2	Al2O3	CaO	SrO	BaO	Na2O	K2O	Total
40B_plag1.1-line32	USPT	65.7	0.04	19.7	0.6	0.04	0.26	5.08	8.01	99.6
40B_plag1.1-line33	USPT	66.6	0.02	19.4	0.6	0.07	0.18	5.35	7.78	100
40B_plag1.1-line34	USPT	66.4	0.05	19.7	0.6	0.08	0.09	6.14	6.58	99.8
40B_plag1.1-line35	USPT	66.1	0.02	18.8	0.2	0	0.1	3.4	10.6	99.7
40B_plag1.1-line36	USPT	66.1	0	21.5	2.1	0.03	0.05	9.97	0.7	101
40B_plag1.1-line37	USPT	66.6	0.03	19.4	0.3	0.02	0.16	5.9	7.45	100
40B_plag1.1-line38	USPT	66.4	0.04	19.7	0.3	0.03	0.15	4.99	8.56	100
40B_plag1.1-line39	USPT	66.0	0.05	19.5	0.3	0.02	0.25	4.92	8.79	100
40B_plag1.1-line4	USPT	66.7	0	19.4	0.5	0.02	0.19	4.83	8.57	100
40B_plag1.1-line40	USPT	67.2	0.06	19.7	0.6	0.05	0.17	5.71	7.27	101
40B_plag1.1-line41	USPT	66.8	0.03	19.5	0.5	0.02	0.12	5.79	7.37	100
40B_plag1.1-line5	USPT	65.9	0.04	20.1	1.1	0.01	0.26	5.62	6.9	100
40B_plag1.1-line6	USPT	66.1	0.09	20.2	1.0	0.08	0.61	5.55	7.27	101
40B_plag1.1-line7	USPT	66.0	0.09	20.2	1.0	0.03	0.61	5.45	7.27	101
40B_plag1.1-line8	USPT	65.9	0.09	20.1	0.9	0.08	0.59	5.26	7.49	101
40B_plag1.1-line9	USPT	65.9	0.06	20.1	0.9	0.06	0.5	5.33	7.38	100
40B_plag2.1	USPT	63.3	0.03	23.8	4.8	0.06	0.04	8.19	0.86	101
40B_plag2.2	USPT	63.9	0.01	23.0	4.1	0.03	0.07	8.39	0.84	101
40B_plag2.3	USPT	66.5	0.1	20.3	0.9	0.05	0.6	5.84	6.82	101
40B_plag2.4	USPT	66.3	0.09	20.3	1.0	0.06	0.37	6.33	6.12	101
40B_plag2.5	USPT	66.1	0.05	20.2	1.0	0.04	0.45	6.11	6.35	100
40B_plag3.1	USPT	66.3	0	19.3	0.4	0.01	0.09	4.63	9.21	100
40B_plag3.2	USPT	66.5	0.02	19.4	0.3	0.03	0	4.39	9.35	100
40B_plag3.3	USPT	66.5	0.01	19.2	0.4	0.03	0	4.51	9	99.8
40B_plag3.4	USPT	67.1	0.01	19.1	0.3	0.02	0.08	4.26	9.55	101
40B_plag3.5	USPT	66.2	0.04	19.5	0.5	0.08	0.16	4.55	8.81	100
40B_plag3.6	USPT	66.2	0.02	19.5	0.5	0.04	0.19	5.01	8.23	100
40B_plag3.7	USPT	67.0	0.01	20.4	0.3	0.03	0.07	10.49	1.3	99.8
40F_kspar1.1	USPT	67.0	0	19.0	0.2	0.04	0.2	4.65	8.89	100
40F_kspar1.2	USPT	67.7	0	19.1	0.2	0.1	0.15	4.75	8.92	101
40F_kspar1.3	USPT	67.5	0.04	19.0	0.2	0.1	0.17	4.62	8.88	101
40F_kspar1.4	USPT	67.4	0.01	19.1	0.2	0.07	0.27	4.47	9.27	101
40F_kspar1.5	USPT	67.6	0.03	19.2	0.3	0.06	0.16	4.97	8.58	101
40F_kspar2.1	USPT	66.9	0.01	19.4	0.2	0.07	0.64	4.48	9.18	101
40F_kspar2.2	USPT	67.2	0.04	19.0	0.2	0.1	0.52	4.54	9.09	101
40F_kspar2.3	USPT	66.8	0.07	19.2	0.2	0.07	0.51	4.27	9.4	101
40F_kspar2.4	USPT	67.0	0.01	19.4	0.2	0.12	0.8	4.3	9.28	101

Sample	Rock Type	SiO2	TiO2	Al2O3	CaO	SrO	BaO	Na2O	K2O	Total
40F_kspar2.5	USPT	67.1	0.04	19.3	0.2	0.08	0.81	4.09	9.49	101
7B_plag1.1	Syenite	64.8	0.04	19.0	0.0	0.03	0.31	1.41	13.1	98.9
7B_plag1.2	Syenite	65.4	0	19.2	0.0	0	0.19	3.09	11.3	99.2
7B_plag1.3	Syenite	64.8	0.01	18.8	0.0	0	0.13	0.29	14.9	99.2
7B_plag1.4	Syenite	65.0	0.01	18.6	0.0	0	0.06	0.16	15.1	99.0
7B_plag1.5	Syenite	65.0	0.05	18.6	0.0	0.01	0.23	0.4	14.8	99.1
7b_plag2.1	Syenite	66.6	0	19.1	0.3	0.03	0.02	4.74	8.78	99.8
7b_plag2.2	Syenite	66.2	0	19.1	0.3	0	0.03	4.29	9.36	99.6
7b_plag2.3	Syenite	66.4	0.03	19.3	0.4	0.02	0	4.81	8.67	99.8
7b_plag2.4	Syenite	66.5	0	19.2	0.4	0	0	5	8.59	100
7b_plag2.5	Syenite	67.1	0.02	19.3	0.4	0.01	0.07	4.94	8.41	100
7b_plag3.1	Syenite	67.1	0	19.3	0.4	0	0	4.98	8.42	100
7b_plag3.2	Syenite	67.1	0.01	19.0	0.4	0	0	4.92	8.52	100
7b_plag3.3	Syenite	67.0	0	19.2	0.4	0	0	5	8.36	100
7b_plag3.4	Syenite	66.7	0.04	19.2	0.5	0.01	0.01	5.12	8.13	100
7b_plag3.5	Syenite	66.7	0	19.3	0.6	0.03	0	5.15	7.98	100
7B_plag4.1-line1	Syenite	66.8	0	19.5	0.5	0	0.02	5.21	8.12	100
7B_plag4.1-line10	Syenite	66.5	0.02	19.3	0.5	0.02	0	5.21	8.13	99.9
7B_plag4.1-line11	Syenite	66.0	0.02	19.3	0.5	0.01	0.08	4.93	8.28	99.3
7B_plag4.1-line12	Syenite	66.6	0.03	19.3	0.5	0	0	5.32	7.85	99.9
7B_plag4.1-line13	Syenite	66.4	0.03	19.1	0.4	0.04	0	4.54	9.15	99.7
7B_plag4.1-line14	Syenite	66.7	0.01	19.3	0.4	0.02	0.06	4.89	8.48	100
7B_plag4.1-line15	Syenite	67.1	0	19.1	0.4	0.02	0	4.85	8.47	100
7B_plag4.1-line16	Syenite	65.9	0.04	19.0	0.4	0.02	0.01	4.17	9.59	99.3
7B_plag4.1-line17	Syenite	64.9	0.05	19.1	0.2	0	0.23	2.77	11.6	99.2
7B_plag4.1-line18	Syenite	65.2	0.04	18.9	0.2	0	0.19	1.25	13.4	99.3
7B_plag4.1-line19	Syenite	65.3	0.01	18.9	0.1	0	0.2	1.39	13.5	99.6
7B_plag4.1-line2	Syenite	66.5	0.04	19.5	0.6	0.01	0	5.4	8.01	100
7B_plag4.1-line20	Syenite	66.1	0	19.3	0.3	0	0.06	4.11	9.61	99.7
7B_plag4.1-line21	Syenite	65.9	0.01	19.2	0.3	0.01	0.08	4.15	9.67	99.5
7B_plag4.1-line3	Syenite	67.1	0.03	19.3	0.6	0.06	0	5.23	8.03	100
7B_plag4.1-line4	Syenite	65.4	0	20.0	0.4	0.01	0	4.43	9	99.6
7B_plag4.1-line5	Syenite	65.3	0.03	19.1	0.1	0.03	0	1.84	13.0	99.6
7B_plag4.1-line6	Syenite	61.8	0.04	21.2	0.2	0	0	1.78	12.2	97.3
7B_plag4.1-line7	Syenite	65.2	0.03	19.8	0.1	0.03	0.02	4.7	9.16	99.1
7B_plag4.1-line8	Syenite	66.7	0.05	19.2	0.5	0.02	0.04	4.5	8.92	100
7B_plag4.1-line9	Syenite	66.8	0.03	19.3	0.5	0	0	5.24	8.07	100
LC-100-c1-1	Syenite	65.2	0.03	18.7	0.6	0.01	0.03	5.12	9.36	99.2
LC-100-c1-2	Syenite	64.7	0.05	18.9	0.6	0.00	0.04	5.14	9.14	98.7

Sample	Rock Type	SiO2	TiO2	Al2O3	CaO	SrO	BaO	Na2O	K2O	Total
LC-100-c1-3	Syenite	65.7	0.05	18.6	0.4	0.00	0.05	4.84	9.77	99.6
LC-100-c1-4	Syenite	64.6	0.01	18.9	0.6	0.00	0.01	5.26	9.07	98.6
LC-100-c1-5	Syenite	62.9	0.00	18.2	0.4	0.01	0.08	4.67	9.01	95.5
LC-100-c1-6	Syenite	64.6	0.03	18.7	0.5	0.03	0.00	5.06	9.41	98.5
LC-100-c2-1	Syenite	65.4	0.01	18.7	0.4	0.03	0.04	4.87	9.82	99.5
LC-100-c2-2	Syenite	64.2	0.02	18.8	0.5	0.04	0.01	5.10	9.64	98.5
LC-100-c2-3	Syenite	65.3	0.04	18.7	0.5	0.04	0.04	4.98	9.63	99.5
LC-100-c2-4	Syenite	65.1	0.05	18.8	0.4	0.02	0.04	5.03	9.55	99.2
LC-100-c3-1	Syenite	65.6	0.00	18.6	0.4	0.03	0.01	4.91	9.89	99.6
LC-100-c3-2	Syenite	65.4	0.00	18.9	0.5	0.00	0.00	5.20	9.24	99.4
LC-100-c3-3	Syenite	65.2	0.00	18.8	0.5	0.00	0.02	5.10	9.49	99.4
LC-100-c3-4	Syenite	65.6	0.04	18.9	0.6	0.04	0.00	5.51	8.65	99.6
LC-100-c3-5	Syenite	65.6	0.02	18.8	0.5	0.03	0.03	5.12	9.35	99.7
LC-2004-15A-C1-1	LSPT	67.2	0.00	18.9	0.4	0.00	0.04	6.14	8.07	101
LC-2004-15A-C1-2	LSPT	67.5	0.03	19.1	0.5	0.00	0.00	6.72	7.28	101
LC-2004-15A-C1-3	LSPT	67.2	0.01	18.9	0.4	0.00	0.00	5.96	8.26	101
LC-2004-15A-C1-4	LSPT	66.9	0.01	18.9	0.4	0.00	0.04	5.91	8.57	101
LC-2004-15A-C2-1	LSPT	67.1	0.02	18.9	0.4	0.00	0.00	6.69	7.27	101
LC-2004-15A-C2-2	LSPT	67.3	0.03	19.1	0.4	0.02	0.00	6.26	7.71	101
LC-2004-15A-C2-3	LSPT	67.1	0.00	19.0	0.4	0.01	0.09	6.48	7.49	101
LC-2004-15A-C2-4	LSPT	65.5	0.02	18.6	0.4	0.06	0.05	6.01	7.89	98.7
LC-2004-15A-C3-1	LSPT	67.0	0.01	18.9	0.4	0.01	0.00	6.00	8.25	101
LC-2004-15A-C3-2	LSPT	67.1	0.00	18.8	0.4	0.00	0.00	6.04	8.14	101
LC-2004-15A-C3-3	LSPT	66.5	0.00	18.7	0.4	0.00	0.00	6.11	7.98	99.9
LC-2004-15A-C3-4	LSPT	67.0	0.01	18.8	0.4	0.00	0.02	5.99	8.13	100
LC-2004-17C-c1-1	Syenite	66.4	0.02	18.8	0.4	0.04	0.18	5.11	9.45	101
LC-2004-17C-c1-2	Syenite	66.3	0.04	18.8	0.5	0.01	0.01	4.91	9.48	100
LC-2004-17C-c1-3	Syenite	66.3	0.01	18.7	0.5	0.00	0.02	4.84	9.56	100
LC-2004-17C-c1-4	Syenite	66.5	0.04	18.7	0.5	0.00	0.03	5.08	9.52	101
LC-2004-17C-c2-1	Syenite	66.1	0.03	18.8	0.4	0.02	0.10	5.01	9.46	100
LC-2004-17C-c2-2	Syenite	65.8	0.06	19.4	1.1	0.05	0.10	5.88	7.62	100
LC-2004-17C-c2-3	Syenite	65.3	0.05	19.3	1.0	0.08	0.17	5.90	7.55	99.6
LC-2004-17C-c2-4	Syenite	65.5	0.07	19.7	1.3	0.04	0.28	6.29	6.54	100
LC-2004-17C-c2-5	Syenite	63.5	0.11	22.4	4.0	0.10	0.08	8.45	1.33	100
LC-2004-17C-c2-6	Syenite	63.8	0.08	21.5	3.1	0.09	0.12	7.50	3.35	99.8
LC-2004-17C-c2-7	Syenite	57.0	0.12	26.7	8.8	0.29	0.11	6.11	0.72	100
LC-2004-17C-c3-1	Syenite	59.8	0.07	24.3	6.5	0.12	0.18	7.56	0.59	99.5
LC-2004-17C-c3-2	Syenite	56.1	0.07	27.4	9.6	0.35	0.09	5.74	0.36	100
LC-2004-17C-c3-3	Syenite	56.8	0.09	26.1	8.6	0.35	0.22	6.26	0.42	99.3

Sample	Rock Type	SiO2	TiO2	Al2O3	CaO	SrO	BaO	Na2O	K2O	Total
LC-2004-17C-c3-4	Syenite	56.0	0.07	26.5	9.1	0.27	0.09	5.98	0.40	98.8
LC-2004-17C-c3-5	Syenite	56.3	0.06	26.9	9.2	0.26	0.05	6.02	0.33	99.5
LC-2004-17C-c4-1	Syenite	66.0	0.00	19.2	0.9	0.04	0.02	6.03	7.69	100
LC-2004-17C-c4-2	Syenite	65.9	0.05	18.5	0.4	0.00	0.05	4.90	9.63	99.6
LC-2004-17C-c4-3	Syenite	66.2	0.02	18.5	0.4	0.00	0.05	4.85	9.73	100
LC-2004-17C-c5-1	Syenite	66.5	0.00	18.6	0.4	0.03	0.04	5.01	9.53	100
LC-2004-17C-c5-2	Syenite	66.5	0.03	18.5	0.4	0.00	0.00	4.87	9.82	100
LC-2004-17C-c5-3	Syenite	66.1	0.00	18.6	0.4	0.00	0.00	4.44	10.0	99.7
LC-2004-17C-c5-4	Syenite	66.4	0.03	18.7	0.5	0.02	0.01	5.11	9.41	100
LC-2004-17C-c5-5	Syenite	66.6	0.04	18.8	0.5	0.00	0.02	4.97	9.37	100
LC-2004-17C-c6-1	Syenite	66.6	0.02	18.9	0.5	0.05	0.12	5.47	8.64	101
LC-2004-17C-c6-2	Syenite	66.6	0.03	18.7	0.4	0.04	0.09	4.93	9.60	101
LC-2004-17C-c6-3	Syenite	66.7	0.03	18.7	0.4	0.03	0.02	4.93	9.76	101
LC-2004-17C-c6-4	Syenite	66.3	0.00	18.7	0.5	0.00	0.01	4.96	9.40	100
LC-2004-17C-c6-5	Syenite	66.4	0.04	18.7	0.4	0.01	0.00	4.85	9.62	100
LC-2004-50a-c1-1	USPT	60.3	0.10	24.2	6.1	0.14	0.20	7.61	0.77	99.7
LC-2004-50a-c1-2	USPT	60.8	0.08	23.8	5.9	0.16	0.21	7.57	0.82	99.7
LC-2004-50a-c1-3	USPT	59.9	0.06	23.7	5.7	0.23	0.24	7.62	0.90	98.8
LC-2004-50a-c1-4	USPT	58.9	0.08	25.1	7.2	0.17	0.12	6.90	0.60	99.4
LC-2004-50a-c1-5	USPT	58.0	0.04	25.1	7.1	0.19	0.18	7.04	0.59	98.7
LC-2004-50a-c1-6	USPT	60.8	0.04	23.7	5.8	0.20	0.14	7.66	0.89	99.6
LC-2004-50a-c2-1	USPT	61.5	0.07	23.5	5.2	0.09	0.11	8.02	0.99	99.9
LC-2004-50a-c2-2	USPT	61.0	0.07	23.5	5.2	0.11	0.13	7.88	0.98	99.2
LC-2004-50a-c2-3	USPT	60.8	0.05	23.9	5.6	0.12	0.20	7.72	0.91	99.7
LC-2004-50a-c2-4	USPT	59.7	0.03	24.1	6.0	0.12	0.21	7.58	0.85	98.9
LC-2004-50a-c3-1	USPT	65.9	0.00	18.8	0.4	0.01	0.04	5.80	8.55	99.6
LC-2004-50a-c3-2	USPT	66.2	0.00	18.9	0.4	0.00	0.05	6.01	8.22	100
LC-2004-50a-c3-3	USPT	66.5	0.02	18.8	0.4	0.01	0.02	5.57	8.79	100
LC-2004-50a-c3-4	USPT	66.4	0.02	18.7	0.4	0.00	0.03	5.61	8.85	100
LC-2004-50a-c3-5	USPT	66.0	0.03	18.6	0.4	0.00	0.00	5.76	8.58	99.6
LC-2004-50a-c4-1	USPT	66.3	0.00	18.7	0.4	0.02	0.03	5.56	8.87	100
LC-2004-50a-c4-2	USPT	65.7	0.01	18.8	0.3	0.00	0.02	5.51	8.86	99.4
LC-2004-50a-c4-3	USPT	65.8	0.02	18.8	0.4	0.00	0.04	5.57	8.73	99.5
LC-2004-50a-c4-4	USPT	65.3	0.03	18.7	0.4	0.00	0.06	5.38	9.16	99.2
LC-2004-50a-c5-1	USPT	65.7	0.01	18.9	0.4	0.01	0.02	5.69	8.64	99.6
LC-2004-50a-c5-2	USPT	65.8	0.01	19.1	0.5	0.00	0.01	5.74	8.46	99.8
LC-2004-50a-c5-3	USPT	65.6	0.03	18.9	0.4	0.04	0.00	5.70	8.83	99.7
LC-2004-50a-c5-4	USPT	60.7	0.00	17.5	0.4	0.02	0.01	5.46	8.86	93.1
LC-2004-50a-c5-5	USPT	65.8	0.02	18.9	0.4	0.02	0.01	5.83	8.30	99.5

Sample	Rock Type	SiO2	TiO2	Al2O3	CaO	SrO	BaO	Na2O	K2O	Total
LC-2004-50cb-c1-1	USPT	66.7	0.02	18.9	0.4	0.01	0.00	5.11	9.57	101
LC-2004-50cb-c1-2	USPT	66.2	0.05	19.2	0.7	0.01	0.06	5.36	9.27	101
LC-2004-50cb-c1-3	USPT	66.4	0.00	18.9	0.5	0.02	0.06	5.11	9.46	101
LC-2004-50cb-c1-4	USPT	66.3	0.02	19.2	0.6	0.00	0.03	5.24	9.29	101
LC-2004-50cb-c2-1	USPT	67.0	0.00	18.7	0.4	0.00	0.02	5.25	9.59	101
LC-2004-50cb-c2-2	USPT	67.0	0.04	18.8	0.5	0.01	0.00	5.83	8.46	101
LC-2004-50cb-c2-3	USPT	66.9	0.04	18.9	0.4	0.00	0.00	5.74	8.59	101
LC-2004-50cb-c2-4	USPT	67.2	0.00	18.9	0.4	0.00	0.02	5.76	8.51	101
LC-2004-50cb-c2-5	USPT	66.8	0.00	19.0	0.5	0.01	0.01	6.13	7.98	101
LC-2004-50cb-c3-1	Pumice in USPT	62.6	0.02	23.1	5.3	0.12	0.12	7.15	1.77	100
LC-2004-50cb-c3-2	Pumice in USPT	61.6	0.02	23.5	5.9	0.06	0.00	6.86	1.96	100
LC-2004-50cb-c3-3	Pumice in USPT	61.9	0.00	23.3	5.5	0.20	0.13	7.39	1.54	100
LC-2004-50cb-c3-4	Pumice in USPT	61.9	0.02	22.9	5.1	0.27	0.09	7.41	1.48	99.4
LC-2004-50cb-c3-5	Pumice in USPT	60.3	0.01	24.4	6.7	0.14	0.10	6.95	1.07	100
LC-2004-50cb-c4-1	Pumice in USPT	59.1	0.03	25.2	7.6	0.22	0.08	6.54	0.90	100
LC-2004-50cb-c4-2	Pumice in USPT	58.9	0.00	24.9	7.4	0.19	0.04	6.47	1.11	99.5
LC-2004-50cb-c4-3	Pumice in USPT	59.3	0.02	25.0	7.4	0.17	0.00	6.49	1.06	99.9
LC-2004-50cb-c4-4	Pumice in USPT	59.5	0.05	24.8	7.2	0.17	0.08	6.65	1.20	100
LC-2004-50cb-c5-1	Pumice in USPT	48.8	0.01	36.7	6.9	0.20	0.04	5.09	0.44	98.5
LC-2004-50cb-c5-2	Pumice in USPT	59.3	0.00	25.1	7.6	0.21	0.11	6.59	1.05	100
LC-2004-50cb-c5-3	Pumice in USPT	59.3	0.02	24.8	7.3	0.19	0.03	6.57	1.07	99.7
LC-2004-50cb-c5-4	Pumice in USPT	59.3	0.06	25.1	7.7	0.14	0.00	6.44	1.04	100
LC-2004-50cb-c6-1	Pumice in USPT	59.0	0.03	25.3	7.9	0.18	0.03	5.43	0.80	99.0
LC-2004-50cb-c6-2	Pumice in USPT	59.8	0.02	24.5	7.0	0.21	0.08	7.03	0.86	99.9
LC-2004-50cb-c6-3	Pumice in USPT	59.6	0.04	24.6	7.1	0.18	0.00	6.06	0.76	98.6
LC-2004-50cb-c6-4	Pumice in USPT	57.7	0.00	25.8	8.7	0.14	0.02	6.20	0.63	99.5
LC-2004-50cb-c6-5	Pumice in USPT	59.6	0.00	24.8	7.2	0.17	0.06	6.66	0.99	99.8
LC-2004-50cb-c6-6	Pumice in USPT	57.3	0.06	26.4	8.9	0.16	0.03	5.99	0.70	99.8
LC-2004-52ca-c1-1	Dacite	56.9	0.09	26.5	8.7	0.21	0.12	6.19	0.62	99.6
LC-2004-52ca-c1-2	Dacite	55.6	0.09	27.2	9.6	0.27	0.05	5.72	0.49	99.4
LC-2004-52ca-c1-3	Dacite	54.5	0.12	28.2	10.6	0.26	0.03	5.21	0.42	99.7

Sample	Rock Type	SiO2	TiO2	Al2O3	CaO	SrO	BaO	Na2O	K2O	Total
LC-2004-52ca-c1-4	Dacite	55.1	0.13	27.6	10.0	0.27	0.04	5.42	0.46	99.5
LC-2004-52ca-c1-5	Dacite	54.4	0.08	27.9	10.2	0.25	0.07	5.17	0.43	98.9
LC-2004-52ca-c1-6	Dacite	55.1	0.05	27.7	10.0	0.27	0.12	5.42	0.48	99.4
LC-2004-52ca-c2-1	Dacite	63.4	0.00	22.6	4.3	0.05	0.01	8.26	1.21	100
LC-2004-52ca-c2-2	Dacite	62.4	0.01	23.2	4.9	0.16	0.00	7.69	1.51	100
LC-2004-52ca-c2-3	Dacite	62.4	0.02	23.5	5.2	0.12	0.04	7.80	1.12	101
LC-2004-52ca-c2-4	Dacite	60.4	0.01	24.5	6.4	0.11	0.01	7.27	0.98	99.9
LC-2004-52ca-c2-5	Dacite	62.6	0.05	22.9	5.0	0.11	0.03	7.70	1.46	100
LC-2004-52ca-c3-1	Dacite	61.4	0.00	23.2	4.8	0.14	0.02	8.03	1.15	99.1
LC-2004-52ca-c3-2	Dacite	62.4	0.04	22.8	4.5	0.16	0.04	7.82	1.62	99.7
LC-2004-52ca-c3-3	Dacite	61.8	0.02	23.2	4.7	0.08	0.05	8.30	0.87	99.4
LC-2004-52ca-c3-4	Dacite	58.3	0.05	26.2	8.3	0.15	0.06	6.31	0.72	100
LC-2004-52ca-c3-5	Dacite	58.8	0.04	25.3	7.3	0.14	0.01	6.81	0.72	99.3
LC-2004-52ca-c3-6	Dacite	63.0	0.03	23.6	4.9	0.11	0.05	8.09	1.10	101
LC-2004-52ca-c4-1	Dacite	62.0	0.01	23.1	4.8	0.13	0.07	7.81	1.32	99.6
LC-2004-52ca-c4-2	Dacite	62.0	0.05	23.0	4.7	0.13	0.04	7.94	1.30	99.5
LC-2004-52ca-c4-3	Dacite	60.9	0.00	23.8	5.5	0.12	0.06	7.66	1.07	99.5
LC-2004-52ca-c4-4	Dacite	60.6	0.02	24.2	6.1	0.12	0.09	7.23	1.12	99.8
LC-2004-52ca-c4-5	Dacite	57.9	0.07	25.4	7.6	0.13	0.06	6.55	0.78	98.8
LC-2004-52ca-c4-6	Dacite	57.7	0.01	25.5	7.4	0.16	0.07	6.52	0.78	98.5
LC-2004-52ca-c5-1	Mafic enclave in dacite	62.2	0.03	23.1	4.7	0.20	0.03	7.64	1.64	99.9
LC-2004-52ca-c5-2	Mafic enclave in dacite	61.3	0.03	23.4	5.3	0.15	0.07	7.49	1.47	99.6
LC-2004-52ca-c5-3	Mafic enclave in dacite	58.7	0.01	25.6	7.6	0.24	0.12	6.63	0.83	100
LC-2004-52ca-c5-4	Mafic enclave in dacite	56.0	0.07	27.1	9.1	0.24	0.07	5.72	0.53	99.1
LC-2004-52ca-c5-5	Mafic enclave in dacite	56.4	0.03	27.0	9.3	0.32	0.05	5.81	0.55	99.7
LC-2004-52ca-c5-6	Mafic enclave in dacite	59.4	0.03	25.0	6.8	0.23	0.09	6.91	0.90	99.7
LC-2004-52ca-c5-7	Mafic enclave in dacite	56.8	0.06	26.6	8.7	0.23	0.08	6.09	0.63	99.5

Sample	Rock Type	SiO2	TiO2	Al2O3	CaO	SrO	BaO	Na2O	K2O	Total
LC-2004-52ca-c6-1	Mafic enclave in dacite	62.4	0.05	22.8	4.5	0.11	0.06	8.08	1.06	99.5
LC-2004-52ca-c6-2	Mafic enclave in dacite	61.9	0.02	23.3	5.0	0.16	0.08	7.72	1.35	99.8
LC-2004-52ca-c6-3	Mafic enclave in dacite	61.7	0.05	23.4	5.7	0.12	0.01	7.48	1.12	99.9
LC-2004-52ca-c6-4	Mafic enclave in dacite	60.7	0.00	23.2	5.1	0.16	0.07	7.80	1.30	98.7
LC-2004-52ca-c6-5	Mafic enclave in dacite	60.3	0.03	24.1	5.8	0.17	0.03	7.27	1.14	99.0
LC-2004-52ca-c6-6	Mafic enclave in dacite	55.5	0.00	27.5	9.7	0.18	0.04	5.50	0.47	99.1
LC-2004-52cb-c1-1	Dacite	58.5	0.06	25.7	8.1	0.19	0.07	6.40	0.76	100
LC-2004-52cb-c1-2	Dacite	55.6	0.16	27.1	9.6	0.26	0.05	5.50	0.76	99.9
LC-2004-52cb-c1-3	Dacite	55.3	0.04	27.7	10.2	0.29	0.05	5.15	0.44	99.5
LC-2004-52cb-c1-4	Dacite	55.5	0.04	27.7	10.0	0.21	0.08	5.42	0.47	99.7
LC-2004-52cb-c2-1	Dacite	62.5	0.02	22.7	4.7	0.17	0.11	7.93	1.25	99.7
LC-2004-52cb-c2-2	Dacite	60.5	0.04	24.2	6.4	0.14	0.12	7.05	1.12	99.8
LC-2004-52cb-c2-3	Dacite	58.7	0.04	25.5	7.7	0.17	0.09	6.43	0.80	99.8
LC-2004-52cb-c2-4	Dacite	58.2	0.05	25.6	8.1	0.20	0.11	6.25	0.75	99.6
LC-2004-52f-c1-1	Pumice in USPT	58.1	0.01	25.8	8.3	0.22	0.09	6.16	0.76	99.8
LC-2004-52f-c1-2	Pumice in USPT	58.1	0.03	26.0	8.5	0.19	0.06	6.21	0.72	100
LC-2004-52f-c1-3	Pumice in USPT	59.0	0.00	24.9	7.3	0.12	0.08	6.61	0.94	99.3
LC-2004-52f-c1-4	Pumice in USPT	58.7	0.00	25.1	7.8	0.23	0.08	6.44	0.86	99.5
LC-2004-52f-c1-5	Pumice in USPT	57.7	0.03	26.0	8.6	0.17	0.08	6.12	0.70	99.7
LC-2004-52f-c2-1	Pumice in USPT	58.9	0.03	25.5	7.9	0.18	0.05	6.39	0.90	100
LC-2004-52f-c2-2	Pumice in USPT	58.6	0.03	25.5	8.0	0.22	0.09	6.34	0.84	100
LC-2004-52f-c2-3	Pumice in USPT	57.9	0.01	26.1	8.4	0.14	0.09	6.21	0.78	100
LC-2004-52f-c2-4	Pumice in USPT	57.6	0.02	26.0	8.4	0.21	0.08	6.02	0.83	99.6
LC-2004-52f-c2-5	Pumice in USPT	57.8	0.00	25.4	8.2	0.15	0.03	6.29	0.86	99.1
LC-2004-52f-c2-6	Pumice in USPT	57.8	0.05	25.9	8.4	0.18	0.00	6.19	0.74	99.5
LC-2004-52f-c3-1	Pumice in USPT	59.3	0.00	25.1	7.6	0.17	0.07	6.55	0.94	100
LC-2004-52f-c3-2	Pumice in USPT	59.2	0.00	25.1	7.6	0.19	0.05	6.53	0.91	99.9
LC-2004-52f-c3-3	Pumice in USPT	58.7	0.00	25.1	7.7	0.18	0.10	6.40	0.93	99.3

Sample	Rock Type	SiO2	TiO2	Al2O3	CaO	SrO	BaO	Na2O	K2O	Total
LC-2004-52f-c3-4	Pumice in USPT	58.8	0.00	25.6	7.9	0.20	0.13	6.41	0.85	100
LC-2004-52f-c4-1	Pumice in USPT	57.9	0.02	25.8	8.3	0.19	0.06	6.24	0.79	99.7
LC-2004-52f-c4-2	Pumice in USPT	57.3	0.03	26.4	8.9	0.19	0.00	5.97	0.72	99.8
LC-2004-52f-c4-3	Pumice in USPT	58.8	0.03	25.1	7.6	0.17	0.11	6.55	0.88	99.6
LC-2004-52f-c4-4	Pumice in USPT	59.0	0.02	25.4	7.6	0.21	0.14	6.78	0.49	100
LC-2004-52f-c5-1	Pumice in USPT	57.9	0.02	26.1	8.4	0.17	0.02	6.09	0.78	99.8
LC-2004-52f-c5-2	Pumice in USPT	57.2	0.03	26.5	9.1	0.18	0.05	5.88	0.67	99.9
LC-2004-52f-c5-3	Pumice in USPT	56.5	0.02	27.2	9.8	0.15	0.02	5.57	0.55	100
LC-2004-52f-c5-4	Pumice in USPT	57.8	0.02	25.9	8.6	0.18	0.06	6.09	0.74	99.7
LC-2004-52f-c5-5	Pumice in USPT	58.0	0.00	26.0	8.5	0.20	0.07	6.13	0.82	100
LC-2004-52f-c5-6	Pumice in USPT	57.4	0.02	26.3	8.9	0.21	0.05	5.92	0.71	99.9
LC-2004-52f-c5-7	Pumice in USPT	57.8	0.03	26.2	8.7	0.15	0.02	5.98	0.73	99.9
LC-2004-52f-c5-8	Pumice in USPT	57.7	0.02	26.1	8.8	0.15	0.08	6.07	0.75	100
LC-2004-52f-c6-1	Pumice in USPT	57.1	0.01	26.1	8.8	0.20	0.05	6.04	0.64	99.5
LC-2004-52f-c6-2	Pumice in USPT	57.7	0.02	25.9	8.6	0.18	0.05	6.02	0.83	99.7
LC-2004-52f-c6-3	Pumice in USPT	57.0	0.02	26.3	8.9	0.19	0.10	5.83	0.72	99.4
LC-2004-52f-c6-4	Pumice in USPT	57.2	0.00	26.2	8.9	0.17	0.04	6.11	0.71	99.6
LC-2004-52f-c6-5	Pumice in USPT	57.6	0.00	25.6	8.3	0.16	0.04	6.19	0.78	98.9
LC-2004-52f-c6-6	Pumice in USPT	58.0	0.02	25.9	8.4	0.16	0.00	6.23	0.80	99.8
LC-2004-52f-c6-7	Pumice in USPT	57.7	0.02	26.1	8.5	0.17	0.06	6.01	0.73	99.7
LC-2004-52f-c7-1	Pumice in USPT	57.5	0.03	25.9	8.5	0.18	0.05	6.19	0.69	99.3
LC-2004-52f-c7-2	Pumice in USPT	56.7	0.00	26.5	9.2	0.19	0.04	5.88	0.58	99.5
LC-2004-52f-c7-3	Pumice in USPT	56.0	0.01	27.2	9.9	0.20	0.09	5.48	0.50	99.7
LC-2004-52f-c7-4	Pumice in USPT	55.1	0.01	27.8	10.5	0.15	0.01	5.18	0.45	99.5
LC-2004-52f-c7-5	Pumice in USPT	57.3	0.02	25.8	8.4	0.12	0.05	6.01	0.83	98.7
LC-2004-52f-c8-1	Pumice in USPT	57.3	0.01	26.2	8.7	0.20	0.04	6.01	0.72	99.5
LC-2004-52f-c8-2	Pumice in USPT	58.1	0.01	25.0	7.6	0.14	0.03	6.45	0.87	98.5
LC-2004-52f-c8-3	Pumice in USPT	56.5	0.02	26.3	8.9	0.14	0.00	5.89	0.70	98.8
LC-2004-52f-c8-4	Pumice in USPT	57.9	0.04	25.5	8.0	0.21	0.04	6.27	0.87	99.1
LC-2004-52f-c8-5	Pumice in USPT	59.3	0.02	24.6	7.1	0.20	0.10	6.76	0.95	99.5
LC-2004-52f-c8-6	Pumice in USPT	58.3	0.04	26.1	8.4	0.19	0.07	6.20	0.79	100

Sample	Rock Type	SiO2	TiO2	Al2O3	CaO	SrO	BaO	Na2O	K2O	Total
LC-2004-52f-c9-1	Pumice in USPT	57.3	0.03	25.8	8.6	0.21	0.09	5.98	0.72	99.1
LC-2004-52f-c9-2	Pumice in USPT	58.5	0.00	25.5	8.2	0.19	0.12	6.39	0.85	100
LC-2004-52f-c9-3	Pumice in USPT	58.1	0.04	25.5	8.2	0.24	0.08	6.34	0.82	99.7
LC-2004-52f-c9-4	Pumice in USPT	57.4	0.03	26.1	8.8	0.18	0.03	5.95	0.71	99.6
LC-2004-52f-c9-5	Pumice in USPT	58.8	0.05	25.0	7.7	0.19	0.12	6.50	0.98	99.7
LC-2004-52f-c9-6	Pumice in USPT	57.5	0.06	26.0	8.8	0.18	0.05	5.98	0.76	99.7
LC-2004-55b-c2-1	Pumice in MSPT	59.5	0.00	25.0	7.3	0.30	0.08	6.68	0.93	100
LC-2004-55b-c2-2	Pumice in MSPT	59.8	0.03	24.8	7.1	0.20	0.07	6.98	0.93	100
LC-2004-55b-c2-3	Pumice in MSPT	59.7	0.00	24.8	7.1	0.18	0.09	6.76	0.92	99.8
LC-2004-55b-c2-4	Pumice in MSPT	59.7	0.02	24.6	7.0	0.24	0.11	6.80	0.93	99.8
LC-2004-57c-c1-1	Pumice in MSPT	66.7	0.01	18.8	0.5	0.04	0.00	5.98	8.15	100
LC-2004-57c-c1-2	Pumice in MSPT	66.7	0.00	18.9	0.5	0.02	0.02	6.10	7.85	100
LC-2004-57c-c1-3	Pumice in MSPT	66.3	0.06	18.8	0.4	0.00	0.00	5.59	8.68	100
LC-2004-57c-c1-4	Pumice in MSPT	66.1	0.02	18.7	0.4	0.01	0.03	5.49	8.99	100
LC-2004-57c-c1-5	Pumice in MSPT	59.7	0.03	24.7	6.9	0.23	0.04	6.93	0.92	99.7
LC-2004-57c-c1-6	Pumice in MSPT	60.6	0.01	25.2	6.4	0.14	0.00	7.30	0.65	101
LC-2004-57c-c1-7	Pumice in MSPT	58.4	0.01	25.5	7.9	0.26	0.07	6.45	0.75	99.7
LC-2004-57c-c1-8	Pumice in MSPT	56.4	0.00	26.1	8.7	0.15	0.01	5.96	0.62	98.2
LC-2004-57c-c1-9	Pumice in MSPT	57.0	0.06	26.6	9.2	0.17	0.02	5.91	0.59	99.8
LC-2004-57c-c2-1	MSPT	66.3	0.01	18.8	0.4	0.00	0.00	5.71	8.64	100
LC-2004-57c-c2-2	MSPT	66.1	0.03	18.7	0.4	0.00	0.01	5.79	8.40	99.6
LC-2004-57c-c2-3	MSPT	66.2	0.00	18.8	0.4	0.01	0.07	5.70	8.39	99.7
LC-2004-57c-c2-4	MSPT	66.1	0.00	18.6	0.4	0.03	0.00	5.83	8.32	99.5
LC-2004-57c-c2-5	MSPT	66.4	0.00	18.8	0.4	0.00	0.00	5.72	8.33	99.9
LC-2004-57c-c3-1	MSPT	60.6	0.03	24.4	6.1	0.25	0.19	7.02	1.65	101
LC-2004-57c-c3-2	MSPT	59.4	0.05	24.4	6.6	0.21	0.14	6.71	1.45	99.4
LC-2004-57c-c3-3	MSPT	60.3	0.08	23.8	6.0	0.26	0.21	6.89	1.75	99.6
LC-2004-57c-c3-4	MSPT	59.4	0.05	24.8	6.9	0.25	0.13	6.74	1.30	99.9
LC-2004-57c-c4-1	MSPT	66.6	0.00	19.0	0.5	0.00	0.02	6.03	8.06	100
LC-2004-57c-c4-2	MSPT	66.2	0.00	18.7	0.4	0.00	0.00	5.76	8.69	99.9
LC-2004-57c-c4-3	MSPT	62.0	0.05	22.7	4.5	0.10	0.10	8.44	1.01	99.1
LC-2004-57c-c4-4	MSPT	59.9	0.05	24.7	6.6	0.12	0.07	7.57	0.60	99.9
LC-2004-57c-c4-5	MSPT	60.3	0.07	24.4	6.4	0.09	0.03	7.55	0.60	99.7
LC-2004-57c-c5-1	MSPT	66.7	0.02	18.7	0.4	0.00	0.03	5.65	8.50	100

Sample	Rock Type	SiO2	TiO2	Al2O3	CaO	SrO	BaO	Na2O	K2O	Total
LC-2004-57c-c5-2	MSPT	66.7	0.00	18.6	0.4	0.01	0.01	5.76	8.32	100
LC-2004-57c-c5-3	MSPT	66.8	0.01	18.9	0.4	0.00	0.03	5.81	8.39	101
LC-2004-57c-c5-4	MSPT	66.9	0.04	18.9	0.5	0.02	0.01	5.89	8.25	101
LC-2004-57c-c5-5	MSPT	66.6	0.00	18.9	0.4	0.00	0.00	5.90	8.20	100
LC-31-c1-1	Monzonite	62.0	0.02	23.1	5.1	0.12	0.07	7.91	1.05	99.7
LC-31-c1-2	Monzonite	62.4	0.01	23.1	4.9	0.12	0.07	7.91	1.32	100
LC-31-c1-3	Monzonite	61.9	0.05	22.6	4.9	0.13	0.00	7.95	1.41	99.2
LC-31-c1-4	Monzonite	61.8	0.04	22.3	4.4	0.09	0.15	6.12	4.51	99.7
LC-31-c2-1	Monzonite	65.6	0.07	18.9	0.4	0.14	0.47	4.13	10.6	100
LC-31-c2-2	Monzonite	65.3	0.09	18.8	0.4	0.12	0.57	4.40	10.1	100
LC-31-c2-3	Monzonite	65.9	0.01	18.8	0.4	0.07	0.51	4.52	10.0	100
LC-31-c2-4	Monzonite	65.9	0.02	18.4	0.1	0.06	0.34	4.07	11.2	100
LC-31-c2-5	Monzonite	65.2	0.06	18.8	0.4	0.10	0.62	4.40	10.3	100
LC-31-c3-1	Monzonite	61.5	0.01	23.2	5.0	0.15	0.08	7.88	1.13	99.3
LC-31-c3-2	Monzonite	61.7	0.01	23.0	5.0	0.13	0.09	7.93	1.30	99.4
LC-31-c3-3	Monzonite	59.1	0.06	24.9	7.0	0.15	0.02	6.95	0.78	99.3
LC-31-c3-4	Monzonite	56.7	0.08	27.0	9.3	0.24	0.09	5.83	0.52	100
LC-31-c4-1	Monzonite	62.0	0.00	23.2	5.0	0.10	0.00	8.19	1.01	99.8
LC-31-c4-2	Monzonite	62.0	0.05	23.1	5.1	0.10	0.06	7.96	1.18	99.9
LC-31-c4-3	Monzonite	61.6	0.04	22.6	5.0	0.08	0.02	7.95	1.41	99.0
LC-31-c4-4	Monzonite	62.1	0.03	23.1	5.1	0.14	0.05	7.74	1.36	100
LC-31-c5-1	Monzonite	65.4	0.05	18.5	0.2	0.07	0.39	4.08	11.0	99.9
LC-31-c5-2	Monzonite	65.4	0.09	18.8	0.3	0.08	0.48	4.22	10.7	100
LC-31-c5-3	Monzonite	65.3	0.05	18.9	0.4	0.08	0.56	4.32	10.4	100
LC-31-c5-4	Monzonite	62.8	0.04	23.0	4.8	0.10	0.03	8.58	0.52	100
LC-31-c5-5	Monzonite	62.6	0.01	22.7	4.7	0.09	0.08	8.32	0.86	99.6
LC-31-c5-6	Monzonite	61.9	0.03	22.6	4.7	0.14	0.00	8.38	0.95	99.1
LC-31-c5-7	Monzonite	62.5	0.03	22.9	4.8	0.08	0.02	8.48	0.80	99.9
LC-31-c5-8	Monzonite	65.2	0.06	18.6	0.4	0.14	0.51	4.22	10.2	99.6
LC-34b-c1-1	LSPT	66.5	0.02	18.8	0.4	0.00	0.00	5.89	8.34	100
LC-34b-c1-2	LSPT	66.2	0.02	18.8	0.4	0.00	0.00	5.51	8.94	100
LC-34b-c1-3	LSPT	66.1	0.04	18.8	0.4	0.02	0.01	5.64	8.90	100
LC-34b-c1-4	LSPT	66.2	0.00	18.9	0.5	0.04	0.00	5.98	8.16	99.9

Sample	Rock Type	SiO2	TiO2	Al2O3	CaO	SrO	BaO	Na2O	K2O	Total
LC-34b-c1-5	LSPT	66.1	0.00	18.8	0.5	0.02	0.00	5.97	8.23	99.7
LC-34b-c1-6	LSPT	66.5	0.03	18.9	0.4	0.04	0.02	5.99	8.18	100
LC-34b-c2-1	LSPT	66.1	0.00	18.9	0.4	0.00	0.02	5.78	8.46	99.9
LC-34b-c2-2	LSPT	66.9	0.06	18.9	0.4	0.00	0.06	5.94	8.31	101
LC-34b-c2-3	LSPT	66.5	0.01	18.8	0.4	0.00	0.00	5.67	8.74	100
LC-34b-c2-4	LSPT	66.2	0.04	18.9	0.4	0.02	0.02	5.86	8.41	100
LC-34b-c4-1	Mafic pumice in LSPT	58.5	0.06	25.6	7.7	0.29	0.23	6.30	1.29	100
LC-34b-c4-2	Mafic pumice in LSPT	57.8	0.09	26.0	8.2	0.32	0.26	5.95	1.12	100
LC-34b-c4-3	Mafic pumice in LSPT	56.4	0.11	27.2	9.5	0.34	0.13	5.41	0.83	100
LC-34b-c4-4	Mafic pumice in LSPT	57.6	0.09	26.1	8.5	0.30	0.21	5.95	1.10	100
LC-34b-c5-1	LSPT	66.2	0.02	19.2	0.6	0.00	0.02	6.48	7.19	99.9
LC-34b-c5-2	LSPT	66.3	0.00	18.8	0.4	0.03	0.02	5.54	8.97	100
LC-34b-c5-3	LSPT	66.6	0.01	18.8	0.4	0.00	0.01	5.68	8.59	100
LC-34b-c5-4	LSPT	65.9	0.04	19.1	0.5	0.00	0.00	6.20	7.91	99.9
LC-34b-c5-5	LSPT	67.0	0.03	19.0	0.6	0.02	0.00	6.34	7.72	101
LC-34b-c5-6	LSPT	66.9	0.03	19.1	0.7	0.04	0.01	6.34	7.34	101
LC-81-c1-1	Rhyolite dyke	65.6	0.01	18.8	0.5	0.00	0.00	5.82	8.27	99.2
LC-81-c1-2	Rhyolite dyke	66.1	0.02	18.7	0.4	0.01	0.02	5.71	8.73	99.8
LC-81-c1-3	Rhyolite dyke	66.4	0.00	18.7	0.4	0.00	0.00	5.93	8.04	99.7
LC-81-c1-4	Rhyolite dyke	66.0	0.02	18.7	0.4	0.04	0.00	5.61	8.35	99.3
LC-81-c1-5	Rhyolite dyke	66.6	0.01	18.7	0.4	0.04	0.02	5.84	8.33	100
LC-81-c2-1	Rhyolite dyke	65.6	0.01	18.6	0.3	0.00	0.04	5.33	9.10	99.1
LC-81-c2-2	Rhyolite dyke	66.1	0.02	18.8	0.4	0.02	0.00	5.62	8.63	99.8
LC-81-c2-3	Rhyolite dyke	66.4	0.02	18.7	0.3	0.02	0.00	5.53	8.98	100
LC-81-c2-4	Rhyolite dyke	66.6	0.00	18.8	0.4	0.00	0.06	5.82	8.46	100
LC-81-c2-5	Rhyolite dyke	66.6	0.03	19.3	0.2	0.00	0.00	6.34	7.77	100
LC-81-c3-1	Rhyolite dyke	65.5	0.01	18.9	0.5	0.03	0.00	5.68	8.36	99.2
LC-81-c3-2	Rhyolite dyke	66.2	0.00	18.6	0.4	0.03	0.00	5.70	8.64	99.7
LC-81-c3-3	Rhyolite dyke	65.9	0.02	18.8	0.5	0.01	0.00	5.68	8.41	99.4
LC-81-c3-4	Rhyolite dyke	65.9	0.01	18.8	0.4	0.01	0.00	5.78	8.35	99.5
LC-81-c3-5	Rhyolite dyke	66.1	0.05	18.9	0.6	0.00	0.00	6.22	7.59	99.6
LC-94-C2-1	Monzonite	98.9	0.01	0.0	0.0	0.00	0.03	0.01	0.02	99.1

Sample	Rock Type	SiO2	TiO2	Al2O3	CaO	SrO	BaO	Na2O	K2O	Total
LC-94-C2-2	Monzonite	62.5	0.02	22.9	4.8	0.10	0.07	8.12	1.06	99.8
LC-94-C2-3	Monzonite	62.2	0.03	23.1	4.8	0.14	0.07	7.78	1.37	99.8
LC-94-C2-4	Monzonite	62.1	0.00	23.2	5.2	0.14	0.07	7.81	1.12	99.9
LC-94-C2-5	Monzonite	56.5	0.05	26.7	9.3	0.12	0.05	5.94	0.45	99.4
LC-94-c3-1	Monzonite	63.7	0.00	22.3	4.1	0.09	0.01	8.59	0.89	100
LC-94-c3-2	Monzonite	62.3	0.04	22.9	5.0	0.13	0.00	8.01	1.22	99.9
LC-94-c3-3	Monzonite	62.4	0.00	23.0	4.9	0.09	0.07	7.89	1.15	99.8
LC-94-c3-4	Monzonite	62.0	0.04	23.1	5.0	0.09	0.00	7.86	1.19	99.6
LC-94-c4-1	Monzonite	64.1	0.01	22.3	3.8	0.11	0.04	8.77	0.97	100
LC-94-c4-2	Monzonite	62.4	0.04	23.0	4.9	0.09	0.02	7.76	1.37	99.8
LC-94-c4-3	Monzonite	62.7	0.00	22.8	4.8	0.11	0.04	7.72	1.48	100
LC-94-c4-4	Monzonite	62.6	0.04	22.9	4.8	0.13	0.06	7.73	1.45	100
LC-94-c5-1	Monzonite	63.2	0.04	22.4	4.4	0.12	0.00	8.43	0.83	99.8
LC-94-c5-2	Monzonite	62.3	0.04	23.2	5.2	0.12	0.03	7.96	0.95	100
LC-94-c5-3	Monzonite	62.5	0.05	22.9	4.9	0.11	0.03	7.99	1.18	99.9
LC-94-c5-4	Monzonite	60.8	0.03	24.2	6.2	0.13	0.03	7.47	0.83	100

Biotite

Table 7: Biotite electron microprobe analyses

Sample	Unit	SiO2	Na2O	CaO	Cl	FeO	MgO	TiO2	K2O	MnO	Al2O3	SrO	BaO	Total
10B_bt1.1	Syenite	35.6	0.633	0.034	0.115	15.2	13.2	6.92	7.39	0.255	14.7	0.0091	2.49	96.5
10B_bt1.2	Syenite	35.2	0.676	0.044	0.080	15.5	12.7	7.75	7.25	0.271	14.5	0.0458	2.45	96.5
10B_bt1.3	Syenite	35.9	0.662	0.006	0.092	15.1	13.1	7.38	7.58	0.270	14.5	0.0148	2.64	97.2
10B_bt1.4	Syenite	35.5	0.579	0.020	0.134	14.2	13.8	7.4	7.48	0.254	14.2	0.0082	2.36	96.1
10B_bt1.5	Syenite	36.1	0.606	0.012	0.116	13.4	14.8	6.23	7.91	0.251	14.2	0	2.15	95.8
10B_bt2.1	Syenite	36	0.572	0.000	0.143	14.4	14.8	5.86	7.85	0.255	14.2	0.025	1.75	95.3
10B_bt2.3	Syenite	36.6	0.627	0.012	0.093	13.0	15.6	5.79	8.15	0.262	13.9	0	1.29	95.8
10B_bt2.4	Syenite	36.6	0.634	0.000	0.114	13.6	15.4	5.67	7.96	0.309	14.1	0.0223	1.58	95.8
10B_bt2.5	Syenite	36.6	0.621	0.016	0.080	13.6	15.3	5.93	7.94	0.261	14.0	0	1.77	95.9
10B_bt2.6	Syenite	36.0	0.675	0.018	0.132	15.0	14.3	6.04	7.88	0.303	14.2	0.0254	1.84	96.5
152_bt1.1	LSPT	36.1	0.561	0.000	0.107	15.6	13.0	7.26	7.74	0.184	14.2	0.0174	2.14	97.2
152_bt1.2	LSPT	35.8	0.635	0.006	0.124	16.0	12.8	7.76	7.69	0.239	14.6	0.0569	2.68	98.5
15D_bt2.1	LSPT	36.8	0.658	0.045	0.055	15.9	12.5	7.44	7.77	0.304	13.7	0.0355	1.54	96.7

Sample	Unit	SiO_2	Na_2O	CaO	Cl	FeO	MgO	TiO_2	K_2O	MnO	Al_2O_3	SrO	BaO	Total
15D_bt2.2	LSPT	36.54	0.594	0.041	0.071	15.9	13.1	7.15	7.81	0.329	13.8	0.0148	1.42	96.8
15D_bt2.3	LSPT	36.5	0.543	0.009	0.14	15.8	13.4	6.23	7.75	0.325	14.0		1.67	96.3
15D_bt2.4	LSPT	36.	0.453	0.078	0.179	17.0	13.5	4.9	7.48	0.368	14.1	0.0036	1.6	96.1
15D_bt3.1	LSPT	36.4	0.595	0.006	0.156	16.1	13.2	6.56	7.78	0.461	13.9		1.94	97.1
15D_bt3.2	LSPT	36.5	0.561	0.002	0.191	16.0	13.3	6.08	7.92	0.541	13.7		1.88	96.8
15D_bt3.3	LSPT	36.	0.584	0.020	0.173	16.4	12.9	6.27	7.94	0.477	13.8		2.03	97.1
15D_bt3.4	LSPT	37.3	0.565	0.004	0.201	16.2	13.5	5.39	8.06	0.533	13.6		1.24	96.7
15D_bt3.5	LSPT	36.0	0.498	0.027	0.204	16.6	14.0	5.94	7.77	0.641	13.3	0.000	1.76	96.8
15D2_bt1.1	LSPT	36.4	0.586	0.050	0.101	15.3	13.1	6.9	7.67	0.342	14.4	0.0006	2.59	97.5
15D2_bt1.2	LSPT	36.0	0.571	0.034	0.119	15.5	13.2	7.26	7.59	0.363	14.3	0.0517	2.37	97.4
15D2_bt1.3	LSPT	35.6	0.629	0.086	0.121	16.8	12.2	7.8	7.21	0.40	14.3	0.0386	2.75	97.9
15D2_bt1.4	LSPT	35.8	0.661	0.069	0.122	16.8	12.0	7.84	7.3	0.406	14.2		2.88	98.1
15D2_bt1.5	LSPT	38.7	0.617	0.020	0.143	16.0	12.0	6.89	7.45	0.395	13.6	0.0299	2.29	98.2
15D2_bt2.1	LSPT	38.0	0.616	0.015	0.146	15.5	14.1	5.87	8.37	0.239	13.5	0.0070	0.68	97.1
15D2_bt2.10	LSPT	38.5	0.496	0.055	0.202	14.8	14.9	5.08	8.58	0.261	13.3	0.0588	0.95	96.5
15D2_bt2.2	LSPT	37.4	0.525	0.735	0.115	15.5	13.1	6.97	7.94	0.273	13.1	0.0585	1.01	96.7
15D2_bt2.3	LSPT	37.4	0.670	0.023	0.088	16.2	13.1	7.15	8.17	0.273	13.7		1.03	97.8
15D2_bt2.4	LSPT	38.0	0.551	0.017	0.170	15.2	14.4	5.74	8.48	0.310	13.3	0.0079	0.33	96.6
15D2_bt2.6	LSPT	36.8	0.486	0.000	0.182	16.1	13.2	6.43	7.95	0.287	13.7		1.99	97.1
15D2_bt2.7	LSPT	38.2	0.543	0.042	0.159	15.0	14.7	5.13	8.49	0.265	13.4	0.0177	0.35	96.3
15D2_bt2.8	LSPT	38.0	0.472	0.123	0.156	15.1	15.2	4.65	8.26	0.301	13.6	0.0105	0.48	96.4
16C_bt1.1	Unknown	35.8	0.504	0.024	0.217	16.2	12.8	6.91	7.78	0.170	14.2		2.39	97.1
16C_bt1.2	Unknown	35.6	0.526	0.000	0.215	16.1	12.6	6.89	7.74	0.174	14.3	0.0069	2.44	96.6
16C_bt1.3	Unknown	35.6	0.543	0.002	0.180	16.0	12.8	7.13	7.78	0.204	14.2		2.22	96.7
16C_bt1.4	Unknown	36.0	0.571	0.009	0.168	16.0	13.1	6.27	7.66	0.177	13.9	0.0518	1.96	96.2
16C_bt2.1	Unknown	37.4	0.230	0.112	0.216	17.2	13.8	4.74	8.37	0.179	13.6		1.15	97.0
16C_bt2.2	Unknown	36.9	0.288	0.016	0.230	17.5	13.4	4.94	8.28	0.200	13.9	0.0179	1.46	97.2
16C_bt2.3	Unknown	36.5	0.214	0.633	0.215	17.3	13.1	4.77	8.24	0.180	13.6	0.0229	1.31	96.2
16C_bt2.4	Unknown	35.0	0.251	0.012	0.233	21.5	13.0	4.56	7.66	0.175	13.3		1.41	97.2
16C_bt3.2	Unknown	35.8	0.511	0.069	0.206	16.6	13.3	5.79	7.88	1.142	13.9		1.92	97.3
16C_bt3.3	Unknown	36.8	0.520	0.031	0.237	17.0	13.5	5.47	8.04	0.225	14.1		1.53	97.5
16C_bt3.4	Unknown	39.2	0.378	0.020	0.187	14.6	16.4	3.85	8.45	0.165	12.7	0.0241	0.61	96.6
16C_bt3.5	Unknown	36.2	0.450	0.024	0.230	17.5	13.0	5.36	7.83	0.203	14.4	0.0007	2.57	97.8
40A2_bt1.1	USPT	36.8	0.671	0.000	0.070	15.6	13.4	6.42	8.07	0.626	14.2	0.0059	1.44	97.3
40A2_bt1.2	USPT	36.8	0.707	0.000	0.046	15.3	13.6	6.58	8.01	0.618	14.4		1.53	97.7
40A2_bt1.3	USPT	37.0	0.662	0.001	0.085	14.1	14.5	6.36	7.94	0.556	14.2		1.55	97.1

Sample	Unit	SiO2	Na2O	CaO	Cl	FeO	MgO	TiO2	K2O	MnO	Al2O3	SrO	BaO	Total
40A2_bt1.4	USPT	37.4	0.596	0.006	0.105	14.6	14.7	5.78	8.17	0.518	14.0	0	0.97	96.9
40A2_bt1.5	USPT	38.2	0.745	0.005	0.132	14.0	15.3	5.31	8.42	0.419	13.6	0.035	0.24	96.5
40A2_bt2.1	USPT	37.2	0.703	0.026	0.037	13.5	14.2	7.25	8.07	0.303	14.1	0.014	1.18	96.6
40A2_bt2.2	USPT	37.3	0.737	0.016	0.038	13.7	14.2	7.24	7.99	0.266	14.2	0.011	1.28	96.9
40A2_bt2.3	USPT	37.4	0.783	0.023	0.030	13.5	14.4	7.33	8.18	0.242	14.3	0.026	1.01	97.3
40A2_bt2.4	USPT	37.4	0.702	0.008	0.021	13.5	14.7	7.2	8.17	0.228	14.3	0	0.80	97.0
40A2_bt2.5	USPT	37.8	0.736	0.031	0.030	13.4	14.5	7.28	8.09	0.220	14.1	0	0.78	97.0
40A3_bt1.1	USPT	37.5	0.842	0.008	0.056	13.5	14.9	6.74	8.25	0.325	13.8	0.006	0.33	96.4
40A3_bt1.2	USPT	37.9	0.746	0.009	0.039	13.3	14.7	6.62	8.32	0.356	13.6	0	0.25	95.9
40A3_bt1.3	USPT	37.5	0.782	0.000	0.057	13.3	14.6	6.64	8.32	0.403	13.6	0.003	0.24	95.5
40A3_bt1.4	USPT	37.8	0.789	0.020	0.051	13.6	14.8	6.66	8.34	0.304	13.7	0	0.41	96.5
40A3_bt2.1	USPT	36.6	0.731	0.003	0.055	14.1	14.0	7.37	7.92	0.361	14.4	0	1.67	97.3
40A3_bt2.2	USPT	36.9	0.792	0.004	0.029	13.8	14.3	7.36	8.05	0.354	14.3	0.016	1.32	97.2
40A3_bt2.3	USPT	37.1	0.774	0.042	0.042	13.7	14.9	6.74	8.29	0.383	13.7	0.018	0.49	96.2
40A3_bt3pt.1	USPT	36.4	0.691	0.016	0.142	15.3	14.2	5.45	7.9	0.483	14.1	0	1.69	96.4
40A3_bt3pt.2	USPT	36.8	0.675	0.013	0.107	15.6	14.1	5.54	8.09	0.572	14.0	0	1.05	96.5
40A3_bt3pt.3	USPT	36.8	0.674	0.015	0.141	15.4	14.4	5.28	8.09	0.458	14.2	0	1.18	96.7
40A3_bt3pt.4	USPT	37.7	0.646	0.003	0.125	14.6	15.2	4.63	8.23	0.467	13.8	0	0.51	95.9
40B_bt1.1	USPT	37.6	0.707	0.012	0.049	14.0	14.2	6.67	8.06	0.316	14.3	0	1.19	97.2
40B_bt1.2	USPT	37.5	0.725	0.000	0.035	14.0	14.2	6.66	8.04	0.327	14.2	0	1.03	96.8
40B_bt1.3	USPT	35.7	0.607	0.015	0.032	15.0	14.8	5.66	6.81	0.501	14.9	0	0.95	95.1
40B_bt2.1	USPT	36.7	0.720	0.022	0.043	13.3	13.8	7.69	7.67	0.188	14.8	0	2.25	97.3
40B_bt2.2	USPT	36.4	0.765	0.014	0.031	13.4	14.0	7.91	7.67	0.220	14.7	0.007	2.15	97.3
40B_bt2.3	USPT	36.6	0.756	0.000	0.041	13.5	14.0	7.79	7.73	0.229	14.9	0.003	2.25	97.9
40B_bt2.4	USPT	36.4	0.713	0.012	0.018	14.0	13.9	7.82	7.7	0.269	14.7	0.040	2.1	97.7
40B_bt2.5	USPT	37.3	0.714	0.000	0.015	13.6	14.5	7.63	7.96	0.243	14.3	0.029	1.41	97.7
40B_bt2.6	USPT	36.6	0.703	0.021	0.039	15.3	13.2	7.5	7.9	0.455	14.1	0	1.29	97.3
40B_bt3.1	USPT	36.3	0.753	0.013	0.074	14.2	14.0	6.85	7.93	0.423	14.2	0.043	1.28	96.1
40B_bt3.2	USPT	35.9	0.746	0.003	0.066	14.4	13.9	6.95	7.73	0.417	14.6	0.026	1.56	96.4
40B_bt3.3	USPT	37.5	0.697	0.020	0.036	15.0	13.6	6.55	8.06	0.451	13.7	0.000	0.36	96.0
40B_bt4.1	USPT	36.8	0.775	0.002	0.055	14.1	14.6	6.38	8.02	0.294	14.2	0.014	1.24	96.6
40B_bt4.2	USPT	37.1	0.632	0.145	0.067	13.9	14.3	6.51	7.68	0.319	14.4	0	1.25	96.3
40B_bt4.3	USPT	36.9	0.705	0.109	0.052	14.1	14.4	6.45	7.89	0.310	14.3	0.013	1.63	96.9
40B_bt4.4	USPT	37.3	0.714	0.042	0.055	14.3	14.2	6.17	7.85	0.345	14.3	0	1.42	96.9
40B_bt4.5	USPT	37.5	0.751	0.003	0.048	14.2	14.5	6.26	8.01	0.414	14.0	0	1.23	96.9
7B_bt1.3	Syenite	37.7	0.697	0.000	0.167	14.8	15.4	4.08	8.51	0.422	13.3	0.034	0.23	95.4

Sample	Unit	SiO2	Na2O	CaO	Cl	FeO	MgO	TiO2	K2O	MnO	Al2O3	SrO	BaO	Total
7B_bt1.4	Syenite	36.6	0.562	0.006	0.172	15.1	14.6	4.56	8.04	0.464	13.7	0	1.63	95.5
7B_bt2.1	Syenite	39.0	0.642	0.012	0.130	13.3	17.0	3.31	8.44	0.42	12.6	0	0	95.0
7B_bt2.3	Syenite	39.1	0.720	0.000	0.151	13.5	16.6	3.5	8.57	0.420	12.4	0.0156	0	95.0
7B_bt2.5	Syenite	38.8	0.733	0.000	0.125	14.0	16.1	4	8.56	0.474	12.6	0.0001	0.05	95.6
7B_bt3.1	Syenite	36.0	0.698	0.010	0.143	14.9	13.8	5.97	7.85	0.439	14.2	0.0228	2.08	96.1
7B_bt3.2	Syenite	35.8	0.665	0.016	0.132	15.6	13.4	6.17	7.71	0.519	14.3	0.0209	1.99	96.4
7B_bt3.3	Syenite	36.0	0.618	0.010	0.116	15.7	13.5	6.43	7.86	0.514	14.0	0	1.88	96.7
7B_bt3.4	Syenite	35.5	0.709	0.039	0.158	15.8	13.1	6.11	7.74	0.479	14.0	0	1.86	95.6

Oxides

Table 8: Oxide electron microprobe analyses

Sample	SiO2	MgO	Cr2O3	TiO2	FeO	Al2O3	NiO	CaO	MnO	V2O3	Total
10B_oxide1.1	0.61	0.043	0.000	6.6	84.0	0.99	0	0.046	0.07	0.344	92.7
10B_oxide1.2	1.27	0.035	0.000	7.1	80.9	1.9	0	0.111	0.09	0.218	91.7
10B_oxide1.3	2.90	0.082	0.000	6.4	79.6	0.66	0	0.161	0.08	0.162	90.0
10B_oxide1.4	1.22	0.039	0.123	8.1	79.8	0.58	0	0.155	0.08	0.210	90.4
10B_oxide1.5	1.03	0.007	0.000	10.4	79.2	0.17	0	0.087	0.08	0.318	91.2
10B_oxide1.6	0.41	0.081	0.010	0.1	0.9	0.00	0	55.0	0.12	0.000	56.6
10B_oxide1.7	0.36	0.056	0.000	0.1	0.9	0.00	0.0457	54.8	0.14	0.034	56.4
10B_oxide2.1	2.00	0.056	0.024	6.9	81.4	0.30	0	0.138	0.06	0.303	91.2
10B_oxide2.2	0.94	0.045	0.022	8.3	80.5	0.19	0	0.118	0.05	0.368	90.5
10B_oxide2.3	1.73	0.022	0.000	5.2	81.7	0.35	0	0.174	0.06	0.191	89.4
10B_oxide2.4	1.27	0.000	0.031	4.0	85.0	0.40	0	0.100	0.04	0.265	91.2
10B_oxide2.5	0.48	0.033	0.006	10.0	80.9	0.25	0	0.063	0.06	0.334	92.1
10B_oxide2.6	0.11	0.043	0.000	95.3	1.3	0.14	0.0202	0.694	0.02	0.822	98.5
10B_oxide2.7	5.00	4.91	0.034	68.4	6.8	4.91	0	0.673	0.10	0.601	91.3
10B_oxide2.8	3.31	3.17	0.000	79.7	4.6	3.53	0.0154	0.520	0.08	0.610	95.5
10B_oxide3.1	0.53	0.024	0.011	8.3	82.2	0.25	0	0.059	0.06	0.354	91.8
10B_oxide3.10	0.11	0.011	0.027	96.6	1.6	0.00	0.0236	0.070	0.01	0.796	99.2
10B_oxide3.2	1.28	0.036	0.000	8.7	79.9	0.31	0	0.096	0.09	0.261	90.7
10B_oxide3.3	2.42	0.007	0.000	7.1	78.9	0.26	0	0.139	0.04	0.308	89.1
10B_oxide3.4	0.50	0.000	0.007	9.0	82.1	0.21	0	0.054	0.06	0.308	92.3
10B_oxide3.5	1.19	0.050	0.000	4.9	85.3	0.46	0	0.121	0.05	0.308	92.4
10B_oxide3.6	0.80	0.020	0.040	5.5	84.6	0.26	0	0.076	0.05	0.203	91.5
10B_oxide3.7	0.11	0.000	0.010	95.6	1.7	0.04	0.0231	0.074	0.00	0.767	98.3
10B_oxide3.8	0.07	0.006	0.000	96.9	0.9	0.07	0.0304	0.252	0.02	0.902	99.2
10B_oxide3.9	0.11	0.018	0.000	96.5	1.6	0.04	0	0.083	0.00	0.826	99.2
10B_oxide4.1	0.43	0.018	0.015	8.4	82.3	0.36	0	0.051	0.09	0.256	91.9

Sample	SiO2	MgO	Cr2O3	TiO2	FeO	Al2O3	NiO	CaO	MnO	V2O3	Total
10B_oxide4.4	0.21	0.064	0.004	7.3	83.3	0.98	0	0.023	0.08	0.314	92.2
10B_oxide4.5	0.62	0.015	0.027	5.5	85.1	0.34	0	0.100	0.05	0.228	92.0
10B_oxide4.6	0.48	0.028	0.026	7.5	82.7	0.20	0	0.127	0.11	0.200	91.4
10B_oxide4.7	0.37	0.007	0.000	6.5	85.3	0.19	0	0.014	0.09	0.178	92.7
10B_oxide4.8	1.49	0.043	0.011	5.8	83.0	0.50	0	0.080	0.11	0.314	91.3
13A_oxide1.1	1.88	0.000	0.000	86.4	3.6	0.44	0	0.175	0.06	0.671	93.2
13A_oxide1.2	0.90	0.018	0.000	87.5	4.7	0.33	0.0018	0.069	0.02	0.779	94.3
13A_oxide1.3	1.60	0.000	0.000	87.9	3.0	0.42	0.0067	0.200	0.07	0.541	93.8
13A_oxide2.1	0.24	0.067	0.042	56.1	25.6	0.49	0	0.065	0.62	0.631	83.9
13A_oxide2.2	0.23	0.221	0.000	58.0	24.5	0.41	0	0.049	0.64	0.671	84.8
13A_oxide2.3	0.31	0.044	0.069	55.9	25.4	0.45	0	0.052	0.51	0.641	83.3
13A_oxide2.4	0.26	0.061	0.039	59.3	27.9	0.50	0	0.050	0.68	0.679	89.4
13A_oxide2.5	0.22	0.089	0.049	54.5	24.6	0.41	0	0.058	1.05	0.794	81.8
13A_oxide3.1	0.15	0.093	0.027	53.1	30.7	0.27	0	0.028	0.71	0.535	85.6
13A_oxide3.2	2.89	0.165	0.023	52.4	27.4	1.88	0	0.134	0.99	0.559	86.5
13A_oxide3.3	0.15	0.080	0.000	54.5	28.4	0.34	0	0.064	0.61	0.634	84.8
13A_oxide3.4	0.27	0.094	0.002	58.1	29.0	0.47	0	0.039	0.40	0.692	89.0
13A_oxide3.5	0.24	0.596	0.018	56.5	26.6	0.51	0	0.064	0.61	0.588	85.7
13A_oxide3.6	0.18	0.075	0.000	52.5	30.2	0.31	0	0.063	0.85	0.492	84.7
13A_oxide3.7	0.31	0.109	0.019	57.3	27.1	0.41	0	0.081	0.64	0.568	86.6
13A_oxide3.8	0.25	0.332	0.009	55.6	29.8	0.18	0	0.049	0.70	0.537	87.5
13A_oxide4.1	1.39	0.003	0.000	87.1	3.8	0.43	0.0085	0.164	0.06	0.726	93.7
13A_oxide4.2	1.79	0.003	0.027	86.4	3.8	0.48	0	0.162	0.08	0.801	93.5
13A_oxide4.3	2.71	0.000	0.010	85.2	3.3	0.83	0	0.181	0.08	0.698	92.9
13A_oxide4.4	1.30	0.000	0.000	87.3	4.2	0.36	0	0.110	0.01	0.695	94.0
16C_oxide1.1	0.07	0.023	0.000	3.1	89.4	0.61	0	0.012	0.06	0.286	93.5
16C_oxide1.2	0.06	0.000	0.076	3.0	89.8	0.51	0	0.000	0.07	0.224	93.7
16C_oxide1.3	0.06	0.000	0.000	2.6	89.8	0.54	0	0.000	0.18	0.207	93.4
16C_oxide1.5	0.04	0.002	0.000	72.5	22.9	0.04	0	0.014	0.37	0.820	96.7
16C_oxidecluster1.1	4.38	0.127	0.012	1.2	87.6	1.94	0	0.119	0.00	0.617	96.0
16C_oxidecluster1.2	0.05	0.031	0.000	42.9	49.7	0.04	0	0.048	3.43	0.454	96.6
16C_oxidecluster1.3	0.05	0.092	0.000	42.4	50.8	0.03	0	0.020	3.45	0.472	97.3
16C_oxidecluster1.4	0.08	0.009	0.000	6.7	85.1	0.37	0	0.037	0.28	0.644	93.3
16C_oxidecluster1.5	4.47	0.203	0.000	40.1	45.5	1.72	0	0.146	4.07	0.338	96.6
40A_oxide1.1	0.47	0.189	0.023	2.6	88.1	1.11	0	0.074	0.09	0.287	92.9
40A_oxide1.2	1.05	0.049	0.024	8.0	81.1	0.63	0	0.175	0.08	0.132	91.3
40A_oxide1.3	1.16	0.233	0.040	26.9	55.2	0.81	0	0.202	0.18	0.325	85.1
40A_oxide1.4	0.51	0.005	0.136	8.5	81.9	1.20	0	0.091	0.12	0.429	92.9

Sample	SiO2	MgO	Cr2O3	TiO2	FeO	Al2O3	NiO	CaO	MnO	V2O3	Total
40A_oxide2.2	0.44	0.013	0.000	9.3	80.9	0.76	0	0.034	0.12	0.357	92.0
40A_oxide2.3	0.25	0.036	0.000	6.1	85.3	0.66	0	0.011	0.14	0.390	92.9
40A_oxide2.4	0.11	0.019	0.054	5.3	85.0	1.34	0	0.033	0.14	0.344	92.3
40A_oxide2.5	0.35	0.176	0.000	0.1	0.5	0.00	0	55.1	0.21	0.000	56.4
40A_oxide3.1	0.38	0.020	0.016	5.8	83.5	0.58	0	0.041	0.18	0.403	90.9
40A_oxide3.2	1.60	0.085	0.000	7.0	81.0	0.66	0	0.079	0.09	0.288	90.8
40A_oxide3.3	0.25	0.023	0.035	4.8	84.5	0.61	0	0.047	0.15	0.247	90.6
40A_oxide3.4	0.36	0.115	0.000	4.1	86.1	0.97	0	0.021	0.09	0.288	92.0
40A_oxide3.5	0.84	0.071	0.000	0.1	0.4	0.00	0	53.4	0.25	0.006	55.0
40A_oxide3.6	1.01	0.073	0.000	0.0	0.4	0.01	0	53.1	0.26	0.034	54.9
40A_oxide4.1	0.75	0.036	0.054	5.3	85.1	0.79	0	0.100	0.05	0.336	92.5
40A_oxide4.2	0.42	0.090	0.000	8.2	79.8	0.87	0	0.026	0.13	0.365	89.9
40A_oxide4.3	0.50	0.014	0.004	4.8	85.8	0.60	0	0.056	0.15	0.130	92.0
40A_oxide4.4	0.38	0.022	0.000	3.5	88.0	0.94	0	0.116	0.15	0.271	93.4
40A_oxide4.5	1.64	0.023	0.000	14.7	72.4	0.59	0	0.280	0.09	0.252	90.0
40A_oxidecluster1.1	0.49	0.534	0.000	3.4	85.1	3.46	0	0.026	0.13	0.458	93.5
40A_oxidecluster1.2	0.95	0.040	0.028	6.9	82.6	0.50	0	0.138	0.15	0.262	91.5
40A_oxidecluster1.3	1.07	0.005	0.016	8.9	81.6	0.59	0	0.133	0.18	0.361	92.8
40A_oxidecluster1.4	0.78	0.028	0.000	8.3	82.0	0.59	0	0.108	0.13	0.208	92.1
40A_oxidecluster1.5	0.73	0.075	0.173	40.0	46.5	0.21	0	0.052	1.66	0.488	89.8
40A3_oxide1.1	1.13	0.000	0.000	26.3	62.9	0.23	0	0.155	0.10	0.295	91.1
40A3_oxide1.2	0.99	0.033	0.000	8.9	80.2	1.05	0	0.207	0.12	0.221	91.8
40A3_oxide1.3	0.89	0.040	0.000	13.7	73.5	0.66	0	0.133	0.13	0.324	89.4
40A3_oxide1.4	0.16	0.013	0.000	8.7	82.4	0.90	0	0.019	0.18	0.352	92.8
40A3_oxide1.5	0.08	0.023	0.000	8.1	83.4	1.03	0	0.000	0.15	0.275	93.0
40A3_oxide1.6	0.28	0.000	0.000	7.2	84.7	0.58	0	0.028	0.12	0.232	93.1
40A3_oxide2.1	1.51	0.430	0.071	26.8	57.7	0.87	0	0.170	0.64	0.328	88.5
40A3_oxide2.2	0.34	0.012	0.000	3.9	88.1	0.60	0	0.039	0.11	0.396	93.4
40A3_oxide2.3	0.49	0.059	0.000	11.6	78.8	0.63	0	0.072	0.15	0.415	92.3
40A3_oxide2.4	0.08	0.028	0.076	3.1	88.5	1.03	0	0.358	0.08	0.333	93.6
40A3_oxide2.5	0.67	0.016	0.033	11.4	78.5	0.49	0	0.130	0.13	0.313	91.7
40A3_oxide3.1	0.53	0.004	0.000	6.6	84.6	1.02	0	0.111	0.09	0.257	93.2
40A3_oxide3.2	0.42	0.027	0.028	7.6	83.2	0.62	0	0.119	0.08	0.275	92.4
40A3_oxide3.3	0.75	0.086	0.004	10.0	81.7	0.29	0	0.058	0.05	0.337	93.2
40A3_oxide3.4	0.57	0.048	0.067	7.4	84.7	0.57	0	0.064	0.08	0.321	93.8
40A3_oxide4.1	0.13	0.000	0.000	7.6	84.0	1.18	0	0.000	0.07	0.376	93.4
40A3_oxide4.2	0.43	0.077	0.000	6.0	84.6	0.87	0	0.010	0.07	0.315	92.4
40A3_oxide4.3	0.38	0.035	0.093	5.9	85.4	0.81	0	0.030	0.08	0.294	93.0

Sample	SiO2	MgO	Cr2O3	TiO2	FeO	Al2O3	NiO	CaO	MnO	V2O3	Total
7B_oxide1.2	0.05	0.036	0.009	7.6	83.8	0.86	0	0.014	0.26	0.459	93.0
7B_oxide1.3	0.05	0.058	0.009	6.6	85.0	0.85	0	0.003	0.24	0.402	93.3
7B_oxide1.4	0.05	0.043	0.002	5.7	86.5	0.55	0	0.000	0.32	0.363	93.6
7B_oxide1.5	0.02	0.033	0.020	6.7	85.1	0.87	0	0.000	0.40	0.458	93.6
7B_oxide1.6	0.06	0.178	0.031	7.3	83.9	0.93	0	0.025	0.79	0.420	93.6
7B_oxide1.7	0.08	0.113	0.000	7.0	84.6	0.90	0	0.018	0.38	0.522	93.6
7B_oxide1.8	0.35	0.020	0.054	12.1	78.1	3.29	0	0.038	0.24	0.465	94.6
7B_oxide1.9	0.36	0.042	0.000	0.1	0.4	0.05	0.0089	54.9	0.17	0.000	56.0
7b_oxide2.1	0.04	0.000	0.037	6.7	85.4	0.59	0	0.017	0.48	0.275	93.6
7b_oxide2.2	0.08	0.000	0.022	7.0	84.7	0.53	0	0.065	0.48	0.280	93.2
7b_oxide2.3	0.04	0.005	0.000	6.7	85.2	0.44	0	0.019	0.44	0.355	93.2
7b_oxide2.4	0.05	0.009	0.004	6.8	85.0	0.59	0	0.010	0.29	0.250	92.9
7b_oxide2.5	0.05	0.034	0.031	6.2	85.2	0.25	0	0.058	0.69	0.253	92.7
7B_oxide3.1	0.07	0.069	0.000	7.5	82.7	0.84	0	0.002	0.81	0.217	92.3
7B_oxide3.2	0.06	0.190	0.018	7.6	83.7	0.50	0	0.000	1.34	0.425	93.8
7B_oxide3.3	0.06	0.169	0.055	6.9	83.8	0.45	0	0.001	1.41	0.301	93.2
7B_oxide3.4	0.07	0.117	0.002	7.1	84.3	0.45	0	0.010	1.31	0.246	93.6
7B_oxide3.5	0.16	0.000	0.000	0.0	0.3	0.00	0	0.006	0.01	0.018	0.5
7B_oxide3.6	0.06	0.058	0.000	6.8	85.0	0.34	0	0.008	0.92	0.368	93.5
7B_oxide3.7	0.06	0.206	0.004	6.7	84.0	0.62	0	0.001	1.51	0.436	93.5
7B_oxide3.8	0.06	0.142	0.000	7.3	83.7	0.60	0	0.006	0.95	0.339	93.1

Appendix 3: Laser Ablation Inductively Coupled Plasma Mass Spectrometry Analyses

Quartz: All analyses are in parts per million (ppm)

Table 9:Quartz Laser ablation inductively coupled mass spectrometry analyses

Sample	Unit	Li	B	Na	Al	P	Ca	Ti	Mn	Ge	Rb	Nb	Sn	La	Ce	Nd	Gd	Pb
		19	0.6		84	23	41	86	0.4	0.	0.	0.	0.	0.	0.0	0.	0.	0.0
13Agr11	Syenite	.4	4	2.3	.9	.6	.9	.9	6	69	05	00	04	00	0	00	01	0
		21	0.6		85	24	41	90	0.3	0.	0.	0.	0.	0.	0.0	0.	0.	0.0
13Agr12	Syenite	.1	5	0.8	.8	.6	.0	.6	5	85	02	00	03	00	0	01	01	0
		19	0.6		82	22	38	86	0.5	0.	0.	0.	0.	0.	0.0	0.	0.	0.0
13Agr13	Syenite	.9	3	0.8	.3	.7	.0	.7	0	81	02	00	06	00	01	00	01	0
		26	3.7		33	23	47	84	3.7	1.	0.	0.	0.	0.	0.0	0.	0.	0.0
13Agr14	Syenite	.0	7	9.8	7	.5	.5	.1	0	17	67	01	09	05	9	02	01	4
		21	0.5		83	24	34	88	0.4	0.	0.	0.	0.	0.	0.0	0.	0.	0.0
13Agr15	Syenite	.0	8	0.8	.4	.2	.8	.2	0	81	02	00	05	00	0	00	01	0
		20	0.5		84	24	52	92	0.4	0.	0.	0.	0.	0.	0.0	0.	0.	0.0
13Agr16	Syenite	.7	6	0.7	.3	.8	.0	.1	1	80	02	00	06	00	0	00	01	0
		21	10.	13.	90	25	40	79	10.	0.	0.	0.	0.	0.	0.2	0.	0.	0.0
13Agr17	Syenite	.8	3	8	.9	.9	.2	.6	20	79	05	02	08	15	7	05	02	7
		20	3.1		88	23	56	87	2.9	0.	0.	0.	0.	0.	0.0	0.	0.	0.0
13Agr18	Syenite	.5	0	5.9	.3	.3	.2	.1	1	76	03	00	05	05	8	02	01	4
		20	0.7		87	27	34	91	0.4	0.	0.	0.	0.	0.	0.0	0.	0.	0.0
13Agr19	Syenite	.5	2	0.7	.7	.8	.6	.2	3	72	02	00	04	00	0	00	00	0
		2.	10.	26.	22	24	61	1.	5.1	3.	1.	0.	0.	0.	0.0	0.	0.	0.1
13Agr21	Syenite	5	1	6	0	.0	.8	1	9	34	78	00	06	01	1	01	01	3
		0.	8.2	19.	78	23	74	1.	3.2	6.	0.	0.	0.	0.	0.0	0.	0.	0.1
13Agr23	Syenite	3	9	1	.1	.9	.3	6	0	94	35	03	05	01	2	00	00	0
		0.	4.4	17.	18	23	97	0.	8.2	4.	1.	0.	0.	0.	0.0	0.	0.	0.0
13Agr27	Syenite	4	8	9	1	.1	.0	9	5	81	10	01	04	02	4	02	01	9
		1.	4.2	19.	19	24	67	1.	7.7	4.	0.	0.	0.	0.	0.0	0.	0.	0.0
13Agr28	Syenite	3	5	4	4	.3	.3	6	5	36	92	01	06	01	1	00	01	9
		2.	4.9	25.	27	22	10	1.	9.0	6.	1.	0.	0.	0.	0.0	0.	0.	0.0
13Agr29	Syenite	0	7	6	7	.7	3	1	2	24	38	01	05	01	1	00	01	8
		17	21.	29.	32	25	12	79	28.	1.	0.	0.	0.	0.	0.6	0.	0.	0.1
13Agr31	Syenite	.4	8	7	0	.0	5	.1	41	04	44	02	24	36	2	15	02	5
		17	0.6		15	21	34	98	0.4	0.	0.	0.	0.	0.	0.0	0.	0.	0.0
13Agr32	Syenite	.1	0	4.3	9	.7	.8	.3	8	73	08	00	11	00	1	00	01	2
		20	0.5		89	22	33	10	0.3	0.	0.	0.	0.	0.	0.0	0.	0.	0.0
13Agr33	Syenite	.7	5	1.5	.3	.9	.3	4	7	76	03	00	07	00	0	00	01	0
		22	0.6		11	20	38	11	0.5	0.	0.	0.	0.	0.	0.0	0.	0.	0.0
13Agr34	Syenite	.5	4	8.4	6	.8	.4	0	5	75	14	01	43	01	3	01	01	2
		21	0.7	10	20	20	43	99	1.8	0.	1.	0.	0.	0.	0.0	0.	0.	0.1
13Agr35	Syenite	.7	4	4	6	.8	.9	.8	2	67	23	24	26	03	8	02	01	5
		22	0.6	18.	93	22	36	10	0.4	0.	0.	0.	0.	0.	0.0	0.	0.	0.0
13Agr36	Syenite	.4	4	2	.4	.6	.6	5	8	92	05	02	20	00	2	01	01	1
		23	0.6	52.	11	22	59	11	0.4	0.	0.	0.	0.	0.	0.0	0.	0.	0.0
13Agr37	Syenite	.1	9	2	4	.3	.7	4	9	87	12	01	13	01	1	01	01	1
		21	0.6	10.	92	21	40	10	0.4	0.	0.	0.	0.	0.	0.0	0.	0.	0.0
13Agr38	Syenite	.4	9	0	.0	.9	.1	3	2	77	06	00	26	00	0	01	01	0
		17	0.6		91	22	38	94	0.4	0.	0.	0.	0.	0.	0.0	0.	0.	0.0
13Agr39	Syenite	.4	6	4.3	.4	.1	.6	.7	0	68	03	00	15	00	1	01	01	1
		19	0.7		83	24	43	10	0.3	0.	0.	0.	0.	0.	0.0	0.	0.	0.0
13Agr41	Syenite	.2	1	0.9	.9	.4	.8	9	4	78	02	00	05	00	0	01	01	0
		21	0.6		82	23	39	94	0.4	0.	0.	0.	0.	0.	0.0	0.	0.	0.0
13Agr410	Syenite	.2	7	1.8	.0	.6	.6	.7	2	73	02	00	10	00	1	02	01	0
		22	0.6		92	23	37	10	0.4	0.	0.	0.	0.	0.	0.0	0.	0.	0.0
13Agr411	Syenite	.8	1	0.8	.4	.9	.0	8	0	70	02	00	04	00	0	01	01	1
		19	0.6		77	24	38	94	0.3	0.	0.	0.	0.	0.	0.0	0.	0.	0.0
13Agr412	Syenite	.1	8	0.9	.5	.8	.1	.9	6	77	02	00	07	00	4	01	01	0
		20	0.6		88	23	40	12	0.4	0.	0.	0.	0.	0.	0.0	0.	0.	0.0
13Agr42	Syenite	.7	8	0.8	.1	.4	.0	0	6	78	02	00	06	00	0	01	01	0

Sample	Type																
		21	0.6		88	23	44	11	0.4	0.	0.	0.	0.	0.	0.0	0.	0.	0.0
13Agr43	Syenite	.8	7	0.8	.7	.7	.9	9	1	77	02	00	04	00	0	00	01	0
		21	0.6		88	23	35	12	0.3	0.	0.	0.	0.	0.	0.0	0.	0.	0.0
13Agr44	Syenite	.9	3	2.8	.2	.0	.9	1	1	72	02	00	10	00	0	01	01	0
		21	0.9	14	24	16	11	12	2.0	0.	0.	0.	1.	0.	0.0	0.	0.	0.2
13Agr46	Syenite	.4	6	1	8	.4	3	7	2	80	40	40	87	03	8	07	02	6
		18	0.6		77	22	36	10	0.2	0.	0.	0.	0.	0.	0.0	0.	0.	0.0
13Agr47	Syenite	.8	2	0.8	.0	.4	.0	6	5	71	02	00	06	00	0	00	00	0
		21	0.6		84	23	36	11	0.4	0.	0.	0.	0.	0.	0.0	0.	0.	0.0
13Agr48	Syenite	.3	0	1.0	.5	.6	.3	5	1	70	02	00	06	00	0	00	01	0
		24	0.6		99	24	36	11	0.5	0.	0.	0.	0.	0.	0.0	0.	0.	0.0
13Agr49	Syenite	.3	3	0.8	.5	.5	.8	0	5	93	02	00	07	00	0	00	00	0
		10	0.9		93	23	55	95	0.5	0.	0.	0.	0.	0.	0.0	0.	0.	0.0
13Agr510	Syenite	.4	6	1.1	.2	.3	.2	.7	6	38	04	01	09	00	0	01	01	1
		12	0.6		96	23	40	95	0.4	0.	0.	0.	0.	0.	0.0	0.	0.	0.0
13Agr511	Syenite	.5	8	4.4	.7	.4	.2	.4	9	84	37	14	06	01	4	01	01	1
		21	0.6		95	25	38	12	0.3	0.	0.	0.	0.	0.	0.0	0.	0.	0.0
13Agr54	Syenite	.2	5	0.8	.6	.2	.1	5	8	87	10	02	08	00	1	00	01	1
		20	0.6		89	22	38	11	0.4	0.	0.	0.	0.	0.	0.0	0.	0.	0.0
13Agr55	Syenite	.8	9	0.8	.6	.9	.1	1	0	80	10	01	06	00	0	00	01	0
		18	0.6		81	26	38	95	0.3	0.	0.	0.	0.	0.	0.0	0.	0.	0.0
13Agr56	Syenite	.6	5	0.8	.0	.0	.1	.9	5	82	02	00	05	00	0	01	01	0
		12	0.6		78	23	57	89	0.2	0.	0.	0.	0.	0.	0.0	0.	0.	0.0
13Agr57	Syenite	.3	5	0.7	.1	.6	.1	.3	5	86	02	00	05	00	0	00	01	0
		20	0.8		11	24	42	99	0.9	0.	0.	0.	0.	0.	0.0	0.	0.	0.0
13Agr58	Syenite	.7	0	2.1	7	.6	.6	.7	9	81	02	00	03	01	2	00	01	1
		1.	1.1	91.	15	20	66	27	1.7	1.	0.	0.	2.	0.	0.1	0.	0.	0.2
13Agr62	Syenite	6	1	1	8	.7	.9	.5	4	17	89	06	80	06	3	07	02	3
		2.	0.6		26	25	39	21	0.2	1.	0.	0.	0.	0.	0.0	0.	0.	0.0
13Agr63	Syenite	1	7	6.8	.0	.4	.0	.0	2	03	02	00	05	00	1	01	01	3
		2.	0.6	24.	68	25	37	20	1.1	1.	0.	0.	0.	0.	0.0	0.	0.	0.0
13Agr64	Syenite	9	7	5	.6	.0	.6	.0	8	05	84	01	08	01	1	00	01	4
		3.	0.5	15.	50	21	47	26	0.3	0.	0.	0.	0.	0.	0.0	0.	0.	0.0
13Agr65	Syenite	3	4	6	.4	.9	.3	.5	8	91	09	00	06	00	1	01	01	2
		4.	1.0	24.	14	17	58	24	10.	1.	0.	0.	0.	0.	0.0	0.	0.	0.7
13Agr66	Syenite	3	2	3	7	.7	.3	.9	07	10	72	06	63	01	4	01	02	1
		3.	1.4	22.	54	23	82	21	1.2	0.	0.	0.	0.	0.	0.0	0.	0.	0.0
13Agr68	Syenite	5	2	9	.5	.6	.8	.8	2	99	14	01	05	01	2	01	01	9
		6.	1.8	37.	17	22	15	26	3.9	1.	0.	1.	0.	0.	0.7	0.	0.	0.1
13Agr69	Syenite	1	7	2	0	.4	9	.6	3	22	46	09	13	41	2	20	02	4
		9.	1.5	20.	81	20	56	11	12.	0.	0.	0.	0.	0.	0.0	0.	0.	0.6
15Agr11	LSPT	5	2	9	.8	.4	.9	6	61	73	35	00	03	00	0	00	01	2
		8.	10.	24	69	23	62	91	74.	0.	2.	0.	0.	0.	0.7	0.	0.	3.6
15Agr110	LSPT	1	2	8	.3	.3	.1	.4	86	88	18	00	48	39	2	09	01	9
		8.	2.7	58.	77	23	47	10	31.	0.	0.	0.	0.	0.	0.0	0.	0.	1.3
15Agr12	LSPT	1	2	6	.8	.1	.6	1	36	67	39	00	08	01	2	01	01	0
		7.	0.9	21.	83	26	10	10	128	0.	0.	0.	0.	0.	0.2	0.	0.	0.5
15Agr14	LSPT	8	7	8	.5	.3	2	3	.3	74	11	00	03	06	2	07	02	1
		10	0.6		10	24	46	12	0.7	0.	0.	0.	0.	0.	0.1	0.	0.	0.3
15Agr15	LSPT	.0	7	7.2	5	.8	.2	6	8	73	02	06	05	06	2	08	03	6
		9.	0.6		91	22	45	12	1.2	0.	0.	0.	0.	0.	0.0	0.	0.	0.0
15Agr16	LSPT	9	7	5.4	.4	.5	.5	1	8	83	34	00	04	00	0	01	01	5
		8.	1.7	33.	88	23	42	99	7.4	0.	0.	0.	0.	0.	0.0	0.	0.	0.3
15Agr17	LSPT	8	6	5	.8	.2	.2	.3	3	70	22	00	04	00	1	00	01	9
		12	8.2	55	80	21	58	10	60.	0.	2.	0.	0.	0.	0.0	0.	0.	2.2
15Agr18	LSPT	.3	9	5	.6	.5	.9	0	74	80	01	00	05	00	2	01	01	2
		9.	0.9		81	25	61	10	3.3	0.	0.	0.	0.	0.	0.0	0.	0.	0.1
15Agr19	LSPT	5	2	6.2	.9	.2	.8	9	1	65	04	00	04	00	0	01	01	5
		8.	0.6		82	22	45	11	0.3	0.	0.	0.	0.	0.	0.0	0.	0.	0.0
15Agr21	LSPT	8	7	1.2	.9	.4	.9	1	0	58	03	00	06	00	0	00	01	0
		6.	1.8	47.	88	23	47	11	13.	0.	0.	0.	0.	0.	0.2	0.	0.	0.8
15Agr210	LSPT	7	6	1	.6	.9	.0	0	83	82	40	46	33	11	0	06	09	0
		8.	1.0		78	22	42	11	0.6	0.	0.	0.	0.	0.	0.0	0.	0.	0.0
15Agr22	LSPT	5	7	8.1	.8	.5	.8	0	6	82	02	00	04	00	0	00	00	2
		9.	0.9		83	23	47	12	2.6	1.	0.	0.	0.	0.	0.0	0.	0.	0.0
15Agr23	LSPT	2	9	4.6	.8	.2	.1	0	5	17	06	00	05	00	0	00	01	7
		9.	1.1	14.	83	27	68	11	6.5	0.	0.	0.	0.	0.	0.0	0.	0.	0.2
15Agr24	LSPT	6	2	4	.7	.3	.1	8	0	77	12	00	04	00	0	01	02	7
		10	3.6	12	81	20	46	11	32.	0.	0.	0.	0.	0.	0.0	0.	0.	1.8
15Agr25	LSPT	.3	6	3	.1	.8	.2	1	45	81	49	00	05	00	0	00	01	2
		8.	0.8		90	25	53	11	1.0	0.	0.	0.	0.	0.	0.0	0.	0.	0.0
15Agr26	LSPT	6	2	4.6	.0	.1	.5	2	1	68	03	00	03	00	0	01	01	4
		8.	2.8	60.	85	25	56	11	20.	0.	0.	0.	0.	0.	0.0	0.	0.	0.9
15Agr27	LSPT	6	8	1	.8	.0	.7	4	69	83	61	00	05	00	0	00	02	0

Sample	Unit	Li	B	Na	Al	P	Ca	Ti	Mn	Ge	Rb	Nb	Sn	La	Ce	Nd	Gd	Pb
15Agr31	LSPT	7.2	2.44	61.9	87.4	24.8	72.7	84.6	13.82	0.73	0.28	0.00	0.07	0.01	0.03	0.01	0.02	0.66
15Agr310	LSPT	8.6	0.73	21.8	91.2	23.9	48.2	90.3	4.46	0.87	0.26	0.00	0.05	0.00	0.01	0.00	0.01	0.22
15Agr32	LSPT	8.6	1.58	30.3	89.8	25.4	56.0	95.9	6.72	0.72	0.16	0.09	0.04	0.02	0.02	0.02	0.01	0.45
15Agr33	LSPT	9.4	7.43	17.1	80.3	23.3	71.2	90.0	28.60	0.74	0.88	0.02	0.06	0.00	0.00	0.01	0.01	1.79
15Agr34	LSPT	9.2	1.82	21.4	83.0	24.3	46.8	101	1.27	0.85	0.09	0.00	0.04	0.01	0.01	0.01	0.01	0.20
15Agr35	LSPT	9.4	9.68	71.5	82.7	21.2	53.7	98.3	42.74	0.79	2.38	0.00	0.06	0.00	0.00	0.01	0.01	1.91
15Agr36	LSPT	10.4	0.80	3.7	90.4	24.1	43.3	109	2.05	0.85	0.08	0.00	0.04	0.00	0.00	0.00	0.01	0.14
15Agr37	LSPT	9.0	4.56	120	89.1	25.3	47.0	86.2	9.57	0.60	0.87	0.00	0.05	0.00	0.00	0.00	0.01	0.77
15Agr38	LSPT	9.1	1.06	17.0	79.6	24.5	51.3	88.7	8.89	0.65	0.26	0.00	0.04	0.00	0.01	0.00	0.01	0.44
15Agr39	LSPT	9.5	1.86	25.0	87.0	25.5	79.4	88.9	10.44	0.87	0.27	0.01	0.06	0.00	0.00	0.02	0.02	0.82
15Agr41	LSPT	8.8	5.54	141	103	25.2	61.4	116	12.44	0.76	0.86	0.01	0.04	0.00	0.01	0.01	0.01	1.41
15Agr42	LSPT	9.6	7.25	199	89.7	21.2	40.1	139	119.7	0.60	5.15	0.00	0.16	0.36	0.46	0.07	0.01	7.48
15Agr43	LSPT	5.8	3.20	67.1	73.0	25.2	56.2	76.2	6.28	0.67	0.42	0.01	0.03	0.00	0.00	0.01	0.01	0.57
15Agr44	LSPT	8.0	1.52	24.2	85.1	23.9	36.6	108	3.60	0.76	0.17	0.09	0.05	0.04	0.11	0.06	0.01	0.18
15Agr45	LSPT	9.7	1.28	16.3	86.5	25.4	46.6	92.6	3.34	0.79	0.06	0.01	0.04	0.00	0.00	0.01	0.01	0.16
15Agr47	LSPT	7.7	3.81	92.0	103	22.8	55.9	101	66.17	0.63	1.05	0.32	0.17	0.04	0.08	0.01	0.02	1.99
15Agr49	LSPT	9.9	0.67	42.0	149	25.0	47.3	98.4	1.95	0.85	0.17	0.05	0.08	0.01	0.02	0.01	0.01	0.10
15Agr51	LSPT	6.5	2.06	33.5	87.9	24.1	49.0	87.3	4.60	0.97	0.14	0.00	0.05	0.00	0.01	0.00	0.01	0.21
15Agr510	LSPT	9.9	10.8	316	118	21.3	55.5	104	93.95	0.75	3.28	0.07	0.16	0.10	0.18	0.01	0.01	4.61
15Agr52	LSPT	8.6	3.03	39.9	172	24.1	55.7	92.2	6.38	0.65	0.83	0.00	0.06	0.00	0.01	0.01	0.01	0.60
15Agr53	LSPT	8.3	2.24	44.4	88.8	21.2	45.2	90.9	12.93	0.53	0.22	0.00	0.06	0.01	0.02	0.01	0.01	1.01
15Agr54	LSPT	9.5	1.50	9.3	112	25.3	45.6	91.1	1.98	0.78	0.34	0.00	0.05	0.00	0.01	0.00	0.01	0.09
15Agr55	LSPT	9.4	1.15	17.4	94.9	22.8	48.2	90.2	3.53	0.65	0.27	0.01	0.04	0.00	0.01	0.01	0.01	0.20
15Agr56	LSPT	9.5	0.77	8.5	89.8	22.7	42.4	105	1.67	0.90	0.10	0.01	0.04	0.00	0.01	0.00	0.01	0.06
15Agr57	LSPT	10.3	0.84	4.2	93.2	21.9	51.2	105	4.54	0.82	0.15	0.00	0.03	0.00	0.00	0.01	0.01	0.17
15Agr58	LSPT	10.2	0.66	2.4	91.6	24.2	40.8	111	1.01	0.85	0.07	0.00	0.04	0.00	0.00	0.00	0.01	0.03
15Agr59	LSPT	9.7	11.9	281	96.4	23.7	36.0	124	77.73	0.66	3.29	0.01	0.04	0.02	0.05	0.01	0.01	5.48
15Agr61	LSPT	7.9	15.0	346	76.8	21.8	45.0	78.3	183.4	0.71	6.63	0.05	0.07	0.01	0.03	0.03	0.01	10.30
15Agr610	LSPT	9.7	1.04	5.8	115	25.2	45.3	95.8	1.41	0.66	0.09	0.02	0.05	0.01	0.03	0.01	0.01	0.05
15Agr62	LSPT	9.3	2.11	40.6	81.4	25.8	41.0	92.4	0.82	0.78	0.12	0.00	0.05	0.00	0.00	0.01	0.01	0.11
15Agr63	LSPT	7.8	0.95	25.2	79.5	24.8	147	90.2	11.57	0.69	0.07	0.01	0.06	0.08	0.27	0.15	0.03	0.14
15Agr64	LSPT	9.1	0.71	10.4	80.7	23.3	40.6	97.1	4.93	0.81	0.08	0.00	0.04	0.00	0.00	0.00	0.01	0.23
15Agr65	LSPT	7.5	1.32	33.9	72.8	25.2	46.9	77.1	5.34	0.84	0.17	0.00	0.06	0.00	0.00	0.01	0.01	0.31
15Agr66	LSPT	10.4	0.81	3.1	87.8	25.2	48.4	93.5	4.35	0.75	0.05	0.00	0.04	0.02	0.07	0.00	0.01	0.23
15Agr67	LSPT	9.1	0.63	2.6	80.5	24.0	40.6	91.3	1.25	0.71	0.02	0.00	0.04	0.01	0.00	0.01	0.01	0.07
15Agr69	LSPT	9.3	0.88	5.4	92.3	25.2	54.1	98.4	1.35	0.97	0.13	0.03	0.04	0.05	0.15	0.05	0.02	0.04
27A2gr15	USPT	9.0	0.72	3.8	89.0	23.4	46.1	94.7	0.57	0.71	0.03	0.00	0.04	0.00	0.01	0.01	0.01	0.00

Sample	Unit	Li	B	Na	Al	P	Ca	Ti	Mn	Ge	R b	N b	Sn	La	Ce	N d	G d	Pb
27A2gr210	USPT	8.3	1.98	36.0	283	25.8	78.4	87.7	1.48	0.76	0.42	0.01	0.06	0.01	0.02	0.01	0.01	0.01
27A2gr24	USPT	13.3	1.81	12.2	155	22.3	54.6	93.8	0.87	0.73	0.14	0.01	0.04	0.00	0.01	0.00	0.01	0.0
27A2gr26	USPT	13.4	0.72	1.9	83.7	22.6	47.8	100	0.51	0.71	0.02	0.00	0.05	0.00	0.00	0.00	0.01	0.0
27A2gr27	USPT	21.0	0.65	3.0	85.8	24.7	39.0	96.7	0.55	0.41	0.02	0.00	0.06	0.00	0.01	0.00	0.01	0.01
27A2gr28	USPT	19.3	0.70	1.3	88.6	24.6	50.4	101	0.36	0.94	0.03	0.00	0.05	0.00	0.00	0.00	0.01	0.0
27A2gr29	USPT	18.3	0.72	2.9	79.4	23.8	44.1	96.0	0.43	0.87	0.12	0.00	0.05	0.00	0.00	0.00	0.01	0.01
27A2gr31	USPT	11.6	0.83	6.9	122	21.4	47.1	95.0	0.48	0.73	0.11	0.01	0.04	0.00	0.00	0.00	0.01	0.0
27A2gr310	USPT	17.6	0.77	0.9	99.0	25.0	48.8	115	0.5	0.68	0.03	0.01	0.03	0.00	0.00	0.00	0.01	0.0
27A2gr311	USPT	19.1	0.69	1.2	86.0	22.8	39.4	114	0.37	0.83	0.02	0.00	0.05	0.00	0.00	0.00	0.00	0.0
27A2gr313	USPT	12.4	0.73	3.4	91.6	22.2	40.3	108	0.36	0.72	0.02	0.00	0.07	0.00	0.00	0.01	0.01	0.0
27A2gr314	USPT	7.9	27.8	56.6	329	22.9	99.6	95.4	16.39	0.94	0.54	0.05	0.12	0.33	0.48	0.08	0.01	0.05
27A2gr315	USPT	13.4	0.70	0.8	84.9	24.5	42.2	101	0.43	0.75	0.03	0.00	0.04	0.00	0.00	0.01	0.01	0.0
27A2gr316	USPT	13.8	2.53	1.7	84.6	27.8	39.6	92.9	0.63	0.80	0.02	0.00	0.04	0.00	0.01	0.00	0.01	0.0
27A2gr317	USPT	17.3	0.69	0.8	80.8	22.9	40.1	92.5	0.32	0.57	0.02	0.00	0.05	0.00	0.00	0.00	0.00	0.0
27A2gr34	USPT	8.8	1.41	103	328	21.7	47.6	103	2.38	1.10	0.82	0.16	0.06	0.03	0.06	0.01	0.01	0.07
27A2gr35	USPT	16.9	0.64	12.1	113	22.4	47.7	106	0.52	0.55	0.04	0.02	0.04	0.01	0.01	0.01	0.01	0.01
27A2gr36	USPT	20.4	0.59	4.6	84.1	23.5	52.6	109	0.40	0.82	0.02	0.01	0.03	0.00	0.00	0.00	0.01	0.0
27A2gr37	USPT	18.1	0.76	1.3	77.5	25.0	45.0	103	0.40	1.12	0.02	0.00	0.04	0.00	0.00	0.01	0.01	0.0
27A2gr38	USPT	9.1	0.86	2.4	119	24.2	49.0	103	0.57	0.78	0.05	0.00	0.05	0.00	0.00	0.00	0.01	0.0
27A2gr39	USPT	13.6	1.15	17.4	106	23.0	50.8	109	0.72	0.76	0.11	0.00	0.07	0.00	0.01	0.01	0.01	0.02
27A2gr410	USPT	15.7	36.1	61.5	336	26.6	178	90.6	9.13	0.78	0.59	0.09	0.18	0.50	0.68	0.41	0.06	0.09
27A2gr411	USPT	18.9	0.72	5.0	83.0	26.3	54.4	98.5	0.88	0.95	0.02	0.00	0.11	0.02	0.07	0.02	0.01	0.03
27A2gr412	USPT	20.2	0.64	2.6	87.1	23.7	38.9	97.2	0.54	0.56	0.02	0.00	0.08	0.00	0.02	0.00	0.01	0.02
27A2gr413	USPT	8.5	2.47	28.3	276	24.2	47.5	105	2.52	0.87	0.44	0.05	0.08	0.02	0.05	0.02	0.01	0.01
27A2gr43	USPT	6.3	1.53	30.6	333	23.7	92.4	101	1.78	0.79	0.41	0.01	0.08	0.02	0.03	0.01	0.01	0.03
27A2gr48	USPT	18.6	0.67	70.3	151	19.5	92.4	104	1.81	0.72	0.32	0.03	1.01	0.17	0.42	0.15	0.03	0.38
27A2gr49	USPT	9.8	0.74	12.9	111	26.4	82.9	101	1.81	0.71	0.08	0.01	0.18	0.05	0.04	0.04	0.01	0.08
27Agr11	USPT	13.7	2.64	23.7	329	24.9	111	101	0.55	0.90	0.41	0.02	0.06	0.01	0.01	0.00	0.01	0.02
27Agr112	USPT	10.7	2.22	31.6	340	22.9	56.2	96.6	0.73	1.03	0.41	0.21	0.04	0.00	0.00	0.00	0.01	0.02
27Agr12	USPT	10.0	0.53	4.2	85.2	20.7	31.4	116	0.37	0.62	0.02	0.00	0.04	0.00	0.00	0.00	0.01	0.05
27Agr13	USPT	11.3	0.59	0.8	87.1	24.3	47.4	124	0.45	0.78	0.02	0.00	0.07	0.00	0.00	0.00	0.01	0.0
27Agr15	USPT	11.3	0.62	0.8	86.9	23.2	37.5	119	0.37	0.57	0.02	0.00	0.04	0.00	0.00	0.00	0.01	0.0
27Agr17	USPT	10.6	0.68	11.1	195	24.8	41.0	119	0.45	0.72	0.02	0.01	0.06	0.00	0.01	0.01	0.01	0.01
27Agr19	USPT	10.1	0.74	0.9	86.5	21.5	42.9	109	0.37	0.60	0.03	0.00	0.04	0.00	0.00	0.01	0.01	0.0
27Agr21	USPT	18.4	1.96	19.3	188	22.3	49.9	80.3	1.47	1.00	0.17	0.03	0.07	0.03	0.04	0.01	0.01	0.05
27Agr210	USPT	9.6	0.67	0.8	84.4	22.8	38.8	96.3	0.35	0.78	0.02	0.00	0.05	0.00	0.00	0.00	0.00	0.0
27Agr22	USPT	10.6	0.66	0.8	91.1	22.9	75.8	101	0.38	0.58	0.02	0.00	0.05	0.00	0.00	0.01	0.00	0.01

Sample	Unit	Li	B	Na	Al	P	Ca	Ti	Mn	Ge	Rb	Nb	Sn	La	Ce	Nd	Gd	Pb
		11	0.7		89	23	45	11	0.3	0.	0.	0.	0.	0.	0.0	0.	0.	0.0
27Agr24	USPT	.7	0	0.8	.3	.2	.7	3	3	67	02	00	06	00	0	00	01	0
		11	0.6		83	22	36	11	0.3	0.	0.	0.	0.	0.	0.0	0.	0.	0.0
27Agr25	USPT	.0	1	0.7	.1	.8	.8	9	7	55	02	00	04	00	0	00	01	0
		11	2.7	22.	32	23	40	10	0.5	0.	0.	0.	0.	0.	0.0	0.	0.	0.0
27Agr26	USPT	.3	3	8	1	.9	.4	1	3	76	46	00	06	00	1	00	01	2
		12	0.5		87	22	33	11	0.3	0.	0.	0.	0.	0.	0.0	0.	0.	0.0
27Agr27	USPT	.0	7	0.7	.0	.1	.6	0	4	85	02	00	06	00	0	00	01	0
		10	0.6		84	24	39	10	0.3	0.	0.	0.	0.	0.	0.0	0.	0.	0.0
27Agr28	USPT	.5	7	0.8	.4	.5	.9	4	2	67	02	00	05	00	0	01	01	0
		9.	0.5		77	19	38	95	0.3	0.	0.	0.	0.	0.	0.0	0.	0.	0.0
27Agr29	USPT	8	8	0.7	.0	.3	.9	.9	4	68	02	00	06	00	0	01	01	0
		10	0.7		95	24	58	12	0.3	0.	0.	0.	0.	0.	0.0	0.	0.	0.0
27Agr31	USPT	.5	1	0.9	.1	.7	.4	1	6	67	02	00	04	00	0	00	01	0
		11	0.6		10	22	37	11	0.4	0.	0.	0.	0.	0.	0.0	0.	0.	0.0
27Agr32	USPT	.0	4	2.6	3	.0	.3	6	0	81	02	00	04	00	0	00	01	0
		11	0.8		15	23	40	11	0.4	0.	0.	0.	0.	0.	0.0	0.	0.	0.0
27Agr33	USPT	.3	5	7.2	1	.9	.0	8	6	77	11	02	05	00	0	00	01	1
		11	0.6		96	22	37	12	0.4	0.	0.	0.	0.	0.	0.0	0.	0.	0.0
27Agr34	USPT	.9	3	1.5	.2	.2	.1	0	4	88	02	00	07	00	0	01	00	0
		10	0.7		85	20	42	11	0.3	0.	0.	0.	0.	0.	0.0	0.	0.	0.0
27Agr35	USPT	.7	2	5.4	.0	.2	.7	8	8	63	02	00	06	00	0	00	01	1
		11	0.5		88	20	29	10	0.4	0.	0.	0.	0.	0.	0.0	0.	0.	0.0
27Agr36	USPT	.8	1	0.6	.5	.1	.1	4	0	80	02	00	05	00	0	00	00	0
		9.	0.5		77	21	33	96	0.3	0.	0.	0.	0.	0.	0.0	0.	0.	0.0
27Agr37	USPT	5	8	0.7	.6	.1	.6	.6	4	77	02	00	06	00	0	00	01	0
		10	1.0		11	23	35	98	0.3	0.	0.	0.	0.	0.	0.0	0.	0.	0.0
27Agr38	USPT	.1	5	5.5	4	.0	.2	.1	9	63	05	00	03	00	0	01	00	0
		11	2.8	21.	26	21	37	89	0.5	0.	0.	0.	0.	0.	0.0	0.	0.	0.0
27Agr39	USPT	.0	8	7	3	.8	.8	.8	0	78	32	01	05	00	0	00	01	1
		9.	0.5		84	21	39	10	0.5	0.	0.	0.	0.	0.	0.0	0.	0.	0.0
27Agr41	USPT	6	1	2.3	.0	.1	.4	5	0	68	02	00	05	00	0	00	00	0
		10	0.5		98	22	31	96	0.3	0.	0.	0.	0.	0.	0.0	0.	0.	0.0
27Agr410	USPT	.3	6	4.4	.4	.2	.6	.8	9	83	03	00	05	00	0	00	01	0
		11	0.5		93	22	31	10	0.3	0.	0.	0.	0.	0.	0.0	0.	0.	0.0
27Agr411	USPT	.1	4	2.1	.1	.8	.8	4	5	88	02	00	06	00	0	01	00	1
		10	0.6		12	20	35	97	0.4	0.	0.	0.	0.	0.	0.0	0.	0.	0.0
27Agr42	USPT	.4	2	6.0	5	.8	.5	.2	8	84	10	00	04	01	3	00	00	1
		9.	1.0		82	25	49	97	0.2	0.	0.	0.	0.	0.	0.0	0.	0.	0.0
27Agr43	USPT	2	0	1.0	.5	.0	.4	.5	9	64	30	01	04	00	0	00	01	0
		11	1.1		13	24	40	90	0.4	0.	0.	0.	0.	0.	0.0	0.	0.	0.0
27Agr44	USPT	.8	3	7.6	3	.8	.7	.4	1	87	06	12	07	00	0	01	01	1
		10	0.6		92	22	36	10	1.9	0.	0.	0.	0.	0.	0.0	0.	0.	0.0
27Agr47	USPT	.4	5	0.7	.3	.6	.1	6	6	80	02	08	07	00	0	00	00	0
		10	0.6		84	22	37	94	0.5	0.	0.	0.	0.	0.	0.0	0.	0.	0.0
27Agr48	USPT	.1	5	3.4	.4	.3	.2	.7	2	75	02	00	03	00	0	00	00	2
		9.	0.6		78	24	37	88	0.4	0.	0.	0.	0.	0.	0.0	0.	0.	0.0
27Agr49	USPT	4	5	0.8	.6	.2	.1	.2	4	72	02	00	06	00	0	00	01	0
		14	0.7		10	21	56	10	0.4	0.	0.	0.	0.	0.	0.0	0.	0.	0.0
40Igr110	USPT	.5	9	2.0	6	.8	.9	1	4	90	02	00	03	00	1	01	01	0
		14	0.7		10	23	51	10	0.4	0.	0.	0.	0.	0.	0.0	0.	0.	0.0
40Igr111	USPT	.6	2	1.7	9	.0	.7	4	3	81	02	00	06	00	0	00	01	0
		13	0.8		11	23	55	97	0.2	0.	0.	0.	0.	0.	0.0	0.	0.	0.0
40Igr12	USPT	.2	1	5.5	7	.0	.0	.3	4	64	06	01	05	00	1	01	01	1
		15	0.8	14.	13	22	48	10	0.2	0.	0.	0.	0.	0.	0.0	0.	0.	0.0
40Igr13	USPT	.8	4	6	5	.8	.0	4	8	94	04	00	04	00	0	00	01	0
		14	0.9	19.	14	22	46	12	1.2	1.	0.	0.	0.	0.	0.0	0.	0.	0.0
40Igr14	USPT	.7	4	9	8	.7	.1	3	4	02	17	01	03	00	1	01	01	8
		17	2.2	39.	29	23	60	10	3.8	0.	0.	0.	0.	0.	0.0	0.	0.	0.1
40Igr15	USPT	.4	5	7	1	.4	.5	4	4	93	72	01	03	01	1	01	02	7
		13	0.8		11	23	62	10	0.8	0.	0.	0.	0.	0.	0.0	0.	0.	0.0
40Igr16	USPT	.0	7	2.1	1	.1	.1	5	5	78	07	00	03	00	0	01	02	1
		13	0.7		10	23	51	11	0.3	0.	0.	0.	0.	0.	0.0	0.	0.	0.0
40Igr17	USPT	.2	1	1.7	0	.2	.2	4	6	89	02	00	03	00	0	01	01	0
		12	0.8		11	26	61	97	0.3	0.	0.	0.	0.	0.	0.0	0.	0.	0.0
40Igr18	USPT	.3	3	9.9	8	.2	.1	.5	5	85	02	00	03	00	0	01	01	0
		14	0.7	10.	11	22	42	97	0.8	0.	0.	0.	0.	0.	0.0	0.	0.	0.0
40Igr19	USPT	.1	0	1	5	.9	.0	.4	6	88	13	00	03	00	0	01	01	1
		15	1.8	19.	20	26	59	12	8.7	1.	0.	0.	0.	0.	0.0	0.	0.	0.5
40Igr21	USPT	.5	6	2	5	.3	.5	0	0	05	23	01	05	01	1	00	00	5
		14	0.9		12	24	59	11	0.4	0.	0.	0.	0.	0.	0.0	0.	0.	0.0
40Igr22	USPT	.1	4	5.4	0	.4	.9	1	9	96	04	00	04	00	0	00	01	1

86

Sample	Unit	Li	B	Na	Al	P	Ca	Ti	Mn	Ge	Rb	Nb	Sn	La	Ce	Nd	Gd	Pb
		14	0.7		11	24	51	13	0.4	1.	0.	0.	0.	0.	0.0	0.	0.	0.0
40Igr24	USPT	.8	2	1.7	2	.2	.1	0	0	12	02	00	04	00	0	01	01	0
		15	1.4	18.	18	27	62	11	3.0	0.	0.	0.	0.	0.	0.0	0.	0.	0.0
40Igr25	USPT	.4	8	2	0	.1	.4	5	7	94	30	00	06	00	0	01	02	6
		14	0.9		11	28	70	10	0.6	0.	0.	0.	0.	0.	0.0	0.	0.	0.0
40Igr26	USPT	.6	9	2.3	7	.0	.9	9	2	82	03	00	06	00	0	00	01	0
		14	0.8		11	27	55	11	0.5	0.	0.	0.	0.	0.	0.0	0.	0.	0.0
40Igr27	USPT	.6	3	1.8	5	.4	.8	0	7	87	02	00	05	00	0	01	01	0
		17	1.0	22.	14	26	72	14	2.8	0.	0.	0.	0.	0.	0.0	0.	0.	0.0
40Igr31	USPT	.0	2	2	1	.4	.4	1	8	87	09	00	05	00	0	01	02	5
		16	0.8		13	26	61	13	0.7	1.	0.	0.	0.	0.	0.0	0.	0.	0.0
40Igr33	USPT	.1	8	2.0	1	.2	.9	0	0	21	03	01	06	00	0	01	01	1
		15	1.0		15	31	72	12	0.6	1.	0.	0.	0.	0.	0.0	0.	0.	0.0
40Igr34	USPT	.5	1	7.9	8	.1	.4	4	9	08	06	00	09	00	0	01	02	1
		17	0.9		14	29	69	12	0.6	1.	0.	0.	0.	0.	0.0	0.	0.	0.0
40Igr35	USPT	.7	5	2.2	2	.6	.5	8	8	06	03	01	06	00	0	01	02	1
		15	0.9		13	29	65	12	0.5	1.	0.	0.	0.	0.	0.0	0.	0.	0.0
40Igr37	USPT	.4	0	2.1	4	.2	.8	0	5	11	03	00	08	00	0	01	01	3
		15	0.8		13	27	64	11	0.5	1.	0.	0.	0.	0.	0.0	0.	0.	0.0
40Igr38	USPT	.1	8	2.0	2	.8	.4	9	2	09	03	00	06	00	0	01	01	0
		18	1.5	39.	18	32	10	12	4.6	1.	0.	0.	0.	0.	0.0	0.	0.	0.1
40Igr39	USPT	.4	7	8	9	.1	9	2	7	31	23	04	06	01	0	01	02	3
		17	1.1		16	33	81	16	0.7	1.	0.	0.	0.	0.	0.0	0.	0.	0.0
40Igr41	USPT	.6	7	2.6	5	.7	.9	8	9	30	04	00	09	00	0	02	02	1
		17	1.5	14.	18	28	10	12	1.1	1.	0.	0.	0.	0.	0.0	0.	0.	0.0
40Igr410	USPT	.7	2	3	0	.2	7	8	3	06	07	01	06	00	0	02	01	2
		16	1.2		16	32	88	12	0.7	1.	0.	0.	0.	0.	0.0	0.	0.	0.0
40Igr411	USPT	.9	5	7.5	5	.8	.1	2	3	08	04	00	11	00	0	01	01	1
		18	0.9		16	30	68	12	0.8	1.	0.	0.	0.	0.	0.0	0.	0.	0.0
40Igr412	USPT	.2	6	9.1	9	.9	.5	3	6	48	03	00	10	00	0	01	02	7
		19	1.3		17	34	97	12	1.0	1.	0.	0.	0.	0.	0.0	0.	0.	0.0
40Igr413	USPT	.2	3	2.8	8	.3	.0	2	2	42	05	00	09	00	0	01	02	1
		20	1.2		18	35	91	17	0.8	1.	0.	0.	0.	0.	0.0	0.	0.	0.0
40Igr42	USPT	.3	6	2.9	7	.2	.8	7	8	41	04	00	08	01	0	01	03	0
		20	1.1	21.	27	31	87	16	1.4	1.	0.	0.	0.	0.	0.0	0.	0.	0.0
40Igr43	USPT	.3	9	4	9	.7	.7	4	4	63	32	00	09	00	0	01	02	4
		18	1.2		17	32	86	15	0.7	1.	0.	0.	0.	0.	0.0	0.	0.	0.0
40Igr44	USPT	.6	2	5.2	9	.1	.7	7	6	33	04	00	38	01	0	01	02	1
		19	1.3		17	33	97	14	0.7	1.	0.	0.	0.	0.	0.0	0.	0.	0.0
40Igr45	USPT	.0	8	9.8	9	.1	.7	8	2	53	04	01	06	00	0	02	03	1
		18	1.2		16	31	93	16	0.6	1.	0.	0.	0.	0.	0.0	0.	0.	0.0
40Igr46	USPT	.3	9	3.5	8	.5	.4	0	0	28	04	00	08	01	0	01	02	1
		22	1.7	30.	29	35	12	14	0.7	1.	0.	0.	0.	0.	0.0	0.	0.	0.0
40Igr47	USPT	.4	9	7	8	.0	1	9	8	39	08	00	08	01	1	02	04	1
		17	1.5		17	32	10	15	0.8	1.	0.	0.	0.	0.	0.0	0.	0.	0.0
40Igr48	USPT	.9	2	3.2	0	.9	5	1	0	53	05	01	08	00	0	01	02	1
		18	1.0		17	33	77	13	0.9	1.	0.	0.	0.	0.	0.0	0.	0.	0.0
40Igr49	USPT	.1	9	5.1	5	.0	.6	1	6	69	04	00	06	00	0	01	01	1
		17	1.4		15	30	95	13	0.6	1.	0.	0.	0.	0.	0.0	0.	0.	0.0
40Igr51	USPT	.7	8	2.8	9	.1	.4	3	4	01	05	01	13	00	0	02	02	1
		18	1.2		16	30	85	15	0.6	1.	0.	0.	0.	0.	0.0	0.	0.	0.0
40Igr510	USPT	.4	1	2.4	6	.5	.5	6	4	47	04	00	07	00	0	02	02	1
		18	1.2		16	29	85	14	0.8	1.	0.	0.	0.	0.	0.0	0.	0.	0.0
40Igr511	USPT	.3	3	2.5	1	.6	.3	4	1	31	04	00	07	00	0	01	02	1
		17	1.2		15	33	87	14	0.6	1.	0.	0.	0.	0.	0.0	0.	0.	0.0
40Igr512	USPT	.4	4	2.7	9	.1	.3	7	8	34	04	00	05	00	0	01	02	1
		17	1.4	29.	18	32	10	12	2.5	1.	0.	0.	0.	0.	0.0	0.	0.	0.0
40Igr513	USPT	.2	4	7	4	.6	2	9	7	67	28	01	10	00	0	01	03	6
		17	1.3		16	34	95	14	0.8	1.	0.	0.	0.	0.	0.0	0.	0.	0.0
40Igr52	USPT	.3	3	8.1	0	.4	.9	0	3	31	05	00	06	00	0	01	02	1
		17	1.5		15	29	95	14	0.5	1.	0.	0.	0.	0.	0.0	0.	0.	0.0
40Igr53	USPT	.3	3	2.7	7	.1	.5	4	4	20	04	01	07	00	0	01	02	1
		17	1.2	15.	17	33	95	15	0.7	1.	0.	0.	0.	0.	0.0	0.	0.	0.0
40Igr54	USPT	.9	5	8	0	.1	.3	5	2	64	04	00	09	00	0	02	02	2
		20	2.5	63.	25	31	86	14	4.6	1.	0.	0.	0.	0.	0.0	0.	0.	0.1
40Igr55	USPT	.1	3	2	2	.8	.3	8	0	60	40	02	09	00	0	02	02	7
		17	1.3		16	33	96	14	0.9	1.	0.	0.	0.	0.	0.0	0.	0.	0.0
40Igr56	USPT	.1	0	2.8	0	.2	.2	3	2	46	05	00	05	00	0	01	01	1
		18	1.8		16	30	95	15	0.6	1.	0.	0.	0.	0.	0.0	0.	0.	0.0
40Igr57	USPT	.5	8	3.4	5	.0	.1	5	7	61	05	01	10	01	0	02	02	1
		17	1.2		15	33	90	14	0.6	1.	0.	0.	0.	0.	0.0	0.	0.	0.0
40Igr59	USPT	.3	4	2.5	9	.2	.0	2	9	74	04	00	05	00	0	01	02	1
		17	1.5		16	33	10	15	0.7	1.	0.	0.	0.	0.	0.0	0.	0.	0.0
40Igr61	USPT	.8	1	3.0	5	.8	5	1	3	26	05	01	09	00	0	02	02	1

Sample	Unit	Li	B	Na	Al	P	Ca	Ti	Mn	Ge	Rb	Nb	Sn	La	Ce	Nd	Gd	Pb
		17	1.2		16	31	90	14	0.7	1.	0.	0.	0.	0.	0.0	0.	0.	0.0
40Igr63	USPT	.9	5	4.1	3	.2	.5	7	9	20	04	01	11	00	0	01	02	1
		11	0.6		88	22	55	11	0.4	0.	0.	0.	0.	0.	0.0	0.	0.	0.0
40Igr64	USPT	.6	5	4.0	.2	.1	.4	8	3	65	03	00	05	01	0	01	01	1
		12	0.9	15.	96	21	52	96	1.5	0.	0.	0.	0.	0.	0.0	0.	0.	0.0
40Igr65	USPT	.3	2	8	.8	.1	.1	.9	0	74	10	00	05	00	0	01	01	3
		9.	0.5		70	20	43	90	0.3	0.	0.	0.	0.	0.	0.0	0.	0.	0.0
40Igr66	USPT	5	9	1.2	.3	.8	.5	.2	5	83	02	00	04	00	0	00	01	0
		11	0.7		83	21	47	94	0.4	0.	0.	0.	0.	0.	0.0	0.	0.	0.0
40Igr67	USPT	.1	1	1.3	.7	.9	.4	.1	2	87	02	00	03	00	0	01	01	0
		12	0.6	15.	10	20	44	88	0.8	0.	0.	0.	0.	0.	0.0	0.	0.	0.0
40Igr68	USPT	.7	3	4	5	.3	.1	.6	8	74	16	00	03	00	0	00	01	3
		12	1.1		86	23	53	11	0.3	0.	0.	0.	0.	0.	0.0	0.	0.	0.0
49Bgr11	MSPT	.9	6	1.4	.6	.3	.5	6	7	36	03	00	04	00	0	01	01	1
		14	0.7		88	23	33	12	0.4	0.	0.	0.	0.	0.	0.0	0.	0.	0.0
49Bgr12	MSPT	.9	4	0.9	.7	.3	.4	7	2	85	02	00	04	00	0	00	01	0
		15	0.7		86	24	35	12	0.3	0.	0.	0.	0.	0.	0.0	0.	0.	0.0
49Bgr13	MSPT	.0	7	0.9	.6	.4	.4	7	6	91	02	00	05	00	0	00	00	0
		10	1.8		10	21	40	10	0.4	0.	0.	0.	0.	0.	0.0	0.	0.	0.0
49Bgr14	MSPT	.5	3	1.6	3	.1	.8	8	7	84	04	00	04	00	0	00	01	1
		13	0.7		85	22	32	11	0.3	0.	0.	0.	0.	0.	0.0	0.	0.	0.0
49Bgr15	MSPT	.0	0	5.7	.5	.9	.4	8	9	65	02	00	06	00	1	00	00	1
		12	0.6		83	22	42	10	0.3	0.	0.	0.	0.	0.	0.0	0.	0.	0.0
49Bgr16	MSPT	.6	3	2.1	.7	.9	.1	8	3	68	02	00	06	00	0	00	00	0
		10	0.9		80	23	43	10	0.3	0.	0.	0.	0.	0.	0.0	0.	0.	0.0
49Bgr17	MSPT	.5	8	1.0	.8	.3	.5	4	5	67	02	00	05	00	0	01	01	0
		8.	0.8		80	21	42	90	0.3	0.	0.	0.	0.	0.	0.0	0.	0.	0.0
49Bgr18	MSPT	5	6	0.9	.6	.9	.6	.9	5	89	02	00	05	00	0	01	01	0
		10	0.9		10	25	44	11	0.6	0.	0.	0.	0.	0.	0.0	0.	0.	0.0
49Bgr21	MSPT	.9	8	1.0	7	.6	.0	0	1	92	04	00	05	00	1	00	01	0
		9.	0.9		81	21	42	91	0.4	0.	0.	0.	0.	0.	0.0	0.	0.	0.0
49Bgr210	MSPT	3	2	0.9	.0	.5	.1	.7	0	85	02	00	04	00	0	00	01	0
		11	1.1		10	23	51	11	0.3	0.	0.	0.	0.	0.	0.0	0.	0.	0.0
49Bgr22	MSPT	.2	7	4.1	3	.5	.8	8	6	80	03	00	07	00	0	00	00	1
		15	2.6	19.	25	20	56	10	1.0	0.	0.	0.	0.	0.	0.0	0.	0.	0.0
49Bgr23	MSPT	.1	6	6	1	.7	.1	4	7	56	25	04	06	01	1	01	01	4
		11	1.3		10	24	62	11	0.7	0.	0.	0.	0.	0.	0.0	0.	0.	0.0
49Bgr24	MSPT	.0	6	2.8	9	.8	.1	7	7	49	05	00	05	00	0	01	02	1
		10	0.9		14	24	43	11	0.4	0.	0.	0.	0.	0.	0.0	0.	0.	0.0
49Bgr25	MSPT	.7	6	1.0	3	.4	.9	4	7	54	10	00	11	00	0	00	01	0
		10	1.1		98	19	35	11	0.7	0.	0.	0.	0.	0.	0.0	0.	0.	0.0
49Bgr26	MSPT	.4	0	2.4	.3	.9	.1	3	3	73	02	00	04	01	1	00	01	0
		10	0.8		99	22	38	11	0.4	0.	0.	0.	0.	0.	0.0	0.	0.	0.0
49Bgr27	MSPT	.7	4	1.2	.0	.3	.3	7	8	62	02	13	05	00	0	01	01	1
		11	0.7		91	19	32	11	0.4	0.	0.	0.	0.	0.	0.0	0.	0.	0.0
49Bgr28	MSPT	.4	3	0.8	.9	.6	.9	7	2	72	02	00	05	00	0	00	00	0
		8.	0.6		79	21	31	93	0.3	0.	0.	0.	0.	0.	0.0	0.	0.	0.0
49Bgr29	MSPT	8	9	0.7	.2	.8	.5	.6	3	75	02	00	05	00	0	00	01	0
		9.	0.8		86	22	43	11	0.3	0.	0.	0.	0.	0.	0.0	0.	0.	0.0
49Bgr31	MSPT	9	2	0.8	.7	.2	.6	3	2	62	02	00	06	00	0	00	01	0
		9.	1.0		10	23	47	11	0.4	0.	0.	0.	0.	0.	0.0	0.	0.	0.0
49Bgr32	MSPT	9	5	1.1	7	.8	.0	6	7	76	04	00	04	00	0	01	01	1
		9.	1.2		90	23	35	11	0.9	0.	0.	0.	0.	0.	0.0	0.	0.	0.0
49Bgr33	MSPT	0	2	0.8	.0	.2	.9	4	6	73	02	00	05	00	1	00	01	1
		9.	0.6		93	22	28	11	0.4	0.	0.	0.	0.	0.	0.0	0.	0.	0.0
49Bgr34	MSPT	7	5	1.5	.0	.7	.8	8	1	81	02	01	08	00	1	00	01	4
		7.	4.3	12.	89	20	43	10	3.9	0.	0.	0.	0.	0.	0.0	0.	0.	0.0
49Bgr35	MSPT	9	8	9	.5	.1	.1	5	2	76	06	01	04	02	4	02	01	1
		8.	7.9	10.	86	20	39	10	5.2	0.	0.	0.	0.	0.	0.0	0.	0.	0.0
49Bgr36	MSPT	3	3	2	.4	.1	.7	6	9	95	07	00	06	03	8	03	01	2
		9.	7.5	11.	17	23	29	10	4.6	0.	0.	0.	0.	0.	0.0	0.	0.	0.6
49Bgr37	MSPT	6	6	8	4	.9	6	3	3	93	19	05	05	04	8	03	01	4
		8.	1.1		94	24	12	10	0.4	0.	0.	0.	0.	0.	0.0	0.	0.	0.0
49Bgr38	MSPT	8	1	1.7	.2	.6	8	7	0	70	03	01	04	00	0	00	01	0
		11	0.8		11	24	38	10	1.1	1.	0.	0.	0.	0.	0.0	0.	0.	0.0
49Bgr41	MSPT	.9	7	0.8	6	.0	.5	5	7	04	02	00	05	00	0	00	01	0
		10	2.4		86	22	36	90	1.0	0.	0.	0.	0.	0.	0.0	0.	0.	0.0
49Bgr42	MSPT	.0	2	2.4	.3	.2	.6	.8	5	81	02	00	06	01	1	01	00	0
		9.	0.6		88	22	30	10	0.3	0.	0.	0.	0.	0.	0.0	0.	0.	0.0
49Bgr43	MSPT	4	7	0.8	.9	.6	.5	6	8	71	02	00	05	00	0	00	01	0
		12	0.8		93	25	51	10	0.2	0.	0.	0.	0.	0.	0.0	0.	0.	0.0
49Bgr44	MSPT	.0	7	0.9	.7	.9	.0	0	7	84	03	00	05	00	0	01	01	0
		13	2.5	30.	34	24	67	10	0.6	0.	0.	0.	0.	0.	0.0	0.	0.	0.0
49Bgr45	MSPT	.0	3	2	8	.1	.5	3	9	97	49	01	07	00	1	00	01	4

Sample	Unit	Li	B	Na	Al	P	Ca	Ti	Mn	Ge	Rb	Nb	Sn	La	Ce	Nd	Gd	Pb
		11	0.8		88	22	37	10	0.3	0.	0.	0.	0.	0.	0.0	0.	0.	0.0
49Bgr47	MSPT	.5	7	0.9	.9	.8	.5	5	7	73	02	00	07	00	0	01	01	0
		10	0.8		11	22	43	94	0.4	0.	0.	0.	0.	0.	0.0	0.	0.	0.0
49Bgr48	MSPT	.7	0	9.0	4	.5	.6	.6	9	63	11	00	05	00	0	00	00	0
		13	3.0	22.	33	23	31	91	1.1	0.	0.	0.	0.	0.	0.0	0.	0.	0.0
49Bgr49	MSPT	.3	9	4	6	.0	.6	.2	2	77	46	01	06	00	0	00	00	2
		18	0.7		89	22	30	11	0.3	0.	0.	0.	0.	0.	0.0	0.	0.	0.0
49Bgr51	MSPT	.1	2	0.7	.8	.7	.7	7	6	69	02	00	05	00	0	00	01	0
		16	0.7		92	22	30	12	0.3	0.	0.	0.	0.	0.	0.0	0.	0.	0.0
49Bgr52	MSPT	.9	2	0.7	.7	.4	.8	3	5	73	02	00	03	00	0	00	01	1
		15	0.8		90	23	39	12	0.5	0.	0.	0.	0.	0.	0.0	0.	0.	0.0
49Bgr53	MSPT	.2	9	1.2	.5	.3	.7	1	4	77	02	00	07	00	0	00	01	0
		12	1.0		93	24	45	10	0.4	0.	0.	0.	0.	0.	0.0	0.	0.	0.0
49Bgr54	MSPT	.6	2	4.5	.1	.7	.3	9	0	68	03	00	04	00	0	00	01	0
		12	0.7		85	22	29	11	0.3	0.	0.	0.	0.	0.	0.0	0.	0.	0.0
49Bgr55	MSPT	.6	0	0.7	.8	.6	.6	7	6	70	02	00	05	00	0	00	01	0
		12	0.7		88	23	31	11	0.4	0.	0.	0.	0.	0.	0.0	0.	0.	0.0
49Bgr56	MSPT	.9	2	0.7	.5	.3	.7	8	0	72	02	00	07	00	0	01	00	0
		10	0.7		89	21	33	11	0.3	0.	0.	0.	0.	0.	0.0	0.	0.	0.0
49Bgr57	MSPT	.4	6	0.8	.9	.7	.3	3	9	70	02	00	07	00	0	00	01	0
		9.	0.9		80	25	41	10	0.4	0.	0.	0.	0.	0.	0.0	0.	0.	0.0
49Bgr58	MSPT	2	9	1.0	.4	.0	.0	5	5	62	02	00	03	01	1	00	01	0
		9.	0.7		81	22	32	11	0.3	0.	0.	0.	0.	0.	0.0	0.	0.	0.0
49Bgr59	MSPT	5	5	0.7	.0	.2	.5	5	9	80	02	00	05	00	0	00	00	0
		9.	0.7		89	23	35	12	0.4	0.	0.	0.	0.	0.	0.0	0.	0.	0.0
49Bgr61	MSPT	8	5	1.4	.1	.5	.6	7	1	77	02	00	04	00	0	01	00	0
		10	0.8		82	22	36	94	0.8	0.	0.	0.	0.	0.	0.0	0.	0.	0.0
49Bgr610	MSPT	.3	4	3.1	.8	.3	.4	.6	2	50	02	00	06	00	0	00	01	0
		14	0.7		90	22	32	13	0.4	0.	0.	0.	0.	0.	0.0	0.	0.	0.0
49Bgr62	MSPT	.0	6	1.8	.3	.6	.0	2	1	71	02	00	08	00	0	00	01	0
		11	0.9		94	22	45	11	0.4	0.	0.	0.	0.	0.	0.0	0.	0.	0.0
49Bgr63	MSPT	.7	7	0.9	.1	.2	.5	6	2	61	03	02	05	00	1	00	00	0
		11	1.0	10.	15	24	39	11	0.5	0.	0.	0.	0.	0.	0.0	0.	0.	0.0
49Bgr64	MSPT	.6	7	6	8	.8	.8	4	1	81	13	05	04	00	0	01	00	1
		9.	0.8		88	21	37	11	0.3	0.	0.	0.	0.	0.	0.0	0.	0.	0.0
49Bgr65	MSPT	3	7	0.8	.4	.4	.7	7	7	76	02	00	07	00	0	01	01	0
		19	2.1	11.	30	24	38	12	1.0	0.	0.	0.	0.	0.	0.0	0.	0.	0.0
49Bgr66	MSPT	.8	6	6	6	.1	.8	1	2	83	27	39	06	00	4	03	01	8
		10	0.8		99	21	34	12	0.3	0.	0.	0.	0.	0.	0.0	0.	0.	0.0
49Bgr67	MSPT	.1	2	8.2	.2	.3	.7	1	0	82	02	00	06	00	0	00	01	0
		8.	1.5		81	21	38	93	1.1	0.	0.	0.	0.	0.	0.0	0.	0.	0.0
49Bgr68	MSPT	2	1	2.1	.0	.8	.5	.7	0	75	02	00	07	00	1	01	00	0
		10	0.7		79	22	32	95	0.2	0.	0.	0.	0.	0.	0.0	0.	0.	0.0
49Bgr69	MSPT	.4	6	0.7	.2	.4	.9	.4	7	46	02	00	04	00	0	01	00	0
		13	0.9		86	22	38	11	0.2	0.	0.	0.	0.	0.	0.0	0.	0.	0.0
49Bgr71	MSPT	.3	0	0.9	.9	.2	.9	8	0	65	02	00	06	00	0	01	01	0
		9.	0.7		98	23	33	12	0.4	0.	0.	0.	0.	0.	0.0	0.	0.	0.0
49Bgr710	MSPT	5	9	0.9	.0	.4	.8	2	1	58	06	01	06	00	0	01	01	1
		9.	0.8		83	23	36	90	0.3	0.	0.	0.	0.	0.	0.0	0.	0.	0.0
49Bgr711	MSPT	2	6	2.3	.4	.6	.4	.9	6	57	02	00	08	00	0	01	01	1
		10	0.7		91	21	31	11	0.4	0.	0.	0.	0.	0.	0.0	0.	0.	0.0
49Bgr72	MSPT	.6	6	0.7	.5	.3	.8	7	1	68	02	00	04	00	0	00	01	0
		12	1.4		17	22	45	12	0.4	0.	0.	0.	0.	0.	0.0	0.	0.	0.0
49Bgr73	MSPT	.4	6	8.2	6	.2	.7	7	6	76	14	67	11	00	0	01	00	4
		13	0.6		95	22	29	13	0.4	0.	0.	0.	0.	0.	0.0	0.	0.	0.0
49Bgr75	MSPT	.2	6	0.7	.4	.5	.3	4	0	77	02	00	04	00	0	00	01	1
		12	0.7		95	23	33	12	0.4	0.	0.	0.	0.	0.	0.0	0.	0.	0.0
49Bgr76	MSPT	.6	4	0.8	.5	.4	.3	0	3	52	02	00	06	00	0	00	01	0
		11	0.7		86	22	37	12	0.3	0.	0.	0.	0.	0.	0.0	0.	0.	0.0
49Bgr77	MSPT	.7	5	0.8	.5	.8	.4	3	8	85	02	00	06	00	0	01	01	0
		13	4.0	15.	13	21	41	93	2.8	0.	0.	0.	0.	0.	0.0	0.	0.	0.0
49Bgr78	MSPT	.0	3	4	1	.7	.0	.3	6	85	12	00	05	03	5	02	01	1
		10	0.8		90	24	56	12	0.5	0.	0.	0.	0.	0.	0.0	0.	0.	0.0
49Bgr79	MSPT	.7	8	0.9	.5	.8	.6	4	1	85	02	00	03	00	0	00	01	0
		9.	1.0		19	19	39	94	0.3	0.	0.	0.	0.	0.	0.0	0.	0.	0.0
49Cgr12	MSPT	9	6	8.5	4	.7	.6	.2	8	84	23	01	04	00	0	01	01	3
		10	0.8		88	21	41	93	1.0	0.	0.	0.	0.	0.	0.0	0.	0.	0.0
49Cgr13	MSPT	.0	2	1.9	.4	.2	.1	.7	3	87	05	01	07	00	0	00	01	2
		10	0.8		96	21	42	10	0.3	0.	0.	0.	0.	0.	0.0	0.	0.	0.0
49Cgr15	MSPT	.7	6	1.6	.8	.5	.5	5	8	69	02	00	05	00	0	01	01	0
		10	0.8		10	18	62	92	0.3	0.	0.	0.	0.	0.	0.0	0.	0.	0.0
49Cgr16	MSPT	.8	4	5.6	1	.9	.3	.0	0	85	02	00	04	00	0	00	01	1
		10	1.0		76	20	12	97	0.3	0.	0.	0.	0.	0.	0.0	0.	0.	0.0
49Cgr22	MSPT	.0	1	1.0	.0	.1	5	.0	1	86	03	01	06	00	0	00	01	1

Sample	Unit	Li	B	Na	Al	P	Ca	Ti	Mn	Ge	Rb	Nb	Sn	La	Ce	Nd	Gd	Pb
		11	1.7	19.	12	24	78	10	1.1	0.	0.	0.	0.	0.	0.0	0.	0.	0.1
49Cgr24	MSPT	.8	2	8	7	.3	.2	9	7	89	09	01	07	01	1	01	00	4
		10	0.7	36.	19	18	51	99	0.8	0.	0.	0.	0.	0.	0.2	0.	0.	0.0
49Cgr27	MSPT	.5	8	4	6	.9	.7	.6	3	71	92	10	05	08	8	04	01	6
		9.	0.8	10.	10	20	65	97	0.5	0.	0.	0.	0.	0.	0.0	0.	0.	0.0
49Cgr28	MSPT	7	2	9	7	.4	.9	.6	3	81	13	01	04	00	3	00	01	2
		9.	0.9		79	23	57	93	0.3	0.	0.	0.	0.	0.	0.0	0.	0.	0.0
49Cgr31	MSPT	5	7	0.9	.6	.1	.8	.1	8	79	02	00	09	00	1	00	01	3
		8.	1.0		14	22	91	87	0.4	1.	0.	0.	0.	0.	0.0	0.	0.	0.0
49Cgr32	MSPT	9	5	6.3	4	.5	.1	.4	5	03	14	01	07	00	0	01	00	1
		12	0.8		86	19	67	14	0.3	0.	0.	0.	0.	0.	0.0	0.	0.	0.0
49Cgr41	MSPT	.8	6	0.9	.0	.2	.9	2	5	80	02	01	07	00	0	00	01	0
		12	0.9	16.	96	20	78	13	0.4	0.	0.	0.	0.	0.	0.0	0.	0.	0.0
49Cgr43	MSPT	.4	0	6	.8	.7	.0	7	8	76	06	01	09	01	2	01	01	1
		12	12.	19	32	29	14	13	8.3	0.	0.	0.	2.	0.	0.1	0.	0.	1.1
49Cgr44	MSPT	.0	9	8	0	.1	2	7	1	67	95	18	61	08	9	08	02	5
		8.	0.8		74	20	69	94	0.2	0.	0.	0.	0.	0.	0.0	0.	0.	0.0
49Cgr45	MSPT	8	0	2.3	.0	.1	.4	.3	5	73	02	00	07	00	0	00	01	2
		10	0.8		85	21	90	12	0.3	0.	0.	0.	0.	0.	0.0	0.	0.	0.0
49Cgr46	MSPT	.0	6	1.3	.2	.4	.4	3	5	84	02	00	07	00	0	00	00	0
		9.	1.0	10.	11	21	75	10	0.5	0.	0.	0.	0.	0.	0.0	0.	0.	0.0
49Cgr48	MSPT	4	0	3	7	.3	.4	3	0	84	12	01	11	00	0	00	01	2
		11	0.7		88	20	42	94	0.4	0.	0.	0.	0.	0.	0.0	0.	0.	0.0
49Cgr49	MSPT	.5	6	0.8	.5	.8	.2	.1	4	90	02	00	06	00	0	00	01	0
		13	5.5	55.	17	27	10	11	6.4	0.	0.	0.	0.	0.	0.0	0.	0.	0.2
49Cgr51	MSPT	.9	8	0	3	.2	6	5	7	65	33	06	31	02	3	02	01	2
		9.	1.8	74.	17	20	94	90	0.3	0.	0.	0.	0.	0.	1.6	0.	0.	0.0
49Cgr510	MSPT	3	0	8	2	.1	.1	.9	4	61	31	07	04	61	5	41	05	5
		14	1.0	25.	17	22	62	10	0.5	0.	0.	0.	0.	0.	0.0	0.	0.	0.0
49Cgr52	MSPT	.6	6	6	6	.4	.4	6	9	77	14	42	09	01	3	00	02	4
		12	2.4	14.	28	22	61	11	1.4	0.	0.	0.	0.	0.	0.0	0.	0.	0.0
49Cgr53	MSPT	.8	7	3	0	.6	.5	1	3	83	51	07	14	00	0	00	01	4
		11	0.9		11	22	57	11	0.5	0.	0.	0.	0.	0.	0.0	0.	0.	0.0
49Cgr55	MSPT	.6	0	8.4	6	.3	.8	3	2	68	85	00	05	01	1	00	00	2
		10	0.9	10.	89	18	61	11	0.3	0.	0.	0.	0.	0.	0.0	0.	0.	0.0
49Cgr56	MSPT	.0	1	6	.6	.7	.5	3	8	93	03	00	04	00	1	00	01	1
		12	1.3	15.	20	22	72	11	0.4	0.	0.	0.	0.	0.	0.0	0.	0.	0.0
49Cgr57	MSPT	.1	7	7	8	.5	.8	0	6	74	19	01	06	00	0	01	01	3
		10	0.8		91	19	49	11	0.4	0.	0.	0.	0.	0.	0.0	0.	0.	0.0
49Cgr58	MSPT	.9	4	0.9	.6	.1	.7	1	6	83	02	00	05	00	0	00	01	1
		9.	0.9		82	21	71	95	0.3	0.	0.	0.	0.	0.	0.0	0.	0.	0.0
49Cgr59	MSPT	9	9	1.3	.8	.1	.8	.2	1	78	02	00	05	00	1	01	01	3
		12	19.		10	23	69	11	0.4	1.	0.	0.	0.	0.	0.0	0.	0.	0.0
49Cgr62	MSPT	.1	4	2.0	3	.8	.1	3	0	06	06	01	05	00	1	01	01	0
		11	1.1 -		92	21	57	10	0.4	0.	0.	0.	0.	0.	0.0	0.	0.	0.0
49Cgr64	MSPT	.0	1	0.8	.1	.7	.2	8	0	75	02	00	05	00	0	00	00	1
		10	0.1		88	19	64	95	0.4	0.	0.	0.	0.	0.	0.0	0.	0.	0.0
49Cgr66	MSPT	.3	2	5.1	.5	.7	.3	.7	7	80	05	01	04	00	0	01	01	1
		10	0.6 -		86	22	43	96	0.4	0.	0.	0.	0.	0.	0.0	0.	0.	0.0
49Cgr67	MSPT	.4	6	2.3	.0	.9	.8	.4	3	76	14	01	04	00	1	00	01	2
		10	1.3		17	23	89	10	0.8	0.	0.	0.	0.	0.	0.0	0.	0.	0.1
49Dgr11	MSPT	.9	8	3.7	8	.7	.3	5	5	76	32	01	11	05	9	05	01	9
		11	0.6		87	21	68	12	0.4	0.	0.	0.	0.	0.	0.0	0.	0.	0.0
49Dgr12	MSPT	.3	8	0.7	.1	.0	.7	3	4	82	02	00	04	00	0	00	01	1
		10	0.7		88	21	76	12	0.4	0.	0.	0.	0.	0.	0.0	0.	0.	0.0
49Dgr14	MSPT	.5	2	4.5	.5	.2	.4	1	7	80	02	01	08	00	1	00	01	4
		10	0.9		95	20	81	12	0.3	0.	0.	0.	0.	0.	0.0	0.	0.	0.0
49Dgr15	MSPT	.6	0	0.9	.9	.6	.6	3	7	58	03	00	05	00	0	00	01	5
		9.	0.9	36.	27	23	18	10	3.0	0.	0.	0.	0.	1.	1.8	0.	0.	54.
49Dgr16	MSPT	2	2	6	4	.4	6	9	6	66	65	30	62	03	4	75	12	8
		9.	0.8		98	24	64	10	0.4	0.	0.	0.	0.	0.	0.0	0.	0.	0.1
49Dgr17	MSPT	0	5	5.3	.6	.1	.7	0	1	64	08	00	13	00	1	01	00	4
		10	1.0		89	23	58	12	0.5	0.	0.	0.	0.	0.	0.0	0.	0.	0.2
49Dgr18	MSPT	.3	5	4.0	.8	.2	.2	6	0	61	04	00	11	00	0	00	01	0
		10	2.7	13.	26	22	86	10	0.6	0.	0.	0.	0.	0.	0.0	0.	0.	1.0
49Dgr19	MSPT	.6	4	1	4	.4	.8	9	2	83	30	05	37	01	2	00	01	8
		9.	1.0		97	21	52	11	0.4	0.	0.	0.	0.	0.	0.0	0.	0.	0.0
49Dgr21	MSPT	4	0	1.7	.1	.5	.2	2	1	56	04	00	09	00	0	00	01	4
		12	2.1	31.	30	23	10	10	0.7	1.	0.	0.	0.	0.	0.0	0.	0.	0.2
49Dgr211	MSPT	.2	8	7	8	.0	5	2	6	05	42	01	13	04	8	04	01	5
		9.	0.9		83	22	12	12	0.5	0.	0.	0.	0.	0.	0.0	0.	0.	0.3
49Dgr22	MSPT	5	6	1.4	.1	.6	4	2	7	78	03	00	10	00	0	01	01	9

Sample	Unit	Li	B	Na	Al	P	Ca	Ti	Mn	Ge	Rb	Nb	Sn	La	Ce	Nd	Gd	Pb
49Dgr24	MSPT	9.8	0.85	3.7	93.6	23.5	52.1	109	0.24	0.73	0.04	0.00	0.06	0.00	0.0	0.00	0.01	0.01
49Dgr27	MSPT	10.5	0.92	3.6	104	20.8	85.0	124	0.52	0.73	0.21	0.01	0.13	0.02	0.7	0.01	0.01	0.12
49Dgr29	MSPT	9.8	0.91	100	347	20.5	84.6	104	0.84	0.66	1.36	0.12	0.20	0.12	0.33	0.05	0.01	0.27
49Dgr41	MSPT	9.0	1.00	1.1	70.6	23.9	58.3	101	0.33	0.80	0.03	0.00	0.04	0.00	0.0	0.00	0.01	0.01
49Dgr42	MSPT	11.4	1.63	29.9	250	19.2	91.1	93.4	0.46	0.98	0.29	0.00	0.05	0.00	0.0	0.00	0.00	0.02
49Dgr43	MSPT	9.2	0.79	3.8	80.1	20.3	84.2	96.0	0.64	0.67	0.02	0.00	0.07	0.01	0.1	0.00	0.01	0.01
49Dgr44	MSPT	9.5	0.85	0.8	77.9	19.6	75.8	101	0.38	0.75	0.02	0.00	0.05	0.00	0.0	0.01	0.01	0.00
49Dgr45	MSPT	9.7	1.03	1.9	86.2	21.6	55.1	102	0.43	0.48	0.05	0.00	0.04	0.00	0.0	0.01	0.00	0.00
49Dgr46	MSPT	9.7	0.81	9.7	84.0	21.0	90.7	98.7	0.43	0.49	0.04	0.00	0.03	0.00	0.1	0.01	0.01	0.01
49Dgr51	MSPT	15.7	2.27	20.6	259	22.2	10.0	126	0.50	1.01	0.53	0.00	0.04	0.00	0.0	0.01	0.01	0.02
49Dgr510	MSPT	11.5	1.22	14.4	207	22.2	65.5	110	0.48	0.87	0.20	0.00	0.04	0.00	0.0	0.00	0.01	0.01
49Dgr512	MSPT	11.1	2.44	34.0	284	20.5	53.4	86.3	0.54	0.82	0.46	0.02	0.04	0.02	0.4	0.00	0.01	0.02
49Dgr513	MSPT	10.4	2.07	30.0	274	20.7	49.1	103	0.55	0.75	0.41	0.77	0.02	0.04	0.12	0.03	0.01	0.06
49Dgr52	MSPT	13.9	0.82	0.8	87.6	21.7	59.6	131	0.33	0.85	0.02	0.00	0.04	0.00	0.0	0.01	0.00	0.00
49Dgr53	MSPT	13.8	0.75	0.7	95.3	18.7	78.0	125	0.48	0.66	0.02	0.00	0.02	0.00	0.0	0.00	0.01	0.00
49Dgr54	MSPT	10.5	0.80	0.7	82.7	21.0	55.0	105	0.31	0.81	0.02	0.00	0.03	0.00	0.0	0.00	0.01	0.00
49Dgr55	MSPT	9.3	0.80	3.5	112	19.9	76.4	107	0.28	0.80	0.07	0.00	0.05	0.00	0.0	0.00	0.01	0.00
49Dgr57	MSPT	9.0	0.83	1.3	79.7	21.8	52.8	106	0.61	0.73	0.02	0.00	0.05	0.00	0.0	0.01	0.01	0.00
49Dgr58	MSPT	10.7	1.30	5.4	103	22.7	65.9	117	0.41	0.82	0.03	0.00	0.05	0.00	0.0	0.01	0.02	0.01
49Dgr59	MSPT	9.0	1.15	1.4	91.5	18.4	63.4	105	0.33	1.00	0.03	0.00	0.08	0.00	0.0	0.00	0.01	0.00
49Dgr61	MSPT	10.1	2.16	14.7	226	20.5	58.4	89.6	0.55	0.73	0.27	0.01	0.04	0.00	0.0	0.01	0.01	0.02
49Dgr62	MSPT	9.5	0.92	0.9	89.7	21.2	94.1	110	0.33	0.73	0.03	0.00	0.03	0.00	0.0	0.00	0.00	0.00
49Dgr63	MSPT	9.8	0.94	0.9	92.9	18.6	60.2	104	0.36	0.81	0.02	0.00	0.04	0.00	0.0	0.00	0.01	0.01
49Dgr64	MSPT	9.2	0.94	0.9	83.8	21.1	45.0	107	0.34	0.56	0.02	0.00	0.06	0.00	0.0	0.01	0.01	0.00
49Dgr65	MSPT	10.4	0.83	0.8	90.1	18.0	48.3	114	0.34	0.65	0.02	0.00	0.03	0.00	0.0	0.01	0.01	0.00
49Dgr66	MSPT	10.2	0.94	0.9	83.8	18.4	53.9	116	0.36	0.76	0.02	0.01	0.03	0.00	0.0	0.00	0.01	0.01
49Dgr67	MSPT	9.6	0.72	0.7	81.7	18.0	48.9	96.9	0.33	0.78	0.02	0.00	0.03	0.00	0.0	0.01	0.01	0.00
49Dgr68	MSPT	9.7	0.95	1.4	77.5	19.8	51.0	92.2	0.34	0.62	0.03	0.00	0.04	0.00	0.0	0.00	0.01	0.00
AGQM12.21	Monzonite	10.8	0.77	14.9	120	24.7	64.1	169	0.61	0.67	0.03	0.00	0.06	0.00	0.0	0.01	0.01	0.03
AGQM12.210	Monzonite	10.1	0.59	1.8	115	23.1	42.4	135	0.24	0.97	0.02	0.00	0.06	0.00	0.0	0.00	0.01	0.00
AGQM12.211	Monzonite	8.8	1.03	10.1	149	28.5	51.7	122	1.84	1.03	0.09	0.01	0.05	0.01	0.1	0.01	0.01	0.18
AGQM12.212	Monzonite	10.8	2.63	475	198	26.9	124	121	55.34	1.10	3.10	0.01	0.07	0.11	0.13	0.05	0.01	2.92
AGQM12.213	Monzonite	7.8	0.59	35.8	110	24.5	46.1	141	5.69	0.71	0.42	0.01	0.07	0.05	0.08	0.02	0.00	0.90
AGQM12.214	Monzonite	11.0	1.21	177	211	23.6	93.8	128	8.49	1.40	1.39	0.12	0.06	0.04	0.7	0.00	0.07	0.47
AGQM12.215	Monzonite	11.1	0.61	34.4	128	25.7	59.1	133	3.14	1.16	0.23	0.00	0.05	0.01	0.2	0.00	0.00	0.51
AGQM12.219	Monzonite	9.4	5.19	610	94.4	24.8	214	134	61.46	0.67	5.13	0.00	0.20	0.14	0.2	0.04	0.01	12.2
AGQM12.22	Monzonite	11.4	0.55	0.5	136	24.0	49.6	180	0.29	0.84	0.02	0.00	0.05	0.00	0.0	0.00	0.00	0.01

Sample	Unit	Li	B	Na	Al	P	Ca	Ti	Mn	Ge	Rb	Nb	Sn	La	Ce	Nd	Gd	Pb
AGQM12	Monzo	13	3.0	17	31	21	13	15	6.7	0.	0.	0.	0.	0.	0.0	0.	0.	2.5
.222	nite	.6	9	2	6	.2	1	2	8	82	92	01	06	01	2	01	01	6
AGQM12	Monzo	7.	0.5	24.	91	24	77	12	5.2	0.	0.	0.	0.	0.	0.0	0.	0.	0.6
.224	nite	3	4	0	.8	.7	.3	0	3	88	35	01	03	03	5	01	01	6
AGQM12	Monzo	10	0.6		11	21	52	16	0.8	0.	0.	0.	0.	0.	0.0	0.	0.	0.0
.225	nite	.4	0	4.3	4	.6	.1	1	4	61	02	00	07	00	0	00	01	3
AGQM12	Monzo	9.	0.5	15.	10	23	70	16	1.9	0.	0.	0.	0.	0.	0.0	0.	0.	0.2
.226	nite	0	5	7	8	.4	.9	1	5	55	11	00	06	01	2	00	01	6
AGQM12	Monzo	10	0.7		13	26	53	15	0.4	0.	0.	0.	0.	0.	0.0	0.	0.	0.0
.227	nite	.4	5	0.7	3	.0	.1	9	5	83	02	00	07	00	0	00	00	0
AGQM12	Monzo	9.	0.6		11	24	75	13	5.3	0.	0.	0.	0.	0.	0.0	0.	0.	0.1
.228	nite	5	3	6.6	6	.1	.5	3	3	90	26	01	04	00	0	00	01	3
AGQM12	Monzo	8.	0.6		10	25	35	13	0.2	0.	0.	0.	0.	0.	0.0	0.	0.	0.0
.23	nite	1	6	3.5	6	.1	.7	2	0	97	02	01	05	00	0	00	01	2
AGQM12	Monzo	8.	1.8		11	25	80	16	5.6	0.	0.	0.	0.	0.	0.0	0.	0.	0.1
.230	nite	4	1	9.4	1	.5	.9	7	7	83	22	01	05	01	1	01	01	5
AGQM12	Monzo	8.	0.7		10	25	32	13	1.0	1.	0.	0.	0.	0.	0.0	0.	0.	0.0
.231	nite	5	3	8.1	2	.5	.5	1	0	27	05	00	06	00	0	00	01	3
AGQM12	Monzo	8.	0.5		86	23	91	12	0.2	0.	0.	0.	0.	0.	0.0	0.	0.	0.0
.233	nite	0	6	4.1	.7	.7	.9	8	1	76	02	00	05	00	0	00	00	1
AGQM12	Monzo	8.	1.3	11	96	23	98	13	4.7	0.	0.	0.	0.	0.	0.0	0.	0.	0.4
.234	nite	9	7	1	.5	.6	.6	1	2	73	27	00	09	01	1	01	01	6
AGQM12	Monzo	9.	2.7	14	10	23	20	16	205	0.	16	0.	0.	0.	0.5	0.	0.	18.
.235	nite	4	4	43	8	.9	5	1	.4	89	.7	02	20	31	1	13	01	4
AGQM12	Monzo	6.	3.7	26	24	23	98	48	9.3	0.	0.	0.	0.	0.	0.0	0.	0.	0.3
.237	nite	7	9	6	6	.3	.1	.4	3	79	96	12	10	01	1	01	01	4
AGQM12	Monzo	12	0.7		13	21	65	15	0.6	1.	0.	0.	0.	0.	0.0	0.	0.	0.0
.238	nite	.1	7	2.2	1	.5	.1	9	3	00	02	00	06	00	0	00	01	4
AGQM12	Monzo	11	0.9	22.	12	25	57	14	2.3	0.	0.	0.	0.	0.	0.0	0.	0.	0.0
.239	nite	.4	3	4	6	.7	.4	8	4	79	09	01	05	01	2	01	02	9
AGQM12	Monzo	9.	0.8	25.	10	22	51	15	3.9	0.	0.	0.	0.	0.	0.0	0.	0.	0.2
.24	nite	0	8	1	4	.1	.9	5	8	69	18	02	05	01	1	01	01	4
AGQM12	Monzo	9.	0.8	18	20	23	11	12	4.2	0.	0.	0.	0.	0.	0.0	0.	0.	0.0
.240	nite	2	5	07	0	.5	1	6	7	92	29	01	07	00	0	00	00	9
AGQM12	Monzo	8.	0.8	32.	21	26	78	12	16.	1.	1.	0.	0.	0.	0.0	0.	0.	1.4
.241	nite	1	5	0	9	.3	.8	3	92	21	58	01	08	02	2	01	01	4
AGQM12	Monzo	8.	1.1	45.	10	24	46	13	5.7	0.	0.	0.	0.	0.	0.0	0.	0.	0.8
.242	nite	7	1	8	2	.0	.5	5	5	89	49	01	07	07	6	04	01	5
AGQM12	Monzo	8.	0.6		10	24	46	13	0.4	0.	0.	0.	0.	0.	0.0	0.	0.	0.0
.243	nite	3	4	4.4	2	.3	.2	5	1	85	02	00	06	00	1	01	01	9
AGQM12	Monzo	12	1.0	18.	15	25	43	16	1.8	0.	0.	0.	0.	0.	0.0	0.	0.	0.3
.25	nite	.6	5	0	4	.6	.3	3	8	61	17	01	04	00	1	01	01	5
AGQM12	Monzo	13	0.7	10.	16	25	49	15	0.5	0.	0.	0.	0.	0.	0.0	0.	0.	0.0
.26	nite	.4	0	5	4	.5	.2	0	7	78	02	00	05	00	0	01	00	1
AGQM12	Monzo	10	0.6		12	24	51	19	0.2	0.	0.	0.	0.	0.	0.0	0.	0.	0.0
.27	nite	.6	1	0.6	1	.5	.0	2	6	75	01	00	05	00	0	00	01	0
AGQM12	Monzo	9.	2.1	40.	11	26	50	12	5.0	0.	0.	0.	0.	0.	0.0	0.	0.	0.1
.28	nite	6	2	6	7	.3	.1	1	0	72	41	01	07	01	1	01	02	4
AGQM12	Monzo	10	1.0	10.	17	23	46	11	1.8	1.	0.	0.	0.	0.	0.0	0.	0.	0.7
.29	nite	.7	4	7	4	.8	.4	2	0	16	10	02	08	01	1	05	01	0
AGQM12	Monzo	10	7.1	42	13	25	15	12	29.	0.	1.	0.	0.	0.	0.0	0.	0.	0.9
1	nite	.8	5	5	2	.0	7	2	44	92	29	00	07	07	8	02	01	0
AGQM12	Monzo	9.	0.8	61.	13	23	57	16	4.3	0.	0.	0.	0.	0.	0.1	0.	0.	0.1
10	nite	1	1	4	1	.7	.9	4	0	61	24	00	07	09	2	02	01	3
AGQM12	Monzo	7.	0.6		10	21	43	15	0.7	0.	0.	0.	0.	0.	0.0	0.	0.	0.0
12	nite	8	0	9.2	0	.7	.8	4	4	73	03	00	04	00	0	01	01	2
AGQM12	Monzo	10	4.6	28	10	23	98	16	6.7	0.	0.	0.	0.	0.	0.0	0.	0.	1.5
13	nite	.5	3	1	7	.2	.0	2	2	75	66	01	04	08	7	01	01	0
AGQM12	Monzo	9.	3.9	10	16	20	12	12	10.	1.	0.	0.	0.	0.	0.0	0.	0.	1.1
14	nite	2	4	7	6	.3	3	1	92	22	60	01	07	02	3	01	01	7
AGQM12	Monzo	9.	0.8	14.	14	24	52	15	0.9	0.	0.	0.	0.	0.	0.0	0.	0.	0.0
15	nite	2	7	3	2	.8	.6	4	5	58	04	00	04	00	0	00	01	3
AGQM12	Monzo	20	1.3	65.	27	25	14	21	10.	0.	0.	0.	0.	0.	0.0	0.	0.	1.5
16	nite	.8	2	2	6	.2	4	1	11	94	93	01	03	03	4	00	01	2
AGQM12	Monzo	22	0.9	23.	30	24	69	22	2.6	0.	0.	0.	0.	0.	0.0	0.	0.	0.0
17	nite	.7	1	9	5	.1	.2	7	6	93	52	01	04	04	5	01	01	6
AGQM12	Monzo	17	0.9		23	26	51	20	9.2	0.	0.	0.	0.	0.	0.0	0.	0.	0.2
18	nite	.8	8	6.2	0	.1	.8	3	7	77	60	01	08	00	0	01	00	2
AGQM12	Monzo	24	5.0	59	25	22	26	20	20.	0.	2.	0.	0.	0.	0.0	0.	0.	0.6
19	nite	.5	6	9	6	.1	1	9	24	59	08	01	07	01	1	01	01	0
AGQM12	Monzo	8.	0.8		87	25	55	13	0.1	0.	0.	0.	0.	0.	0.0	0.	0.	0.0
2	nite	4	8	0.7	.9	.0	.1	9	6	74	02	00	06	00	0	00	01	0
AGQM12	Monzo	17	4.8	42	32	24	29	18	80.	0.	4.	0.	0.	0.	0.2	0.	0.	4.4
20	nite	.4	8	3	3	.5	7	6	57	93	02	02	10	26	6	05	01	5

Sample	Unit	Li	B	Na	Al	P	Ca	Ti	Mn	Ge	Rb	Nb	Sn	La	Ce	Nd	Gd	Pb
AGQM12 22	Monzonite	13.4	0.69	10.2	156	24.3	42.5	209	1.22	0.80	0.09	0.00	0.03	0.00	0.00	0.00	0.00	0.04
AGQM12 23	Monzonite	7.6	0.74	19.4	96.0	25.1	61.2	131	2.37	0.76	0.15	0.00	0.05	0.01	0.01	0.00	0.01	0.15
AGQM12 24	Monzonite	8.5	1.17	19.6	99.0	23.2	83.2	130	2.27	0.79	0.11	0.01	0.06	0.00	0.00	0.01	0.01	0.11
AGQM12 26	Monzonite	8.7	0.73	3.3	120	25.1	63.1	166	34.48	0.57	0.02	0.00	0.04	0.01	0.07	0.01	0.01	1.23
AGQM12 27	Monzonite	9.1	0.60	1.5	103	22.1	70.3	165	0.51	0.87	0.03	0.00	0.07	0.00	0.00	0.00	0.01	0.03
AGQM12 29	Monzonite	13.3	1.08	22.7	189	25.3	57.5	169	5.62	0.52	2.39	0.15	0.08	0.02	0.02	0.01	0.02	1.18
AGQM12 30	Monzonite	9.2	0.60	0.6	102	22.2	64.9	170	0.30	0.77	0.02	0.00	0.07	0.00	0.00	0.00	0.00	0.01
AGQM12 31	Monzonite	8.2	0.82	5.4	88.5	21.9	56.4	135	0.85	0.72	0.04	0.00	0.03	0.00	0.00	0.00	0.01	0.02
AGQM12 33	Monzonite	9.1	1.36	42.2	106	22.7	124	148	9.86	0.68	0.79	0.01	0.05	0.02	0.03	0.02	0.01	1.24
AGQM12 34	Monzonite	8.7	0.89	13.2	89.4	23.9	82.2	133	25.08	0.91	1.82	0.01	0.06	0.09	0.14	0.02	0.02	3.60
AGQM12 35	Monzonite	12.5	0.69	7.1	152	22.1	34.0	194	0.61	0.77	0.02	0.01	0.06	0.00	0.00	0.00	0.01	0.07
AGQM12 36	Monzonite	8.8	1.12	40.1	97.9	22.2	42.3	129	3.86	0.91	0.22	0.01	0.06	0.01	0.02	0.01	0.00	0.83
AGQM12 37	Monzonite	8.0	1.11	6.6	107	22.6	51.9	125	0.18	0.81	0.03	0.01	0.06	0.00	0.00	0.01	0.01	0.01
AGQM12 39	Monzonite	8.2	4.60	21.1	123	27.0	260	161	12.49	0.90	0.43	0.01	0.04	0.02	0.14	0.06	0.01	1.29
AGQM12 4	Monzonite	9.5	0.91	1.9	109	25.1	79.6	145	0.25	0.82	0.32	0.01	0.05	0.00	0.00	0.01	0.01	0.02
AGQM12 40	Monzonite	10.0	1.00	67.0	195	26.5	43.0	129	3.53	0.68	0.41	2.05	0.10	0.02	0.07	0.04	0.01	0.33
AGQM12 42	Monzonite	9.0	0.86	6.3	100	25.2	43.1	147	0.84	0.73	0.03	0.01	0.07	0.00	0.00	0.01	0.01	0.06
AGQM12 6	Monzonite	9.7	1.21	19.8	286	23.1	76.4	146	18.01	0.86	3.47	0.01	0.16	0.13	0.19	0.07	0.01	4.47
AGQM12 7	Monzonite	6.1	2.09	96.1	227	24.8	107	59.9	5.76	0.87	0.64	0.05	0.05	0.02	0.05	0.01	0.01	0.27
AGQM12 8	Monzonite	9.2	2.70	25.8	103	23.6	189	133	26.52	1.04	1.35	0.00	0.06	0.02	0.03	0.01	0.00	0.93
Syenite1g r11	Syenite	8.9	1.36	23.4	101	19.3	85.2	96.8	6.12	0.89	0.15	0.01	1.50	0.01	0.04	0.02	0.02	1.94
Syenite1g r110	Syenite	11.5	0.64	0.9	85.3	27.1	38.7	106	0.33	0.86	0.02	0.00	0.06	0.00	0.00	0.01	0.01	0.01
Syenite1g r111	Syenite	11.3	0.69	0.9	84.0	27.7	39.8	110	0.46	0.71	0.04	0.00	0.06	0.00	0.00	0.01	0.01	0.00
Syenite1g r112	Syenite	9.5	0.57	11.0	80.3	25.7	36.0	90.5	0.37	0.67	0.03	0.00	0.04	0.00	0.00	0.00	0.01	0.02
Syenite1g r113	Syenite	10.3	0.72	0.9	78.8	28.0	40.3	94.7	0.40	0.73	0.02	0.00	0.06	0.00	0.00	0.00	0.01	0.01
Syenite1g r12	Syenite	12.1	3.81	1.1	91.0	24.2	39.0	99.1	0.87	0.64	0.02	0.00	0.06	0.00	0.01	0.00	0.01	0.12
Syenite1g r13	Syenite	11.1	0.66	1.2	79.6	22.6	38.8	110	0.38	0.62	0.02	0.00	0.05	0.00	0.00	0.00	0.01	0.00
Syenite1g r15	Syenite	10.7	0.68	1.0	89.4	25.2	42.3	103	0.64	0.67	0.02	0.00	0.08	0.00	0.00	0.00	0.01	0.29
Syenite1g r16	Syenite	10.9	0.61	0.9	85.3	27.5	39.8	114	0.56	0.69	0.02	0.00	0.09	0.00	0.00	0.01	0.01	1.20
Syenite1g r17	Syenite	10.8	0.67	0.9	79.0	26.1	42.1	104	0.32	0.69	0.02	0.00	0.08	0.00	0.01	0.00	0.01	0.21
Syenite1g r18	Syenite	11.0	0.74	1.4	83.3	25.3	44.3	107	0.49	0.76	0.03	0.00	0.10	0.00	0.00	0.01	0.01	0.06
Syenite1g r19	Syenite	11.7	0.74	4.8	97.0	27.1	45.7	110	0.49	0.61	0.05	0.00	0.05	0.00	0.00	0.00	0.01	0.07
Syenite1g r21	Syenite	11.3	0.83	8.7	106	28.1	51.6	110	0.85	0.62	0.05	0.00	0.05	0.00	0.00	0.01	0.01	0.02
Syenite1g r210	Syenite	9.3	1.94	14.3	195	24.2	63.7	69.4	1.50	0.90	0.18	0.05	0.05	0.02	0.13	0.01	0.01	0.45
Syenite1g r211	Syenite	11.5	0.71	4.7	116	27.6	44.5	103	0.24	0.74	0.04	0.00	0.06	0.00	0.01	0.00	0.01	0.00
Syenite1g r22	Syenite	12.9	0.68	10.6	132	28.2	32.9	113	0.33	1.06	0.04	0.00	0.06	0.00	0.00	0.01	0.01	0.23
Syenite1g r23	Syenite	14.1	9.75	19.5	138	26.5	52.8	78.0	4.06	0.79	0.27	0.01	0.04	0.00	0.00	0.01	0.01	6.51

93

Sample	Unit	Li	B	Na	Al	P	Ca	Ti	Mn	Ge	Rb	Nb	Sn	La	Ce	Nd	Gd	Pb
Syenite1g		11	0.6		91	26	41	12	0.4	0.	0.	0.	0.	0.	0.0	0.	0.	0.0
r25	Syenite	.8	9	1.5	.5	.2	.7	1	4	95	02	00	05	00	0	01	00	2
Syenite1g		11	0.5		84	24	31	12	0.3	0.	0.	0.	0.	0.	0.0	0.	0.	0.0
r27	Syenite	.5	2	1.1	.5	.0	.4	0	2	79	02	00	03	00	0	00	00	1
Syenite1g		10	0.6		78	27	39	10	0.4	0.	0.	0.	0.	0.	0.2	0.	0.	0.0
r29	Syenite	.7	1	1.5	.5	.9	.6	0	1	85	02	00	06	14	2	03	01	0
Syenite1g		11	0.5		85	24	36	10	0.4	0.	0.	0.	0.	0.	0.0	0.	0.	0.0
r31	Syenite	.4	9	4.7	.7	.8	.7	4	3	79	02	00	04	00	0	01	01	6
Syenite1g		11	0.6		87	25	41	10	0.4	0.	0.	0.	0.	0.	0.0	0.	0.	0.0
r310	Syenite	.7	6	0.9	.4	.6	.7	3	6	84	02	00	06	00	0	01	01	3
Syenite1g		11	1.0	29.	10	25	41	98	0.4	0.	0.	0.	0.	0.	0.0	0.	0.	0.1
r311	Syenite	.4	7	2	.3	.4	.2	5	89	08	09	04	00	0	00	01		2
Syenite1g		10	0.8	15.	94	26	49	89	4.6	0.	0.	0.	0.	0.	0.0	0.	0.	0.2
r312	Syenite	.3	1	2	.0	.7	.8	.7	4	69	17	00	08	01	1	00	01	2
Syenite1g		11	0.8		89	25	51	90	0.4	0.	0.	0.	0.	0.	0.0	0.	0.	0.0
r313	Syenite	.5	8	1.2	.6	.9	.9	.7	5	85	03	00	04	00	0	00	00	1
Syenite1g		10	0.6		77	23	39	10	0.2	0.	0.	0.	0.	0.	0.0	0.	0.	0.0
r32	Syenite	.1	4	0.9	.6	.5	.7	2	9	64	02	00	05	00	0	01	01	0
Syenite1g		11	3.4	31	99	23	25	14	123	0.	7.	0.	0.	0.	0.4	0.	0.	9.2
r33	Syenite	.9	7	5	.8	.2	2	2	.4	85	20	56	29	36	4	07	02	0
Syenite1g		10	2.5		90	25	43	21	0.3	0.	0.	0.	0.	0.	0.0	0.	0.	0.0
r34	Syenite	.3	6	7.5	.2	.6	.0	.0	1	59	08	00	05	00	0	00	01	3
Syenite1g		12	0.8		99	26	48	11	0.4	0.	0.	0.	0.	0.	0.0	0.	0.	0.0
r35	Syenite	.7	0	1.1	.4	.4	.4	1	4	63	03	00	05	00	0	01	01	0
Syenite1g		12	0.7		91	24	45	10	0.4	0.	0.	0.	0.	0.	0.0	0.	0.	0.0
r36	Syenite	.0	2	1.0	.8	.7	.4	6	5	66	02	00	03	00	0	01	01	0
Syenite1g		12	0.7		87	26	43	11	0.4	0.	0.	0.	0.	0.	0.0	0.	0.	0.0
r37	Syenite	.0	0	0.9	.3	.5	.4	5	1	74	02	00	04	00	0	01	01	0
Syenite1g		11	0.6		81	26	40	10	0.4	0.	0.	0.	0.	0.	0.0	0.	0.	0.0
r38	Syenite	.2	5	0.9	.5	.5	.2	2	1	71	02	00	04	00	0	01	01	0
Syenite1g		11	0.9		90	26	41	10	0.3	0.	0.	0.	0.	0.	0.0	0.	0.	0.0
r41	Syenite	.5	2	0.9	.9	.7	.3	5	5	76	02	00	03	00	0	00	01	0
Syenite1g		11	0.6		89	26	38	12	0.4	0.	0.	0.	0.	0.	0.0	0.	0.	0.0
r42	Syenite	.7	6	1.2	.3	.5	.0	1	9	73	02	00	04	00	0	00	01	0
Syenite1g		12	0.7		93	26	43	12	0.4	0.	0.	0.	0.	0.	0.0	0.	0.	0.0
r43	Syenite	.6	2	3.6	.9	.8	.9	8	3	94	02	00	06	00	0	00	01	0
Syenite1g		13	0.6		93	24	40	12	0.7	0.	0.	0.	0.	0.	0.0	0.	0.	0.0
r44	Syenite	.2	9	1.3	.6	.3	.3	5	1	84	02	00	05	00	0	00	01	8
Syenite1g		12	0.6	54.	14	28	40	12	1.5	0.	0.	0.	0.	0.	0.1	0.	0.	0.0
r46	Syenite	.5	7	0	7	.6	.7	9	4	70	44	02	05	05	2	02	01	4
Syenite1g		13	0.9	28.	13	28	54	14	4.9	0.	0.	0.	0.	0.	0.8	0.	0.	0.0
r47	Syenite	.4	8	4	4	.5	.6	0	9	81	12	17	06	68	2	09	01	6
Syenite1g		10	0.7		12	26	43	12	0.6	0.	0.	0.	0.	0.	0.0	0.	0.	0.0
r48	Syenite	.7	3	8.9	1	.7	.8	4	7	68	19	01	12	01	4	01	01	3
Syenite1g		12	1.4		94	24	50	10	0.3	0.	0.	0.	0.	0.	0.0	0.	0.	0.0
r49	Syenite	.1	0	0.9	.3	.7	.3	4	3	64	02	00	03	00	0	00	00	0

Appendix 4: Temperature Calculations

Titanium in quartz geothermometer

Table 10: Titanium in quartz geothermometer calculations

Sample	Unit	Wark & Watson 2006	Thomas et al. 2010			Huang & Audetat 2012		
			5km	10km	15km	5km	10km	15km
13Agr11	Syenite	780	584	616	648	679	733	772
13Agr12	Syenite	785	588	620	652	683	738	777
13Agr13	Syenite	780	584	616	648	678	733	771
13Agr14	Syenite	776	581	613	645	675	729	768

Sample	Unit	Wark & Watson 2006	Thomas et al. 2010			Huang & Audetat 2012		
			5km	10km	15km	5km	10km	15km
13Agr16	Syenite	788	590	622	654	685	740	779
13Agr17	Syenite	769	576	607	639	669	723	761
13Agr18	Syenite	780	584	616	648	679	733	772
13Agr19	Syenite	786	589	621	653	684	739	777
13Agr21	Syenite	414	301	323	344	356	392	418
13Agr23	Syenite	436	319	341	363	376	413	439
13Agr27	Syenite	406	295	316	337	349	385	410
13Agr28	Syenite	436	319	341	363	376	413	439
13Agr29	Syenite	416	303	324	345	358	394	419
13Agr31	Syenite	768	575	607	638	668	722	760
13Agr32	Syenite	796	596	629	661	693	748	787
13Agr33	Syenite	803	602	634	667	699	754	794
13Agr34	Syenite	812	608	641	673	706	762	801
13Agr35	Syenite	798	598	630	662	694	750	789
13Agr37	Syenite	816	611	644	677	710	766	806
13Agr38	Syenite	802	601	633	666	698	753	793
13Agr39	Syenite	791	593	625	657	688	743	782
13Agr41	Syenite	809	606	639	672	704	760	799
13Agr410	Syenite	791	593	625	657	688	743	782
13Agr411	Syenite	808	605	638	671	703	759	798
13Agr412	Syenite	792	593	625	657	689	744	782
13Agr42	Syenite	823	617	650	683	716	773	813
13Agr43	Syenite	822	616	649	682	715	771	811
13Agr44	Syenite	825	618	651	684	717	774	814
13Agr46	Syenite	831	622	656	689	723	780	820
13Agr47	Syenite	806	603	636	669	701	757	796
13Agr48	Syenite	818	613	645	678	711	768	807
13Agr49	Syenite	811	607	640	673	705	761	801
13Agr510	Syenite	793	594	626	658	690	745	783
13Agr511	Syenite	792	593	626	658	689	744	783
13Agr54	Syenite	829	621	654	688	721	778	818
13Agr55	Syenite	813	609	642	674	707	763	803
13Agr56	Syenite	793	594	626	658	690	745	784
13Agr57	Syenite	784	587	619	651	682	736	775
13Agr58	Syenite	798	598	630	662	694	750	789
13Agr62	Syenite	651	486	514	542	566	614	648
13Agr63	Syenite	625	466	494	521	543	590	623
13Agr64	Syenite	620	463	490	517	539	585	618

95

Sample	Unit	Wark & Watson 2006	Thomas et al. 2010			Huang & Audetat 2012		
			5km	10km	15km	5km	10km	15km
13Agr66	Syenite	641	479	506	534	557	605	638
13Agr69	Syenite	647	483	512	540	563	611	644
15Agr11	LSPT	818	613	646	679	712	768	808
15Agr110	LSPT	787	589	621	653	684	739	778
15Agr12	LSPT	799	599	631	664	696	751	790
15Agr14	LSPT	803	601	634	666	699	754	793
15Agr15	LSPT	830	622	655	688	722	779	819
15Agr16	LSPT	824	617	650	683	717	773	813
15Agr17	LSPT	798	597	630	662	694	749	788
15Agr18	LSPT	799	598	631	663	695	750	789
15Agr19	LSPT	811	607	640	672	705	761	801
15Agr21	LSPT	812	608	641	674	706	762	802
15Agr210	LSPT	811	607	640	673	705	761	801
15Agr22	LSPT	811	607	640	673	705	761	801
15Agr23	LSPT	823	617	650	683	716	773	813
15Agr24	LSPT	821	615	648	681	714	770	810
15Agr25	LSPT	812	608	641	674	706	762	802
15Agr26	LSPT	813	609	642	675	707	763	803
15Agr27	LSPT	817	612	644	677	710	767	806
15Agr28	LSPT	806	604	637	669	702	757	797
15Agr29	LSPT	785	588	620	652	683	737	776
15Agr31	LSPT	777	582	613	645	676	730	768
15Agr310	LSPT	785	588	620	652	683	738	776
15Agr32	LSPT	793	594	626	658	690	745	784
15Agr33	LSPT	785	588	620	652	683	737	776
15Agr34	LSPT	800	599	632	664	696	751	791
15Agr35	LSPT	796	596	629	661	693	748	787
15Agr37	LSPT	779	584	615	647	678	732	771
15Agr38	LSPT	783	586	618	650	681	735	774
15Agr39	LSPT	783	587	618	650	681	736	774
15Agr41	LSPT	818	613	646	678	712	768	808
15Agr42	LSPT	844	632	666	699	734	792	832
15Agr43	LSPT	764	572	603	635	664	718	756
15Agr44	LSPT	809	606	639	671	704	760	799
15Agr45	LSPT	788	590	622	655	686	741	779
15Agr47	LSPT	800	599	632	664	696	751	791
15Agr49	LSPT	796	596	629	661	693	748	787
15Agr51	LSPT	781	585	617	648	679	734	772

Sample	Unit	Wark & Watson 2006	Thomas et al. 2010			Huang & Audetat 2012		
			5km	10km	15km	5km	10km	15km
15Agr52	LSPT	788	590	622	654	685	740	779
15Agr53	LSPT	786	589	621	653	684	738	777
15Agr54	LSPT	786	589	621	653	684	739	777
15Agr55	LSPT	785	588	620	652	683	737	776
15Agr56	LSPT	805	603	636	668	701	756	796
15Agr57	LSPT	805	603	636	668	701	756	796
15Agr58	LSPT	813	609	642	674	707	763	803
15Agr59	LSPT	828	620	654	687	720	777	817
15Agr61	LSPT	767	574	606	637	667	721	759
15Agr610	LSPT	793	594	626	658	690	745	784
15Agr62	LSPT	788	590	622	654	686	740	779
15Agr63	LSPT	785	588	620	652	683	737	776
15Agr64	LSPT	795	595	627	660	691	746	785
15Agr65	LSPT	765	573	604	636	666	719	757
15Agr67	LSPT	787	589	621	653	684	739	778
15Agr69	LSPT	796	596	629	661	693	748	787
27A2gr15	USPT	791	593	625	657	688	743	782
27A2gr16	USPT	793	594	626	658	690	745	784
27A2gr210	USPT	781	585	617	649	680	734	773
27A2gr24	USPT	790	592	624	656	687	742	781
27A2gr26	USPT	799	598	630	663	695	750	789
27A2gr27	USPT	794	595	627	659	691	746	785
27A2gr28	USPT	799	599	631	663	695	751	790
27A2gr29	USPT	793	594	626	658	690	745	784
27A2gr31	USPT	792	593	625	657	689	744	783
27A2gr310	USPT	821	615	648	681	714	770	810
27A2gr311	USPT	816	611	644	677	710	766	806
27A2gr313	USPT	809	606	638	671	703	759	799
27A2gr314	USPT	792	593	626	658	689	744	783
27A2gr315	USPT	800	599	631	664	696	751	790
27A2gr316	USPT	789	591	623	655	686	741	780
27A2gr317	USPT	788	590	622	654	686	740	779
27A2gr34	USPT	802	601	634	666	698	754	793
27A2gr35	USPT	806	603	636	668	701	756	796
27A2gr36	USPT	811	607	640	672	705	761	801
27A2gr37	USPT	802	601	633	666	698	753	793
27A2gr38	USPT	803	601	634	666	699	754	793
27A2gr39	USPT	810	607	640	672	705	761	800

Sample	Unit	Wark & Watson 2006	Thomas et al. 2010			Huang & Audetat 2012		
			5km	10km	15km	5km	10km	15km
27A2gr411	USPT	796	597	629	661	693	748	787
27A2gr413	USPT	804	602	635	667	700	755	795
27A2gr43	USPT	800	599	632	664	696	751	791
27A2gr44	USPT	807	605	637	670	702	758	797
27A2gr48	USPT	804	602	635	667	699	755	794
27A2gr49	USPT	800	599	632	664	696	751	791
27Agr11	USPT	800	599	631	664	696	751	790
27Agr112	USPT	794	595	627	659	691	746	785
27Agr12	USPT	818	613	646	678	712	768	808
27Agr13	USPT	827	620	653	686	720	777	817
27Agr15	USPT	822	616	649	682	715	771	811
27Agr17	USPT	823	616	649	682	716	772	812
27Agr19	USPT	810	607	640	672	705	761	800
27Agr21	USPT	770	577	608	640	670	724	762
27Agr210	USPT	793	594	626	659	690	745	784
27Agr22	USPT	800	599	632	664	696	752	791
27Agr23	USPT	815	610	643	676	709	765	805
27Agr24	USPT	815	611	643	676	709	765	805
27Agr25	USPT	822	616	649	682	715	772	812
27Agr26	USPT	800	599	632	664	696	751	791
27Agr27	USPT	811	608	640	673	706	762	801
27Agr28	USPT	804	602	635	667	700	755	795
27Agr29	USPT	793	594	626	658	690	745	784
27Agr31	USPT	824	617	650	683	717	773	813
27Agr32	USPT	818	613	646	679	712	768	808
27Agr33	USPT	821	615	648	681	714	771	811
27Agr34	USPT	824	617	650	683	717	773	813
27Agr36	USPT	803	602	634	667	699	754	794
27Agr37	USPT	794	595	627	659	691	746	785
27Agr38	USPT	796	596	628	661	692	748	787
27Agr39	USPT	784	587	619	651	682	737	776
27Agr41	USPT	805	603	636	668	700	756	795
27Agr410	USPT	794	595	627	659	691	746	785
27Agr411	USPT	804	602	635	667	700	755	794
27Agr42	USPT	795	595	628	660	691	747	785
27Agr43	USPT	795	595	628	660	692	747	786
27Agr44	USPT	785	588	620	652	683	738	776
27Agr47	USPT	806	604	636	669	701	757	796

Sample	Unit	Wark & Watson 2006	Thomas et al. 2010			Huang & Audetat 2012		
			5km	10km	15km	5km	10km	15km
27Agr49	USPT	782	586	618	649	680	735	773
40Igr110	USPT	799	599	631	663	695	751	790
40Igr111	USPT	804	602	634	667	699	755	794
40Igr12	USPT	795	595	628	660	692	747	786
40Igr13	USPT	803	602	634	667	699	754	793
40Igr14	USPT	826	619	652	685	719	775	816
40Igr15	USPT	803	602	634	667	699	754	794
40Igr16	USPT	805	603	635	668	700	756	795
40Igr17	USPT	816	611	644	677	710	766	805
40Igr18	USPT	795	596	628	660	692	747	786
40Igr19	USPT	795	595	628	660	692	747	786
40Igr21	USPT	823	617	650	683	716	773	813
40Igr22	USPT	812	608	641	674	706	762	802
40Igr23	USPT	827	620	653	686	720	777	817
40Igr25	USPT	817	612	645	678	711	767	807
40Igr26	USPT	811	607	640	672	705	761	801
40Igr27	USPT	812	608	641	673	706	762	802
40Igr31	USPT	846	634	667	701	736	793	834
40Igr33	USPT	834	625	658	691	726	783	823
40Igr34	USPT	828	620	653	686	720	777	817
40Igr35	USPT	832	623	657	690	724	781	821
40Igr37	USPT	824	617	650	683	716	773	813
40Igr38	USPT	822	615	648	681	715	771	811
40Igr39	USPT	825	618	651	684	718	774	814
40Igr41	USPT	872	653	687	722	758	817	859
40Igr410	USPT	832	623	656	690	724	781	821
40Igr411	USPT	826	618	651	685	718	775	815
40Igr412	USPT	827	619	652	685	719	776	816
40Igr413	USPT	825	618	651	684	718	775	815
40Igr42	USPT	880	659	693	728	765	824	866
40Igr43	USPT	869	651	685	719	756	814	856
40Igr44	USPT	861	645	679	713	749	808	849
40Igr45	USPT	853	639	673	707	742	800	841
40Igr46	USPT	864	647	682	716	752	810	852
40Igr47	USPT	854	639	673	707	742	800	842
40Igr48	USPT	856	641	675	709	745	803	844
40Igr49	USPT	836	626	659	693	727	784	825
40Igr51	USPT	838	627	661	694	729	786	826

Sample	Unit	Wark & Watson 2006	Thomas et al. 2010			Huang & Audetat 2012		
			5km	10km	15km	5km	10km	15km
40Igr511	USPT	849	636	670	704	739	797	837
40Igr513	USPT	833	624	657	690	725	781	822
40Igr52	USPT	845	633	667	700	735	793	834
40Igr53	USPT	849	636	669	703	738	796	837
40Igr54	USPT	860	644	678	712	748	806	847
40Igr55	USPT	853	639	673	706	742	800	841
40Igr56	USPT	848	635	669	702	737	795	836
40Igr57	USPT	860	644	678	712	748	807	848
40Igr59	USPT	847	634	668	702	737	794	835
40Igr61	USPT	856	641	675	709	745	803	844
40Igr62	USPT	868	650	684	719	755	814	855
40Igr63	USPT	852	638	672	705	741	799	840
40Igr64	USPT	821	615	648	681	714	770	810
40Igr65	USPT	794	595	627	659	691	746	785
40Igr66	USPT	785	588	620	652	683	738	776
40Igr67	USPT	790	592	624	656	688	743	781
40Igr68	USPT	783	586	618	650	681	735	774
49Bgr11	MSPT	819	613	646	679	712	768	808
49Bgr12	MSPT	831	622	656	689	723	780	820
49Bgr13	MSPT	831	623	656	689	723	780	820
49Bgr14	MSPT	809	606	639	671	704	760	799
49Bgr15	MSPT	821	615	648	681	714	770	810
49Bgr16	MSPT	809	606	638	671	703	759	799
49Bgr17	MSPT	803	602	634	667	699	754	794
49Bgr18	MSPT	786	589	621	653	684	738	777
49Bgr21	MSPT	811	607	640	673	705	761	801
49Bgr210	MSPT	787	590	622	654	685	739	778
49Bgr23	MSPT	804	602	634	667	699	755	794
49Bgr24	MSPT	820	614	647	680	713	769	809
49Bgr25	MSPT	816	611	644	677	710	766	805
49Bgr26	MSPT	815	610	643	676	709	765	805
49Bgr27	MSPT	819	614	646	679	713	769	809
49Bgr28	MSPT	820	614	647	680	713	769	809
49Bgr29	MSPT	790	591	624	656	687	742	781
49Bgr31	MSPT	815	610	643	676	709	765	805
49Bgr32	MSPT	819	613	646	679	712	768	808
49Bgr33	MSPT	816	611	644	677	710	766	806
49Bgr34	MSPT	821	615	648	681	714	770	810

Sample	Unit	Wark & Watson 2006	Thomas et al. 2010			Huang & Audetat 2012		
			5km	10km	15km	5km	10km	15km
49Bgr35	MSPT	805	603	635	668	700	756	795
49Bgr36	MSPT	806	604	636	669	701	757	797
49Bgr37	MSPT	803	601	634	666	698	754	793
49Bgr38	MSPT	808	605	638	670	703	759	798
49Bgr39	MSPT	801	600	633	665	697	753	792
49Bgr41	MSPT	805	603	636	668	700	756	795
49Bgr42	MSPT	786	588	620	652	684	738	777
49Bgr43	MSPT	807	604	637	669	702	757	797
49Bgr44	MSPT	798	598	630	663	695	750	789
49Bgr45	MSPT	802	601	633	666	698	753	792
49Bgr46	MSPT	810	607	639	672	705	761	800
49Bgr47	MSPT	805	603	635	668	700	756	795
49Bgr48	MSPT	791	593	625	657	688	743	782
49Bgr49	MSPT	786	589	621	653	684	739	777
49Bgr51	MSPT	820	614	647	680	713	770	809
49Bgr53	MSPT	824	617	651	684	717	774	814
49Bgr54	MSPT	810	606	639	672	704	760	800
49Bgr55	MSPT	819	614	647	680	713	769	809
49Bgr56	MSPT	820	615	648	680	714	770	810
49Bgr57	MSPT	815	611	643	676	709	765	805
49Bgr58	MSPT	805	603	636	668	701	756	796
49Bgr59	MSPT	817	612	645	678	711	767	807
49Bgr61	MSPT	831	622	656	689	723	780	820
49Bgr610	MSPT	791	593	625	657	688	743	782
49Bgr62	MSPT	837	627	660	694	728	785	826
49Bgr63	MSPT	818	613	646	678	712	768	808
49Bgr64	MSPT	817	612	645	677	710	767	806
49Bgr65	MSPT	820	614	647	680	714	770	810
49Bgr66	MSPT	825	618	651	684	717	774	814
49Bgr67	MSPT	824	617	650	683	717	773	813
49Bgr68	MSPT	790	592	624	656	687	742	781
49Bgr69	MSPT	792	593	626	658	689	744	783
49Bgr71	MSPT	811	608	640	673	706	762	801
49Bgr710	MSPT	825	618	651	684	718	775	815
49Bgr711	MSPT	786	589	621	653	684	738	777
49Bgr72	MSPT	820	614	647	680	713	770	810
49Bgr73	MSPT	831	623	656	689	723	780	820
49Bgr75	MSPT	839	628	662	695	730	787	827

Sample	Unit	Wark & Watson 2006	Thomas et al. 2010			Huang & Audetat 2012		
			5km	**10km**	**15km**	**5km**	**10km**	**15km**
49Bgr77	MSPT	826	619	652	685	719	775	815
49Bgr78	MSPT	789	591	623	655	687	742	780
49Bgr79	MSPT	827	620	653	686	720	777	817
49Cgr12	MSPT	791	592	624	656	688	743	782
49Cgr13	MSPT	790	592	624	656	687	742	781
49Cgr15	MSPT	805	603	635	668	700	756	795
49Cgr16	MSPT	787	590	622	654	685	740	779
49Cgr22	MSPT	794	595	627	660	691	746	785
49Cgr23	MSPT	787	590	622	654	685	740	778
49Cgr24	MSPT	810	607	640	672	705	761	800
49Cgr27	MSPT	798	598	630	662	694	749	789
49Cgr28	MSPT	795	596	628	660	692	747	786
49Cgr31	MSPT	789	591	623	655	687	741	780
49Cgr32	MSPT	781	585	617	649	679	734	772
49Cgr41	MSPT	847	634	668	702	737	794	835
49Cgr43	MSPT	842	631	664	698	732	790	830
49Cgr44	MSPT	842	631	664	698	733	790	831
49Cgr45	MSPT	791	592	624	656	688	743	782
49Cgr46	MSPT	827	619	652	685	719	776	816
49Cgr48	MSPT	802	601	633	666	698	753	792
49Cgr49	MSPT	790	592	624	656	688	743	781
49Cgr51	MSPT	817	612	645	678	711	767	807
49Cgr510	MSPT	786	589	621	653	684	738	777
49Cgr52	MSPT	806	604	636	669	701	757	796
49Cgr53	MSPT	813	609	641	674	707	763	803
49Cgr55	MSPT	814	610	643	676	708	765	804
49Cgr56	MSPT	814	610	643	676	709	765	804
49Cgr57	MSPT	811	607	640	673	705	761	801
49Cgr58	MSPT	812	608	641	674	707	763	802
49Cgr59	MSPT	792	593	625	657	689	744	783
49Cgr64	MSPT	808	606	638	671	703	759	799
49Cgr66	MSPT	793	594	626	658	690	745	783
49Cgr67	MSPT	794	594	627	659	690	745	784
49Dgr11	MSPT	805	603	635	668	700	756	795
49Dgr12	MSPT	826	619	652	685	719	776	816
49Dgr14	MSPT	824	617	650	683	717	773	813
49Dgr15	MSPT	826	619	652	685	719	775	815
49Dgr16	MSPT	810	607	640	672	705	761	800

102

Sample	Unit	Wark & Watson 2006	Thomas et al. 2010			Huang & Audetat 2012		
			5km	10km	15km	5km	10km	15km
49Dgr18	MSPT	829	621	654	688	722	778	819
49Dgr19	MSPT	810	607	640	672	705	761	800
49Dgr21	MSPT	814	610	642	675	708	764	804
49Dgr211	MSPT	801	600	632	665	697	752	792
49Dgr22	MSPT	826	619	652	685	719	775	815
49Dgr23	MSPT	861	645	679	713	749	807	849
49Dgr24	MSPT	811	607	640	673	705	761	801
49Dgr27	MSPT	828	620	654	687	721	777	817
49Dgr29	MSPT	804	602	635	667	699	755	794
49Dgr41	MSPT	799	599	631	664	696	751	790
49Dgr42	MSPT	789	591	623	655	687	742	780
49Dgr43	MSPT	793	594	626	658	690	745	784
49Dgr44	MSPT	800	599	631	664	696	751	790
49Dgr45	MSPT	801	600	633	665	697	752	792
49Dgr46	MSPT	797	597	629	661	693	748	787
49Dgr51	MSPT	830	622	655	688	722	779	819
49Dgr510	MSPT	811	607	640	673	705	761	801
49Dgr513	MSPT	803	601	634	666	698	754	793
49Dgr52	MSPT	835	626	659	692	727	784	824
49Dgr53	MSPT	829	621	654	687	721	778	818
49Dgr54	MSPT	805	603	636	668	701	756	796
49Dgr55	MSPT	807	605	637	670	702	758	797
49Dgr57	MSPT	806	604	637	669	702	757	797
49Dgr58	MSPT	820	614	647	680	713	769	809
49Dgr59	MSPT	805	603	636	668	701	756	795
49Dgr61	MSPT	784	587	619	651	682	737	775
49Dgr62	MSPT	811	607	640	673	705	761	801
49Dgr63	MSPT	804	602	635	667	700	755	794
49Dgr64	MSPT	808	605	638	670	703	759	798
49Dgr65	MSPT	817	612	644	677	710	766	806
49Dgr66	MSPT	818	613	646	679	712	768	808
49Dgr67	MSPT	794	595	627	659	691	746	785
49Dgr68	MSPT	788	590	622	654	685	740	779
AGQM12.21	Monzonite	873	654	688	723	759	818	860
AGQM12.210	Monzonite	839	629	662	696	730	787	828
AGQM12.211	Monzonite	825	618	651	684	718	775	815
AGQM12.212	Monzonite	825	618	651	684	718	774	814

Sample	Unit	Wark & Watson 2006	Thomas et al. 2010			Huang & Audetat 2012		
			5km	10km	15km	5km	10km	15km
AGQM12.214	Monzonite	833	624	657	691	725	782	822
AGQM12.215	Monzonite	837	627	661	694	728	786	826
AGQM12.219	Monzonite	839	629	662	695	730	787	828
AGQM12.22	Monzonite	882	661	695	730	767	827	869
AGQM12.220	Monzonite	836	626	659	693	727	784	824
AGQM12.224	Monzonite	823	616	649	682	716	772	812
AGQM12.225	Monzonite	866	648	683	717	753	812	853
AGQM12.226	Monzonite	866	649	683	717	753	812	853
AGQM12.227	Monzonite	863	647	681	715	751	809	851
AGQM12.228	Monzonite	837	627	661	694	729	786	826
AGQM12.229	Monzonite	807	605	637	670	702	758	797
AGQM12.23	Monzonite	837	627	660	694	728	785	826
AGQM12.230	Monzonite	871	653	687	721	758	817	858
AGQM12.231	Monzonite	835	625	659	692	726	784	824
AGQM12.233	Monzonite	833	624	657	690	724	781	822
AGQM12.234	Monzonite	835	626	659	692	727	784	824
AGQM12.235	Monzonite	866	649	683	717	753	812	853
AGQM12.237	Monzonite	710	531	561	591	618	669	705
AGQM12.238	Monzonite	864	647	681	715	751	810	851
AGQM12.239	Monzonite	853	639	673	707	742	800	841
AGQM12.24	Monzonite	860	644	678	712	748	806	847
AGQM12.240	Monzonite	830	622	655	688	722	779	819
AGQM12.241	Monzonite	826	619	652	685	719	775	815
AGQM12.242	Monzonite	840	629	663	696	731	788	829
AGQM12.243	Monzonite	840	629	663	696	731	788	829
AGQM12.25	Monzonite	867	650	684	718	754	813	855
AGQM12.26	Monzonite	855	640	674	708	744	802	843
AGQM12.27	Monzonite	893	668	703	738	776	836	878
AGQM12.28	Monzonite	824	617	650	683	717	774	814
AGQM12.29	Monzonite	814	609	642	675	708	764	803
AGQM121	Monzonite	826	619	652	685	718	775	815
AGQM1213	Monzonite	867	649	683	718	754	812	854
AGQM1214	Monzonite	824	617	650	683	717	774	814
AGQM1215	Monzonite	859	643	677	711	747	805	846
AGQM1216	Monzonite	908	680	715	750	789	850	893
AGQM1217	Monzonite	919	688	724	759	799	860	904
AGQM1218	Monzonite	901	675	710	745	784	844	887

Sample	Unit	Wark & Watson 2006	Thomas et al. 2010			Huang & Audetat 2012		
			5km	10km	15km	5km	10km	15km
AGQM122	Monzonite	844	632	665	699	734	791	832
AGQM1220	Monzonite	888	665	700	735	772	832	874
AGQM1221	Monzonite	918	687	723	758	798	859	902
AGQM1222	Monzonite	906	678	713	749	787	848	891
AGQM1223	Monzonite	836	626	659	693	727	784	824
AGQM1224	Monzonite	835	625	659	692	726	783	824
AGQM1226	Monzonite	870	651	686	720	757	815	857
AGQM1227	Monzonite	869	651	685	719	756	815	856
AGQM1228	Monzonite	825	618	651	684	718	774	814
AGQM1229	Monzonite	873	654	688	723	759	818	860
AGQM1230	Monzonite	874	654	689	723	760	819	861
AGQM1231	Monzonite	840	629	662	696	730	788	828
AGQM1233	Monzonite	853	639	673	707	742	800	841
AGQM1234	Monzonite	838	627	661	694	729	786	826
AGQM1235	Monzonite	894	669	704	739	777	837	880
AGQM1236	Monzonite	833	624	657	691	725	782	822
AGQM1237	Monzonite	828	621	654	687	721	777	818
AGQM1239	Monzonite	866	649	683	717	753	812	853
AGQM1240	Monzonite	833	624	657	690	724	781	822
AGQM1242	Monzonite	852	638	672	706	741	799	840
AGQM126	Monzonite	852	638	672	705	741	799	840
AGQM127	Monzonite	734	550	580	611	639	691	728
AGQM128	Monzonite	837	627	660	694	728	785	826
Syenite1gr11	Syenite	794	595	627	659	691	746	785
Syenite1gr111	Syenite	811	607	640	673	705	761	801
Syenite1gr112	Syenite	785	588	620	652	683	738	777
Syenite1gr113	Syenite	791	593	625	657	688	743	782
Syenite1gr12	Syenite	797	597	629	662	694	749	788
Syenite1gr13	Syenite	811	607	640	673	705	761	801
Syenite1gr14	Syenite	788	590	622	654	685	740	779
Syenite1gr15	Syenite	803	601	634	666	698	754	793
Syenite1gr16	Syenite	816	612	644	677	710	766	806
Syenite1gr17	Syenite	803	602	634	667	699	754	794
Syenite1gr18	Syenite	807	604	637	670	702	758	797
Syenite1gr19	Syenite	811	607	640	673	706	761	801
Syenite1gr21	Syenite	811	607	640	673	705	761	801
Syenite1gr210	Syenite	752	563	594	625	654	707	745
Syenite1gr211	Syenite	802	601	633	666	698	753	793

Sample	Unit	Wark & Watson 2006	Thomas et al. 2010			Huang & Audetat 2012		
			5km	10km	15km	5km	10km	15km
Syenite1gr23	Syenite	766	574	605	637	667	721	758
Syenite1gr24	Syenite	809	606	639	671	704	760	799
Syenite1gr25	Syenite	825	618	651	684	717	774	814
Syenite1gr27	Syenite	823	616	649	682	716	772	812
Syenite1gr31	Syenite	803	602	634	667	699	754	794
Syenite1gr310	Syenite	802	601	633	665	698	753	792
Syenite1gr311	Syenite	796	596	628	661	693	748	787
Syenite1gr312	Syenite	784	587	619	651	682	737	775
Syenite1gr313	Syenite	786	588	620	652	684	738	777
Syenite1gr32	Syenite	802	600	633	665	697	753	792
Syenite1gr33	Syenite	847	634	668	702	737	795	835
Syenite1gr34	Syenite	625	466	494	521	543	590	623
Syenite1gr35	Syenite	813	609	642	674	707	763	803
Syenite1gr36	Syenite	807	604	637	669	702	758	797
Syenite1gr37	Syenite	817	612	645	678	711	767	807
Syenite1gr38	Syenite	801	600	632	665	697	752	791
Syenite1gr42	Syenite	824	617	650	683	717	773	813
Syenite1gr43	Syenite	832	623	656	690	724	780	821
Syenite1gr44	Syenite	829	621	654	687	721	778	818
Syenite1gr46	Syenite	833	624	658	691	725	782	822
Syenite1gr47	Syenite	845	633	667	700	735	793	834
Syenite1gr48	Syenite	827	620	653	686	720	776	817
Syenite1gr49	Syenite	803	602	634	667	699	754	794

Putirka 2 Feldspar Geothermometer

Table 11: Putirka (2008) two-feldspar geothermometer results

Sample	Unit	Pressure (kbar)	Temp	Equilibrium Test		
				delta-a(An)	delta-a(Ab)	delta-a(Or)
LC-2004-40A2	USPT	2.7	887	-0.10	-0.01	-0.03
LC-2004-40A2	USPT	2.7	920	0.24	-0.04	-0.06
LC-2004-40A3	USPT	2.7	856	-0.20	-0.01	0.01
LC-2004-40A3	USPT	2.7	884	0.13	0.01	-0.09
LC-2004-40B	USPT	2.7	896	0.07	0.01	-0.21
LC-2004-15D	LSPT	2.7	958	0.41	-0.01	-0.30
LC-2004-15D	LSPT	2.7	910	0.28	0.02	-0.32

Ghiorso & Evans Fe-Ti oxide Geothermometer

Input to calculation:

Magnetite	wt %	Ilmenite	wt %
SiO_2	0.0813	SiO_2	0.0476
TiO_2	6.74	TiO_2	42.4
Al_2O_3	0.3735	Al_2O_3	0.0286
Fe_2O_3	0.0	Fe_2O_3	0.0
V_2O_3	0.6439	V_2O_3	0.4718
Cr_2O_3	0	Cr_2O_3	0.0
FeO	85.11	FeO	50.83
MnO	0.2835	MnO	3.45
MgO	0.0087	MgO	0.0921
CaO	0.0367	CaO	0.0196
ZnO	0.0	ZnO	0.0
NiO	0.0	NiO	0.0

Results of calculation:

T °C (Fe-Ti exchange)	759
$log_{10}f_{O2}$ (relative to NNO)	0.73
T °C (Fe-Mg exchange)	-227
a TiO_2 (liquid, realtive to rutile saturation)	0.654

Figure 25: output report for the Ghiorso and Evans Fe-Ti oxide geothermometer